Simultaneous Range/Velocity Detection with an Ultra-Wideband Random Noise Radar through Fully Digital Cross-Correlation in the Time Domain

THESIS

James R. Lievsay, Captain, USAF

AFIT/GE/ENG/11-24

DEPARTMENT OF THE AIR FORCE
AIR UNIVERSITY

AIR FORCE INSTITUTE OF TECHNOLOGY

Wright-Patterson Air Force Base, Ohio

AFIT/GE/ENG/11-24

Simultaneous Range/Velocity Detection with an Ultra-Wideband Random Noise Radar through Fully Digital Cross-Correlation in the Time Domain

THESIS

Presented to the Faculty

Department of Electrical and Computer Engineering

Graduate School of Engineering and Management

Air Force Institute of Technology

Air University

Air Education and Training Command

In Partial Fulfillment of the Requirements for the

Degree of Master of Science in Electrical Engineering

James R. Lievsay, B.S.E.E., M.S.E.E.

Captain, USAF

March 2011

AFIT/GE/ENG/11-24

Simultaneous Range/Velocity Detection with an Ultra-Wideband Random Noise Radar through Fully Digital Cross-Correlation in the Time Domain

James R. Lievsay, B.S.E.E., M.S.E.E.

Captain, USAF

Approved:

/signed/	7 Mar 2011
Maj Geoffrey Akers, PhD (Chairman)	date
/signed/	7 Mar 2011
Dr. Peter Collins (Member)	date
/signed/	7 Mar 2011
Dr. Matthew Fickus (Member)	date

Abstract

This research effort examines the theory, application, and results of applying two-dimensional cross-correlation in the time domain to ultra-wideband (UWB) random noise waveforms for simultaneous range and velocity estimation. When applying common Doppler processing techniques to random noise waveforms for the purpose of velocity estimation, the velocity resolution degrades as the signal bandwidth or the target speed increase. To mitigate the degradation, the Doppler approximation is not utilized, and instead, wideband signal processing theory is applied in the time domain. The results show that by accurately interpolating each sample in the digitized reference signal, a target's velocity and range can be extracted simultaneously. However, the drawback consists of the amount of time involved in processing the data. As technology continues to advance, it is believed that the Air Force Institute of Technology UWB Random Noise Radar (RNR) will be capable of simultaneously estimating a target's range and velocity near real-time through 2D non-coherent cross-correlation in the time domain.

Acknowledgements

It is my pleasure to thank those who made this thesis possible. First and foremost, I would like to thank my wife, who stood out in below freezing weather to help me collect the data I needed. Without her love, support, and assistance, my thesis would have suffered greatly. Secondly, I would like to thank my advisor, Maj Geoffrey Akers, whose knowledge, expertise, and feedback significantly helped in completing my thesis. I also appreciate Dr. Matthew Fickus of the Department of Mathematics & Statistics for the helpful comments and suggestions. I would next like to express my gratitude to my fellow graduate students who selflessly took time away from their thesis to help me brainstorm. Some of those brainstorming sessions sparked ideas that greatly impacted this thesis. Finally, I would like to offer thanks to all my family and friends for showing their support and in particularly, my mother, father, and sister who traveled hundreds of miles for my defense and graduation.

James R. Lievsay

Table of Contents

Page

List of Figures

List of Tables

Simultaneous Range/Velocity Detection with an Ultra-Wideband Random Noise Radar through Fully Digital Cross-Correlation in the Time Domain

I. Introduction

1.1 Problem Description

The main purpose of a radar is to extract a target's range and/or Doppler information from an environment. The capability a radar possesses depends on a wide variety of topics that include radar waveform characteristics, radar hardware components, radar operating environment, etc. Particularly, the waveform of the radar offers some of the best insight to a radar's potential performance.

The waveform for an ultra-wideband (UWB) random noise radar (RNR) offers some of the best theoretical accuracies when estimating the time delay, τ, and Doppler frequency, f_d, from a target reflected signal. These accuracies are observed through the waveform's ambiguity response shown in Figure 1.1 where the response produces what is commonly known as a "thumbtack" response. The thumbtack ambiguity response communicates to a radar designer the potential accuracy the waveform has in extracting a target's true range and velocity. Furthermore, the thumbtack response allows the capability of detecting multiple targets with similar characteristics.

A problem, though, comes from the fact the ambiguity function produces a thumbtack response. With a thumbtack response, the radar will miss a target if not exactly matched to the particular time delay and Doppler shift. Therefore, for 2D correlation the number of combinations between reference time delays and Doppler shifts increases significantly putting computational stress on the signal processing.

An additional problem that arises from an UWB random noise waveform stems from the large bandwidth combined with the random characteristics signal. When

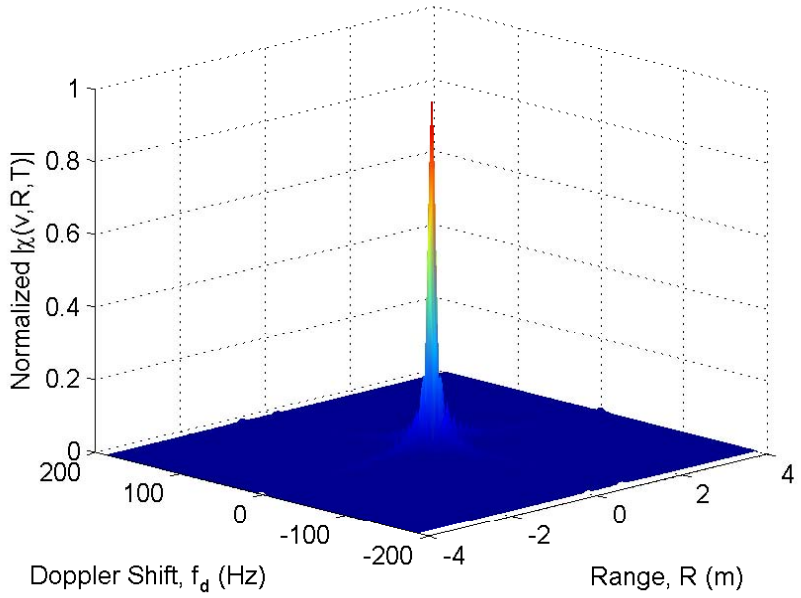

Figure 1.1: Commonly known as a "thumbtack" ambiguity response. The response conveys the radar waveform's excellence in very accurately estimating a target's range and velocity.

extracting a target's velocity, the common approach consists of measuring the relative Doppler shift between the radar and target, and then convert the shift to a velocity. The magnitude of Doppler shift is directly proportional to the target's velocity and carrier frequency, f_c, of the waveform. Since the target's speed is generally unknown and not controlled, the focus will be on the f_c.

In a random noise waveform, the instantaneous frequency is random, causing the instantaneous Doppler shift to become random. Over time, a mean frequency is established, which represents the carrier frequency. As the bandwidth increases, the variance of the frequencies increases, which leads to a high variance in Doppler shifts. The Doppler shift variance reduces the measurement accuracy and therefore, leads to poor velocity estimation.

The final problem this paper addresses pertains to performing the 2D digital correlation with the AFIT UWB RNR. In the AFIT UWB RNR, the transmit and receive signals are digitized near the antennas. No modulation occurs in the system,

which means there is not an I/Q detector that preserves the instantaneous phase. Therefore, only non-coherent integration may be used for the 2D correlation.

1.2 Research Motivation

Doppler processing has been theoretically derived for RNR and experimented with using narrowband and UWB RNR. However, UWB RNR Doppler processing produces low resolution results and has only been accomplished through analog correlation. If accurate Doppler estimation is achieved, then UWB RNR could be effectively utilized in covert operations as a through-wall-imaging radar while maintaining the low probability of intercept (LPI) characteristics.

1.3 Research Goals

The primary goal is to demonstrate the AFIT RNR's capability to extract a moving target's velocity through non-coherent digital correlation. The secondary goal expands the previous goal to include extracting a target's velocity and range simultaneously with the AFIT RNR through non-coherent 2D digital correlation.

1.4 Background

The theory behind random noise radar (RNR) first came about in the 1950s as a way to produce high range-Doppler resolution. An RNR system transmits a random, low-power noise waveform. Ideally, this waveform produces the desired thumbtack ambiguity function needed for high resolution in both range and Doppler.

The earliest reported investigations in noise technology were in 1959 and 1962 from Horton [18] and Craig [12]. A short time later, in 1963 and 1967, Grant et al. [16], Cooper et al. [11], and McGillem [25] formulated a theoretical analysis and built prototypes that used a polarity coincidence correlator after converting from microwave to video frequencies. Further experiments were conducted to show possible target detection in very poor SNR.

Research died down due to the enormous amount of data processing required by UWB systems. Then in the 1990s, with the technology advancements, RNR discussions began resurfacing. In 1995 Narayanan and his co-authors at the University of Nebraska implemented a complex noise radar that used a variable delay line with an intermediate mixing frequency to measure the in-phase and quadrature-phase components [27]. Then from 1997-99, Walton and his coworkers at Ohio State University developed an RNR that used a fixed range gate for moving target identifications [33,34].

Narayanan continued his work with the polarmetric RNR to demonstrate the Doppler estimation capability [13, 26], where the Doppler estimates were averaged over ten trials through a heterodyne correlation detailed in [14]. Narayanan and his co-authors concluded: 1.) Doppler frequency extraction from a moving target works with polarmetric RNR, 2.) the estimated Doppler frequency of a narrowband RNR closely resembles the Doppler estimate for a fixed frequency, 3.) Doppler spread increases at larger bandwidths and higher target velocities. The Doppler visibility effects from the third conclusion along with the hardware in the polarmetric UWB RNR used by Narayanan is given in further detail in [23].

Axelsson outlined the range/Doppler processing theory behind RNR in [1–3,5,6], where simulated transmit and receive signals are used to estimate Doppler. The random noise waveform Axelsson's model used is produced with random phase and is frequency modulated where the AFIT RNR waveform is unmodulated, band-limited, thermal noise. Axelsson often distinguished the difference between narrowband RNR and wideband RNR where he observed, like Narayanan, the Doppler spread worsened with increased bandwidth.

Finally, Dawood [15] and Axelsson [7] produced a generalized ambiguity function for an UWB RNR, which displays the potential range/Doppler resolutions. Dawood continued with the generalized ambiguity function to derive the ambiguity function that incorporated his polarmetric UWB RNR complex waveform.

II. Theory

2.1 Overview

This chapter first covers the minimum specifications required for an ultra-wideband (UWB) system, which is then followed by basic radar properties and how they differ between wideband and narrowband. Then the signal models for wideband and narrowband will be defined. Next an introduction to random noise radars (RNR) and the theory behind RNR will be given. The importance of radar ambiguity functions are then discussed where the narrowband, wideband, and AFIT RNR ambiguity functions will be given. Finally the theory and implementation behind 2D digital cross-correlation in the time domain with the AFIT RNR will be discussed.

2.2 Ultra-Wideband Definition

According to the Federal Communications Commission (FCC) an UWB system is defined by [8]:

- *Ultra-wideband (UWB) system.* An intentional radiator that, at any point in time, has a fractional bandwidth equal to or greater than 0.20 or has a UWB bandwidth equal to or greater than 500 MHz, regardless of the fractional bandwidth.
  - *UWB bandwidth.* The UWB bandwidth, B, is the frequency band bounded by the points that are 10 dB below the highest radiated emission, as based on the complete transmission system including the antenna. The upper boundary is designated f_H and the lower boundary is designated f_L.
  - *Center frequency.* The center frequency,f_C, equals $(f_H + f_L)/2$.
  - *Fractional bandwidth.* The fractional bandwidth is $2(f_H - f_L)/(f_H + f_L)$.

These definitions will be used throughout the paper.

2.3 Radar Properties

When a transmitted signal, $s(t)$, reflects off a target (point scatter), the received signal, $s_r(t)$, differs from $s(t)$ based on the target's position, relative motion between the receiver and target, and the scattering characteristics of the target. The distance between the target and radar causes a time delay difference between the signals, while the relative motion introduces a time scale difference.

2.3.1 Time Delay. If the relative velocity between the radar (assuming a monostatic radar system[1]) and target is zero, then the roundtrip time for the transmitted energy to travel from the radar to the target and back is defined as the time delay, τ and expressed as

$$\tau = \frac{2R}{c}, \tag{2.1}$$

where R is the range between the radar and target and c is the speed of light. In this scenario $s_r(t) \propto s(t - \tau)$.

When the relative velocity does not equal zero, the range between the radar and target becomes a function of time, $R(t)$. Subsequently, the time delay is then expressed as a function of time,

$$\tau(t) = \frac{2}{c}R(t), \tag{2.2}$$

and the received signal changes to $s_r(t) \propto s(t - \tau(t))$. When the target reflects the transmitted signal at time t, the range is $R(t)$. Then the reflected energy returns to the radar at time $t - \tau(t)/2$ and the range becomes $R(t - \tau(t)/2)$. Therefore, the time delay is [35]

$$\tau(t) = \frac{2}{c}R\left[t - \frac{\tau(t)}{2}\right]. \tag{2.3}$$

[1]In a monostatic radar system, the transmit and receive antenna(s) are collocated.

Following Weiss [35], expanding $\tau(t)$ into a Taylor series about $t = \tau_o$, where τ_o is the constant $2R_o/c$ and R_o is the range of the target at time zero, gives

$$\tau(t) = \tau(\tau_o) + \tau'(\tau_o)(t - \tau_o) + \tau''(\tau_o)\frac{(t-\tau_o)^2}{2} + \cdots , \tag{2.4}$$

where $'$ denotes differentiation with respect to t. The first term is chosen so $\tau(\tau_o) = \tau_o$. Then let $v(t) = R'(t)$ be the velocity of the target at time t. By differentiating (2.3) with respect to t and evaluating at $t = \tau_o$, the second term of (2.4) becomes

$$\begin{aligned} \tau'(t) &= \frac{2}{c}R'\left[t - \frac{\tau(t)}{2}\right]\left(1 - \frac{\tau'(t)}{2}\right) \\ \tau'(\tau_o) &= \frac{2}{c}v\left[\tau_o - \frac{\tau(\tau_o)}{2}\right]\left(1 - \frac{\tau'(\tau_o)}{2}\right) \\ \tau'(\tau_o) &= \frac{2v(\tau_o/2)}{c + v(\tau_o/2)}. \end{aligned} \tag{2.5}$$

Next let $a(t) = R''(t)$ be the acceleration of the target at time t. Going through the same process yields the third term [35],

$$\tau''(\tau_o) = \frac{2a(\tau_o/2)\left(1 - \dfrac{2v(\tau_o/2)}{c + v(\tau_o/2)}\right)^2}{c + 2v(\tau_o/2)}. \tag{2.6}$$

Therefore, (2.4) becomes

$$\tau(t) = \tau_o + \frac{2v(\tau_o/2)}{c + v(\tau_o/2)} \cdot (t - \tau_o) + \frac{2a(\tau_o/2)\left(1 - \dfrac{2v(\tau_o/2)}{c + v(\tau_o/2)}\right)^2}{c + 2v(\tau_o/2)} \cdot \frac{(t-\tau_o)^2}{2} + \cdots . \tag{2.7}$$

For a target with constant velocity, $v(\tau_o/2) = v$ and $a(t) = 0$, (2.7) simplifies to

$$\tau(t) = \tau_o + \frac{2v}{c + v} \cdot (t - \tau_o). \tag{2.8}$$

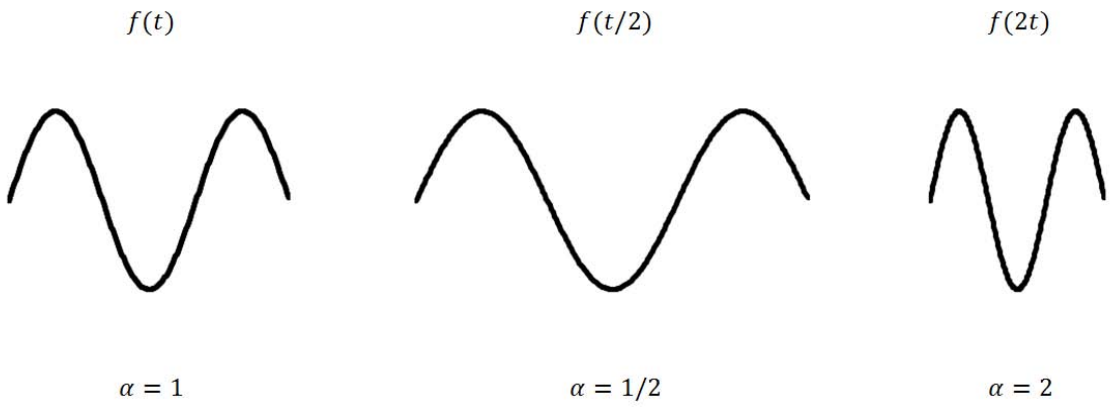

Figure 2.1: Illustration of a time scaled signal.

2.3.2 Time Scale. When a target is in motion with a constant radial velocity[2], v, the reflected transmitted signal is time scaled by α where α is defined as

$$\alpha = \frac{c - v}{c + v} \tag{2.9}$$

The time scale is often approximated with a Doppler shift in the frequency domain. The relation can be seen in the time domain in Figure 2.1 where $\alpha < 1$ produces a negative Doppler shift and $\alpha > 1$ causes a positive Doppler shift. So time scaling the signal by a factor α can be represented as $s_r(t) \approx s(\alpha t)$. When $\alpha = 1$ then the relative velocity is zero following (2.9).

2.4 Signal Models

Using an accurate signal model is key to analyzing the theoretical radar performance. The most common signal model is the narrowband model that is approximated from the wideband model. The two models and their respective limits will be addressed in this section [35].

[2]An ingressing target's velocity is negative while an egressing target possesses positive velocity

2.4.1 Wideband Signal Model. As previously stated, the received signal from a moving target is given as $s_r(t) = s(t - \tau(t))$. Taking the time argument, $t - \tau(t)$, of the received signal and substituting (2.8) gives

$$t - \tau(t) = \frac{c - v}{c + v}(t - \tau_o) = \alpha(t - \tau_o), \tag{2.10}$$

allowing the received signal to be expressed as $s_r(t) \propto s(\alpha(t - \tau_o))$. However, τ_o is the same as (2.1); therefore, the received signal is

$$s_r(t) \propto s(\alpha(t - \tau)). \tag{2.11}$$

Equation (2.11) is known as the wideband signal model. The significant declaration the model presents is the relationship of time scale and time delay. Ultimately, a target's velocity affects both scale and delay.

2.4.2 Narrowband Signal Model. Typically, a narrowband model is used by approximating the time scale, α, with a Doppler shift, f_d. By first rewriting α as

$$\alpha = \frac{c - v}{c + v} = \frac{1 - \frac{v}{c}}{1 + \frac{v}{c}}, \tag{2.12}$$

and then performing the long division and multiplication, α becomes

$$\begin{aligned} \alpha &= \left(1 - \frac{v}{c}\right)\left(1 - \frac{v}{c} + \left(\frac{v}{c}\right)^2 - \cdots\right) \\ &= 1 - \frac{2v}{c} + 2\left(\frac{v}{c}\right)^2 - \cdots . \end{aligned} \tag{2.13}$$

When $|v| \ll c$ (2.13) simplifies to

$$\alpha \approx 1 - \frac{2v}{c}, \ \textit{or}\ (\alpha - 1) \approx \frac{-2v}{c}. \tag{2.14}$$

For a transmit signal with a carrier frequency of f_c, the Doppler shift, f_d, is defined as

$$f_d \equiv \frac{-2v}{c} f_c \approx (\alpha - 1) f_c. \tag{2.15}$$

Thus, when $|v| \ll c$ the time scale is approximated by a Doppler shift and the narrowband received signal model is

$$s_r(t) \approx s(t - \tau) e^{j2\pi f_d (t-\tau)}. \tag{2.16}$$

2.4.3 Limitation of the Doppler Shift Approximation. The approximation given in (2.15) implicitly states that all frequencies in the signal experience the same shift. Consider a signal consisting of three tones at 100, 1000, and 10000 Hz, as depicted in black in Figure 2.2. If an ingressing target causes the scale to be $\alpha = 1.1$, then the received signal changes to tones at frequencies of 110, 1100, and 11000 Hz as depicted in green in Figure 2.2. However, when using (2.15) where $f_c = (10000 - 100)/2 = 4950$ Hz, the Doppler shift becomes $f_d = (1.1 - 1) \cdot 4950 = 495$ Hz and is applied to all tones. This causes the tones to appear at frequencies of 595, 1495, 10495 Hz as depicted in red in Figure 2.2. This signal has a fractional bandwidth (as defined in Section 2.2) of 1.96 and demonstrates the error that results from approximating a scale change with a Doppler shift.

The significant difference between time scaling a signal and frequency shifting a signal is frequency shifting assumes a separation is possible between the carrier frequency, f_c, and all other phase modulation components in the signal [35]. This is a narrowband assumption and is not always true for wideband signals.

Another common narrowband assumption states the targets in the environment are slowly fluctuating for the duration of the signal, T. That is, the targets do not change position relative to the positional resolution of the signal [10], i.e.,

$$vT \ll \frac{c}{2B}, \tag{2.17}$$

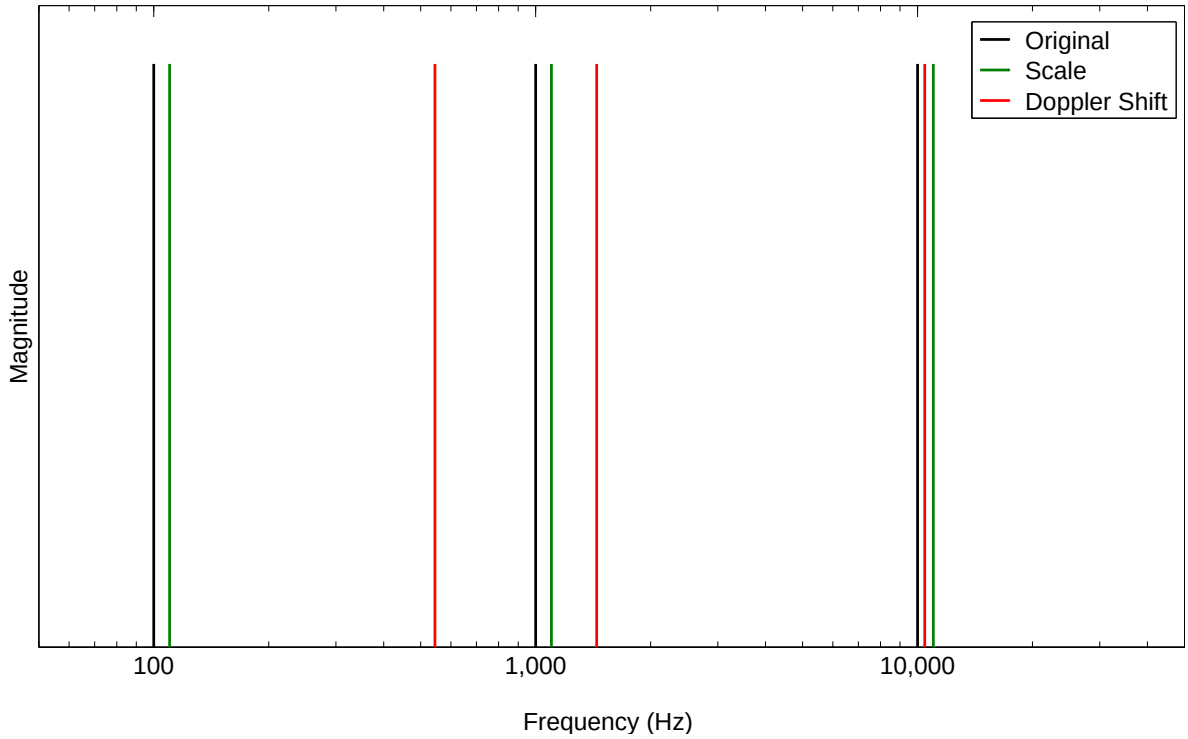

Figure 2.2: Here is an example of a transmit signal comprised of three tones at 100, 1000, and 10000 Hz as represented in black. If a target causes a scale change of $\alpha = 1.1$ then the received signal has tones appearing at 110, 1100, 11000 Hz as represented in green. If the scale is approximated with a Doppler shift, then the tones will be incorrectly placed at 595, 1495, 10495 Hz as represented in red.

where c is the speed of light and B is the bandwidth of the signal. Equation (2.17) is more commonly written as

$$\frac{2v}{c} \ll \frac{1}{TB}, \tag{2.18}$$

where this form is called the narrowband condition and TB refers to the time-bandwidth product of the signal. So it can be seen that the processing duration, T, is limited by the velocity of the target ($T \ll c/(2Bv)$). When the narrowband condition, (2.18), holds true, then the narrowband model, (2.16), is used for narrowband processing. So (2.18) is violated by either fast moving targets (large v) or a large time-bandwidth product, TB.

So the wideband model (2.11) should be used when (2.18) is violated and/or the fractional bandwidth is large (generally greater than 0.1) [35].

Wideband processing has its own limitations, namely a target's acceleration. Just as the narrowband model requires the changes in a target's position to be small relative to the range resolution of the radar, the wideband model requires the changes in in a target's velocity (scale) be small relative to the velocity (scale) resolution of the radar over the measurement window, T. Young gives the wideband condition as [36]

$$T < \sqrt{\frac{c}{2aB}}. \tag{2.19}$$

This condition is derived from the requirement that $\Delta v/a < T$ where Δv represents the velocity interval of interest. Start by computing the differential of (2.9).

$$\begin{aligned} \Delta\alpha &= \frac{(c+v)(-\Delta v) - (c-v)(\Delta v)}{(c+v)^2}, \\ &= \frac{-2c\Delta v}{(c+v)^2}. \end{aligned} \tag{2.20}$$

Next, solve (2.20) for Δv when $\Delta\alpha = 1/TB$.

$$\Delta v = \frac{(c+v)^2}{2cTB}. \tag{2.21}$$

Then substituting (2.21) into the initial requirement, $\Delta v/a < T$, gives the wideband condition

$$\begin{aligned} T^2 &< \frac{(c+v)^2}{2cBa}, \\ T &< \sqrt{\frac{c}{2aB}}; \quad \text{where } v \ll c. \end{aligned}$$

If (2.19) is violated then the received signal cannot be accurately represented by a wideband signal model.

2.5 Random Noise Radars

The theory behind the random noise radar (RNR) first came about in the 1950s as a way to produce high range-Doppler resolution. An RNR system transmits a random, low-power noise waveform. Ideally, this waveform produces the desired thumbtack ambiguity function needed for high resolution in both range and Doppler.

The earliest reported investigations in noise technology were in 1959 and 1962 from Horton [18] and Craig [12]. A short period later, in 1963 and 1967, Grant et al. [16], Cooper et al. [11], and McGillem [25] formulated a theoretical analysis and built prototypes. Further experiments were conducted to show possible target detection in very poor SNR.

Research died down due to the enormous amount of data processing required by UWB systems. It was not until the 1970s when technology advancements allowed further research to continue [30].

2.5.1 Pros and Cons of Random Noise Radars. The concept of the random noise radar (RNR) was first considered in the 1950s as a way to eliminate all the range-Doppler ambiguities (thumbtack ambiguity function) [30]. The thumbtack response is due to the aperiodicity or non-repeating nature of the transmitted waveform. Another advantage comes from the low transmitted peak power of an RNR. Considering both of these strengths at once, a random, low-power noise waveform, leads to the third and fourth advantages of low probability of intercept (LPI) and low probability of identification (LPID). If the RNR is UWB, then the electronic counter-countermeasures (ECCM)[3] improve [17]. As an example, the effectiveness of jamming decreases as the bandwidth of the system increases. Large bandwidths also improve the range resolution (ΔR), because

$$\Delta R = \frac{c}{2B}. \tag{2.22}$$

[3]ECCM - electronic warfare undertaken to insure effective friendly use of the electromagnetic spectrum in spite of the enemy's use of electronic warfare [20]

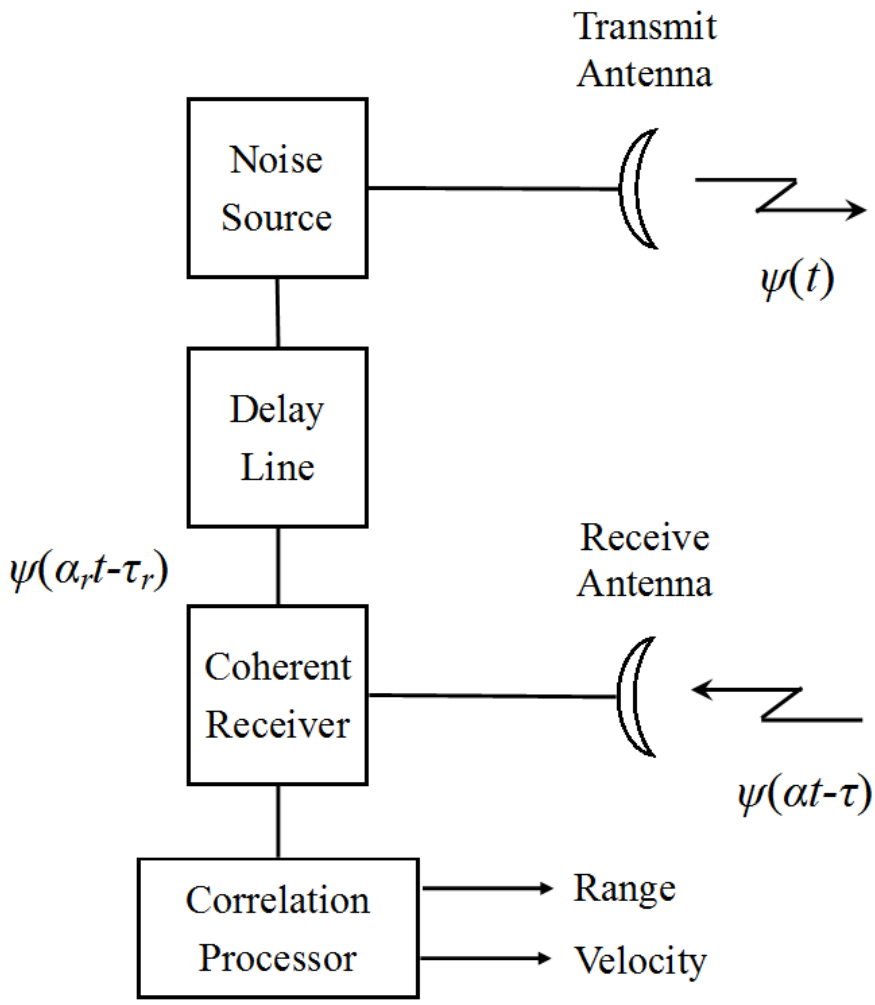

Figure 2.3: Main components of a noise radar using a delay line [30]

Since a target's range and velocity are generally unknown, it is necessary to apply a set of filters matched to all possible range-velocity pairs [9] in order to get the thumbtack ambiguity function. This requires very high computational power and is the biggest drawback to RNR. Considering an UWB RNR, the hardware costs increase because it is more difficult to build devices that cover a large bandwidth with the same efficiency as narrowband devices [30].

2.5.2 Range Estimation Theory. Fig. 2.3 shows the main components of an RNR. A continuous wave (CW) noise signal, $\psi(t)$, is transmitted, reflected by the

target, and returns to the receive antenna for coherent detection after a delay of τ. A copy of $\psi(t)$, delayed by τ_r, is used as the reference signal and cross-correlated with $\psi(\alpha t - \tau)$. When $\tau_r = \tau$ a strong correlation peak occurs and the range can be calculated as

$$R = \frac{c}{2}\tau = \frac{c}{2}\tau_r. \tag{2.23}$$

2.5.3 Doppler Processing Theory. The theory covered here follows Axelsson's [4] derivation for Doppler processing on RNR systems. Considering a point target detection, the transmitted noise signal can be modeled as [4]

$$s(t) = X(t)\cos(\omega_o t) - Y(t)\sin(\omega_o t), \tag{2.24}$$

where ω_o is the center frequency and $X(t)$ and $Y(t)$ are statistically independent, stationary, stochastic, Gaussian processes with zero means and autocorrelation functions $R_X(\gamma) = R_Y(\gamma) = R(\gamma)$ where γ is an arbitrary time difference, $t_2 - t_1$, [4]. In terms of complex signals, $s(t) = \mathrm{Re}[\psi(t)]$; therefore, $\psi(t)$ is

$$\psi(t) = [X(t) + jY(t)]e^{j\omega_o t}. \tag{2.25}$$

For moving targets, the received signal is expanded or compressed in time as a result of the relative radial velocity between the point target and the radar. Recalling, for a point target positioned at R and a relative velocity v, the received signal is $\psi(\alpha(t-\tau))$. However, Axelsson makes a narrowband approximation by modeling the received signal as $\psi(\alpha t - \tau)$. The approximation effectively causes the scale and time delay to become independent and will be used for the remainder of the section.

Cross-correlating $\psi(\alpha t - \tau)$ with the reference signal $\psi(\alpha_r t - \tau_r)$, which is delayed by τ_r, time compressed by $\alpha_r = 1 - 2v_r/c$, and τ_r, α_r, and v_r are reference parameters, becomes proportional to [1]

$$C(\tau, \alpha;\ \tau_r, \alpha_r) = \int_0^T w(t)\psi(\alpha t - \tau)\psi^*(\alpha_r t - \tau_r)dt, \tag{2.26}$$

where $w(t)$ is a window function chosen to improve the Doppler sidelobe suppression and T is the length of the cross-correlation.

Inserting (2.25) into (2.26) yields

$$C(\tau,\alpha;\tau_r,\alpha_r) = \int_0^T w(t)\Big[X(\alpha t-\tau)+jY(\alpha t-\tau)\Big] \cdot\Big[X(\alpha_r t-\tau_r)-jY(\alpha_r t-\tau_r)\Big] \cdot e^{[-j\omega_c(\tau-\tau_r)+j(\alpha-\alpha_r)\omega_c t]}dt. \tag{2.27}$$

Letting $\Delta\alpha$ and $\Delta\tau$ represent the error in estimating time scale and time delay respectively, $\Delta\alpha = \alpha - \alpha_r$ and $\Delta\tau = \tau - \tau_r$, and recalling $R_X(\gamma) = R_Y(\gamma)$, the average of (2.27) is

$$R_c(\Delta\tau,\Delta\alpha) = 2e^{-j\omega_c\Delta\tau}\int_0^T w(t)\Big[R_X(\Delta\alpha t-\Delta\tau)-jR_{XY}(\Delta\alpha t-\Delta\tau)\Big] \cdot e^{j\Delta\alpha\omega_c t}dt. \tag{2.28}$$

Recall, $X(t)$ and $Y(t)$ are statistically independent because of the properties of an RNR waveform, which in turn, causes the cross-correlation, R_{XY}, to become zero. Therefore, (2.28) reduces to

$$R_c(\Delta\tau,\Delta\alpha) = 2e^{-j\omega_c\Delta\tau}\int_0^T w(t)R_X(\Delta\alpha t-\Delta\tau)e^{j\Delta\alpha\omega_c t}dt. \tag{2.29}$$

The reference signal parameters, α_r and τ_r, are varied until the maximum correlation (with α and τ respectively) is found. These estimated maximum correlation signal parameters, represented by α_{r0} and T_{r0}, are used to estimate the velocity and range in (2.23) and (2.9) [30].

For narrowband random noise processes, the phase term in (2.28) and (2.29) produces the most decorrelation. Therefore, $\Delta\alpha\omega_c t$ needs to be kept low over the integration time to prevent a drop in the correlation peak [30]. Assuming ω_c cannot

be changed and the velocity of the target is completely unknown, the integration time is forced to be very small.

If using the following relationship,

$$\Delta\alpha = \frac{-2\Delta v}{c} = \frac{\Delta f_d}{f_o},$$

$$\text{where} \qquad \Delta v = v - v_r$$
$$\Delta f_d = \frac{-2\Delta v f_o}{c},$$

then (2.29) becomes an extension of the Woodward ambiguity function [6], where

$$\chi(\Delta R, \Delta f_d) = \Big| R_c(\Delta\tau, \Delta f_d,) \Big|. \tag{2.30}$$

As previously stated in (2.22), the range resolution depends on the bandwidth B. There is a limiting relationship between the range resolution (ΔR), relative velocity of the target (v), and the correlation time (T). The time taken for the target to pass through a range resolution cell is

$$T_p = \frac{\Delta R}{v}. \tag{2.31}$$

To keep the ambiguity function from degrading, the correlation time needs to be smaller than T_p. Combining this fact with (2.22) and (2.31), the limiting factor molds into the form

$$\frac{\Delta R}{v} = \frac{c}{2Bv} > T.$$

From here it is possible to let the number of statistically independent samples be represented by $N = 2BT$, which then allows an upper limit to be derived

$$N = 2BT < \frac{c}{v}. \tag{2.32}$$

For example, the average human walks at approximately 3 mph, which equates to $N < 2.237 \times 10^8$ samples. For the hardware used in this paper where $B \approx 370\ MHz$ [29], the limit on the correlation time becomes $T < 0.30\ s$. This makes sense because T and $\Delta\alpha$ are inversely proportional.

2.5.4 Doppler Processing in Practice. Doppler shift in UWB RNR is a little bit of a misnomer. Recall that Doppler shift is directly proportional to the carrier frequency. In a narrowband RNR, the mean frequency can be thought of as the carrier frequency. For UWB there is still a mean frequency, but the variance is much greater. This causes the variance of the average Doppler shift to increase greatly making Doppler estimation worse. The results given in [23] and [26] show Doppler estimation worsening with increased bandwidth.

2.6 Radar Ambiguity Function

The radar ambiguity function is normally used by radar designers as a means of comparing different waveforms. The function can provide insight about how different radar waveforms may be suitable for the various radar applications. It is also used to determine the range (time delay) and Doppler (velocity) accuracies[4] and resolutions[5] for a specific radar waveform.

2.6.1 Narrowband Ambiguity Function. The radar ambiguity function represents the output of the matched filter. The ambiguity function evaluated at $(\tau, f_d) = (0, 0)$ is equal to the matched filter output that is matched perfectly to the signal reflected from the target of interest. In other words, when the filter is perfectly matched returns from the nominal target are located at the origin of the ambiguity function. Thus, the ambiguity function at nonzero τ and f_d represents returns for some range

[4]Levanon states measurement accuracy is proportional to the shape of the matched filter response close to the peak (the second derivative of the response) [22].

[5]Resolution is the minimum distance needed to distinguish between two targets and is proportional to the ambiguity function main lobe width (usually measured at the $-3\ dB$ point) [22].

and Doppler difference from the nominal target [24]. For a signal $u(t)$, the narrowband ambiguity function, $\chi(\tau, f_d)$, is defined as [22]

$$\left|\chi(\tau, f_d)\right| = \left| \int_{-\infty}^{\infty} u(t)u^*(t-\tau)e^{j2\pi f_d t}dt \right|. \tag{2.33}$$

Since, the narrowband ambiguity function is defined with the narrowband signal model, (2.33) becomes a 2D function of time delay, τ, and Doppler shift, f_d.

2.6.2 Wideband Ambiguity Function. The wideband ambiguity function still represents the output of the matched filter. The difference is the wideband signal model is incorporated into (2.33). Therefore, for a signal, $u(t)$, the wideband ambiguity function, $\chi(\tau, \alpha)$, is defined as [21]

$$\left|\chi(\tau, \alpha)\right| = \left| \int_{-\infty}^{\infty} u(t)u^*(\alpha(t-\tau))dt \right|, \tag{2.34}$$

and is now a 2D function of time delay, τ, and time scale, α.

2.6.3 AFIT RNR Wideband Ambiguity Function. The cross-correlation of the received signal with a reference signal given in equation (2.26) represents the output of the matched filter and can be used to define the generalized ambiguity function. With the substitution of $\beta = \alpha/\alpha_r$ and $\Delta\tau = \tau - \beta\tau_r$, Axelsson [7] defines the generalized ambiguity function of an UWB random waveform as

$$|\chi(\Delta\tau, \beta)| = \left| \int \psi(\beta t - \Delta\tau)\psi^*(t)dt \right|. \tag{2.35}$$

Assuming $\psi(t)$ is ergodic then (2.35) becomes a time average over the measurement time T, such that,

$$\begin{aligned}|\langle\chi(\Delta\tau,\beta,t)\rangle| &= \left|\text{Real}\left[\int_t^{t+T} E\left[\psi(\beta\zeta-\Delta\tau)\psi^*(\zeta)\right]\times w(t-\zeta)d\zeta\right]\right| \\ &= \left|\text{Real}\left[\int_t^{t+T} E\left[u(\beta\zeta-\Delta\tau)u^*(\zeta)\right]\times e^{j2\pi f_c(\beta-1)\zeta} w(t-\zeta)d\zeta\right]\right| \\ &= \left|\int_t^{t+T} R_u\left[(\beta-1)\zeta-\Delta\tau\right]\times\cos(j2\pi f_c(\beta-1)\zeta)w(t-\zeta)d\zeta\right|, \quad (2.36)\end{aligned}$$

where $E[\cdot]$ is the expected value operator and $w(\cdot)$ is the chosen window.

Dawood and Narayanan [15] give the analytical solution of $R_u(\cdot)$ from (2.36) as

$$R_u\left[(\beta-1)\zeta-\Delta\tau\right] = \frac{\sin\left[\pi B((\beta-1)\zeta-\Delta\tau)\right]}{\pi B((\beta-1)\zeta-\Delta\tau)}. \quad (2.37)$$

Therefore, the ambiguity function for the AFIT UWB RNR depicted in Figure 2.4 is

$$|\langle\chi(\Delta\tau,\beta,t)\rangle| = \left|\int_t^{t+T} \text{sinc}\left[\pi B((\beta-1)\zeta-\Delta\tau)\right]\times\cos(j2\pi f_c(\beta-1)\zeta)w(t-\zeta)d\zeta\right|. \quad (2.38)$$

Figures 2.5–2.8 represents the ambiguity function over an array of reference velocities and ranges where a perfectly matched filter corresponds to $|\chi(0,0,T)|$.

Since it is well known the signal bandwidth, B, controls range resolution (recall (2.22)), the signal parameters that control velocity resolution are discussed. Through varying all possible signal parameters in (2.38) and plotting only $|\chi(0,\beta,T)|$, it is hypothesized that the signal's maximum frequency, f_H, and measurement time, T, mold the velocity resolution. Figure 2.9 illustrates the benefits of increasing either f_H or T.

2.7 2D Digital Cross-Correlation and RNR

Dawood and Narayanan [15] develop a generalized wideband ambiguity function for a coherent RNR. In the development of the ambiguity function, they note that the

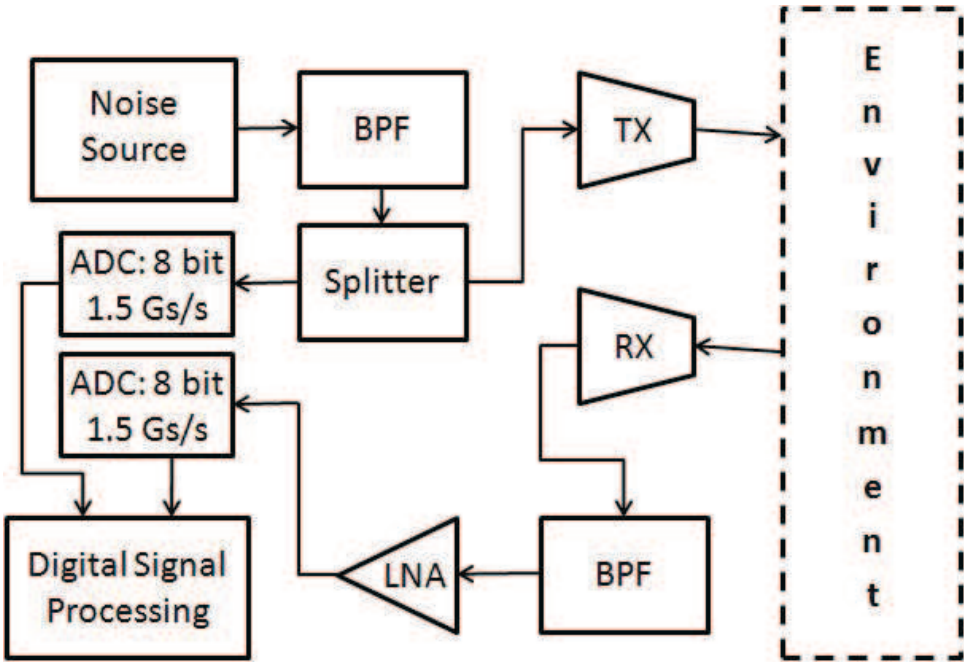

Figure 2.4: Block diagram of the AFIT RNR, which is based on Narayanan's design [28]

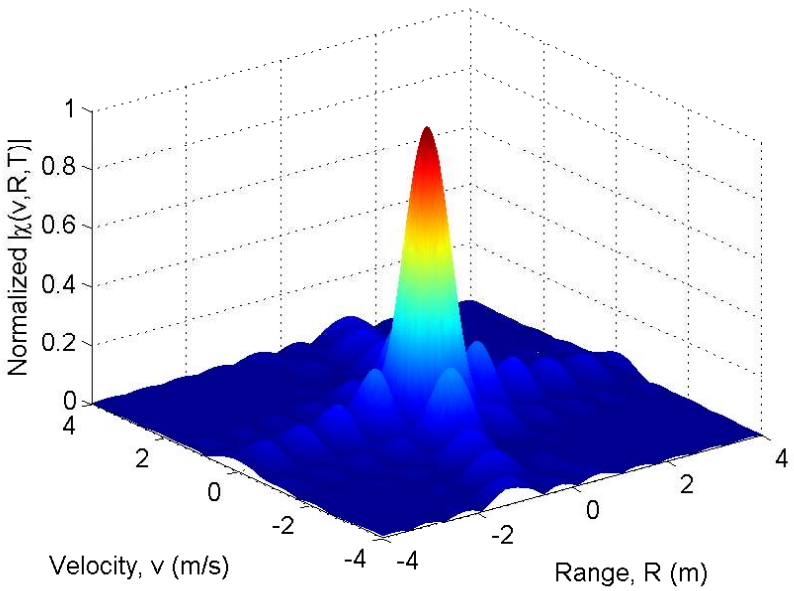

Figure 2.5: The ambiguity plot depicts the range and velocity resolutions for the AFIT RNR design parameters of $B = 400$ MHz, $f_c = 550$ MHz, and for a chosen measurement time of $T = 160$ ms.

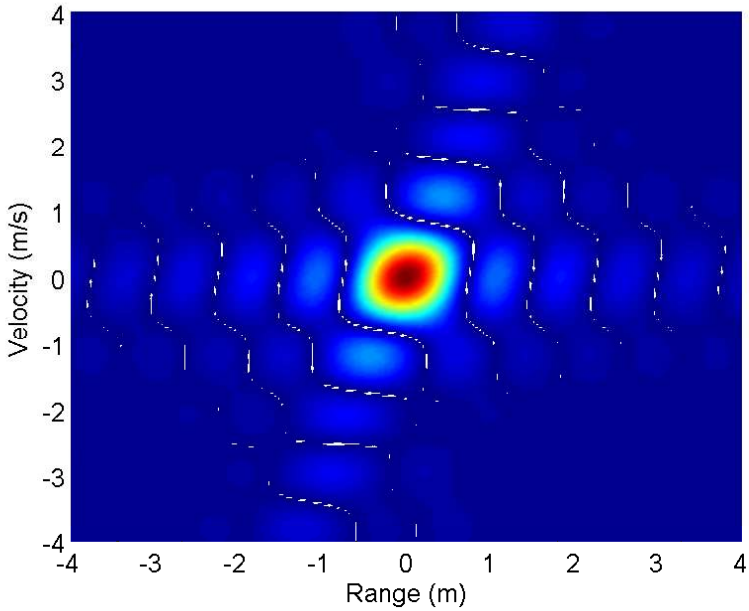

Figure 2.6: The top view of Figure 2.5. From this viewpoint it can be easily be seen that range and velocity are not independent.

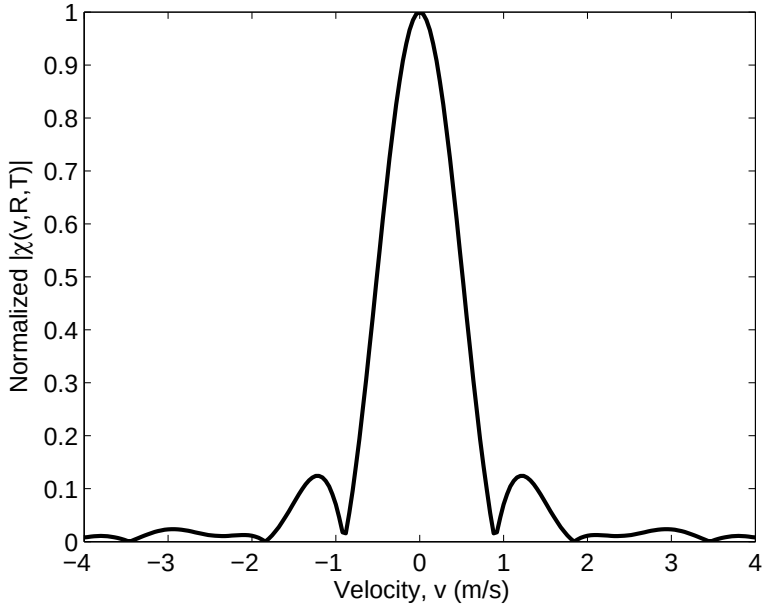

Figure 2.7: This cut from Figure 2.5 depicts the theoretical velocity resolution/accuracy of the AFIT RNR waveform when the radar is perfectly matched in range and $T = 160$ ms, $|\chi(0, \beta, T)|$.

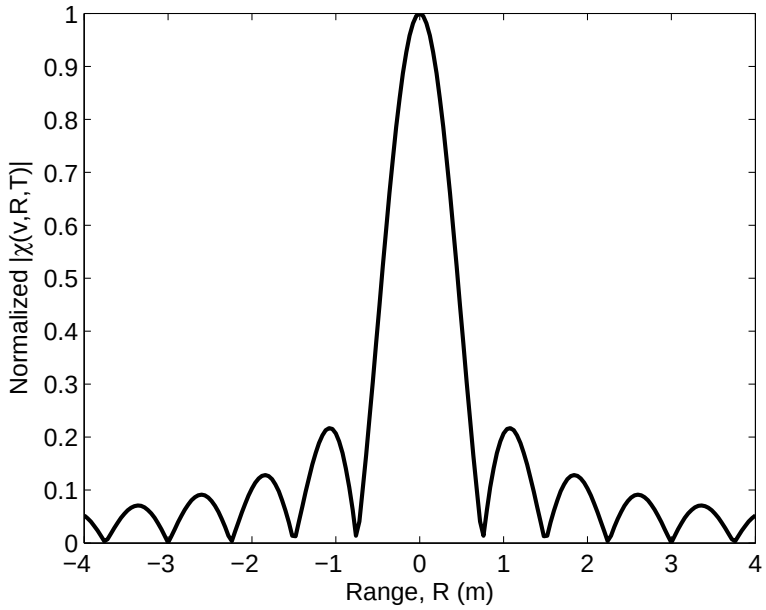

Figure 2.8: This cut from Figure 2.5 depicts the theoretical range resolution/accuracy of the AFIT RNR waveform when the radar is perfectly matched in velocity and $T = 160$ ms, $|\chi(\Delta\tau, 0, T)|$.

correlator must be matched to the velocity and time delay of the target due to the Doppler-spread parameter of UWB waveforms. Creating a correlation filter matched to the time delay and velocity of the target has been discussed by Pace [30, Sec 7.3]; however, the author is unaware of any attempts to implement this approach in the time domain utilizing a fully digital correlator. The likely reason for the reluctance to implement the two-dimensional filter is the computational requirements. The number of variables to be considered in the filter design and the range of those variables must be weighed carefully against the available computation resources, including time.

When implementing the digital correlator in the time domain, each discrete sample of the reference signal, s_{ref}, must be interpolated based on the time shift Δt that each sample goes through due to the reference velocity v_r. Recall $\alpha_r = (c - v_r)/(c + v_r)$. After every sample shifts in time, the reference signal's measurement time changes by $T_r = T/\alpha_r$. Therefore, the total time difference, ΔT, between the reference and transmitted signals is $\Delta T = T_r - T$. Assuming the target's radial

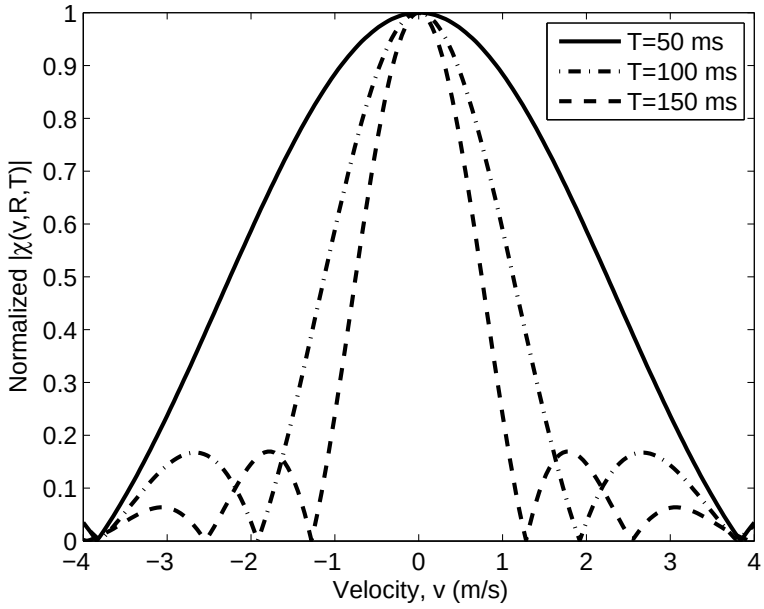

(a)

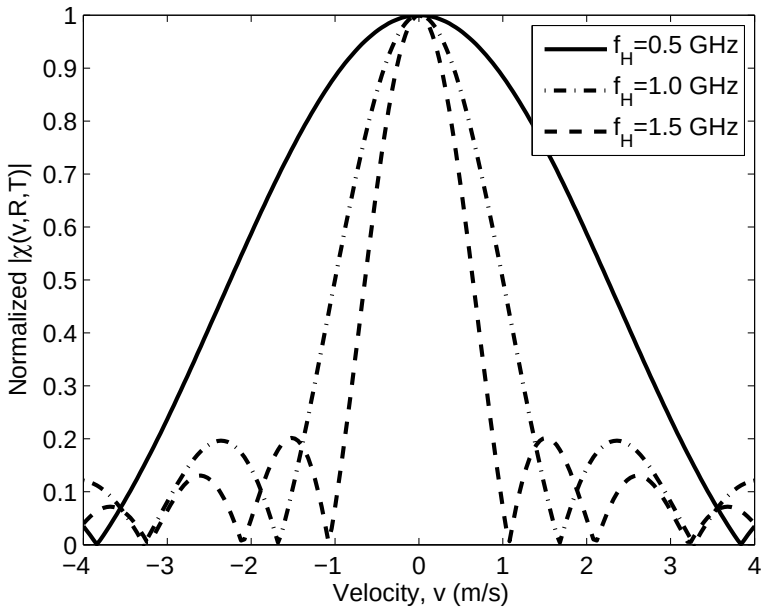

(b)

Figure 2.9: The theoretical velocity resolution/accuracy of an RNR waveform when varying either T or f_H while the radar is perfectly matched in range, $|\chi(0, \beta, T)|$. The maximum frequency, f_H, and the measurement time, T, are the parameters that control the velocity resolution. In (a) $f_H = 500$ MHz is kept constant while T is varied, and in (b) $T = 50$ ms is kept constant while f_H is varied.

velocity is constant over T, the relative time shift each sample experiences can be derived as

$$\begin{aligned}\Delta t &= \frac{\Delta T}{f_s \cdot T} = \frac{T_r - T}{f_s \cdot T} = \frac{\frac{T}{\alpha} - T}{f_s \cdot T} \\ &= \frac{T(\frac{1}{\alpha} - 1)}{f_s \cdot T} = \frac{\frac{c+v}{c-v} - 1}{f_s} = \frac{c+v-c+v}{(c-v)f_s} \\ &= \frac{2v}{(c-v)f_s}, \end{aligned} \tag{2.39}$$

where f_s represents the sampling frequency and a negative velocity corresponds to a radially ingressing target. Figure 2.10 illustrates how if every sample experiences a relative time shift of Δt, then the overall time shift each sample gets interpolated to is

$$s_{ref}[k] = s[k - (k-1)\Delta t], \tag{2.40}$$

where $k \in 1 : L$ and $L = \lceil f_s \cdot T \rceil$.

The major difficulty in estimating velocity through digital correlation comes from the number of samples in the measurement vector, L. The computational requirements grow with L. As Figure 2.9 illustrated the dependent parameters, these parameters in turn control L since $f_s = 2f_H$ and $L = \lceil f_s \cdot T \rceil$. Table 2.1 gives the lengths that are required to achieve the velocity resolutions depicted in Figure 2.9.

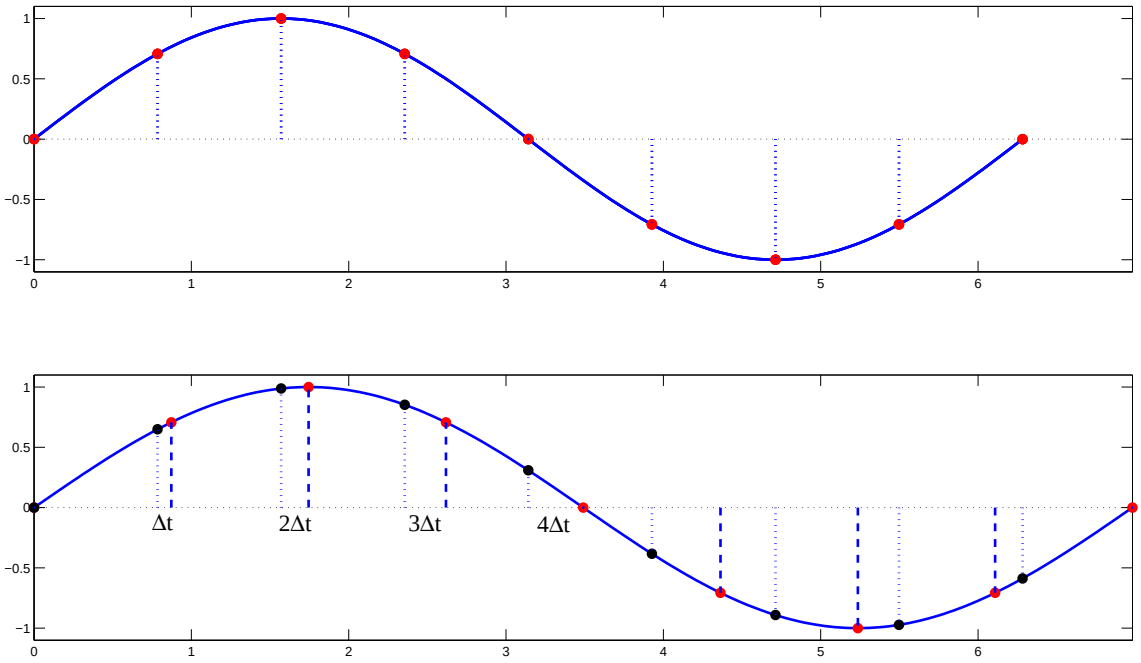

Figure 2.10: In order to simulate reference signals, interpolation must be used so the sampling frequency f_s does not change. The top plot can be viewed as a transmit signal where the small dashed lines correspond to the sampled signal at a rate of f_s. The bottom plot would be a received/reference signal where the original samples, represented by large dashed lines, have shifted in time. In order to keep the same f_s as in the hardware, each sample is interpolated back to the original time locations represented again by the small dashed lines.

Table 2.1: Length of Signals in Figure 2.9

f_H (GHz)	T (ms)	f_s (GHz)	L (million)
0.5	50	1.0	50
0.5	100	1.0	100
0.5	150	1.0	150
0.5	50	1.0	50
1.0	50	2.0	100
1.5	50	3.0	150

III. Test and Methodology

3.1 Overview

This chapter begins by characterizing the transmit signal based on the AFIT ultra-wideband (UWB) random noise radar (RNR) hardware. Then the following sections cover the simulation and experimental procedures.

3.2 AFIT RNR Transmit Signal

The key signal generation components in the AFIT UWB RNR system are pictured in Figure 3.1. The radar was initially designed for a bandwidth of 400 MHz with a maximum frequency of 800 MHz [31]. However, the bandpass filter (BPF), which is a low pass filter (LPF) and high pass filter (HPF) in series, as shown in Figure 3.1, limits the bandwidth to approximately 470 MHz with a maximum frequency of roughly 795 MHz as seen in Figure 3.2. The passband for the LPF is DC – 720 MHz, while the passband for the HPF is 395 – 3200 MHz. The AFIT UWB RNR bandwidth of 410 MHz follows the bandwidth definition given in Section 2.2. The half-power (3 dB) bandwidth, B_3, is also shown in Figure 3.2 and approximately equals 270 MHz with a maximum frequency of roughly 630 MHz. These are the parameters of the reference signal, $s_{ref}(t)$, passed to the computer for digital signal processing (DSP).

Printed log periodic dipole array (LPDA) antennas, pictured in Figure 3.3, are used as the transmit and receive antennas for the AFIT UWB RNR. The antennas are Ramsey Electronics® model LPY-41and were initially chosen by Schmitt [31] because the antennas are inexpensive, readily available, and designed for 400 – 1000 MHz. So the antenna further limits the signal's bandwidth and also ends up spectrally coloring the signal. Nelms [29] characterized the half-power bandwidth from the receive antenna as roughly 185 MHz with a maximum frequency of approximately 520 MHz as illustrated in Figure 3.4 [29]. Therefore, the simulations and experiments planned/performed assumed the receive signal, $s_r(t)$, parameters were $B_3 = 185$ MHz and $f_H = 520$ MHz. However, after the experiments in Chapter IV were accomplished, a frequency response for the antenna was obtained from Ramsey Electronics and

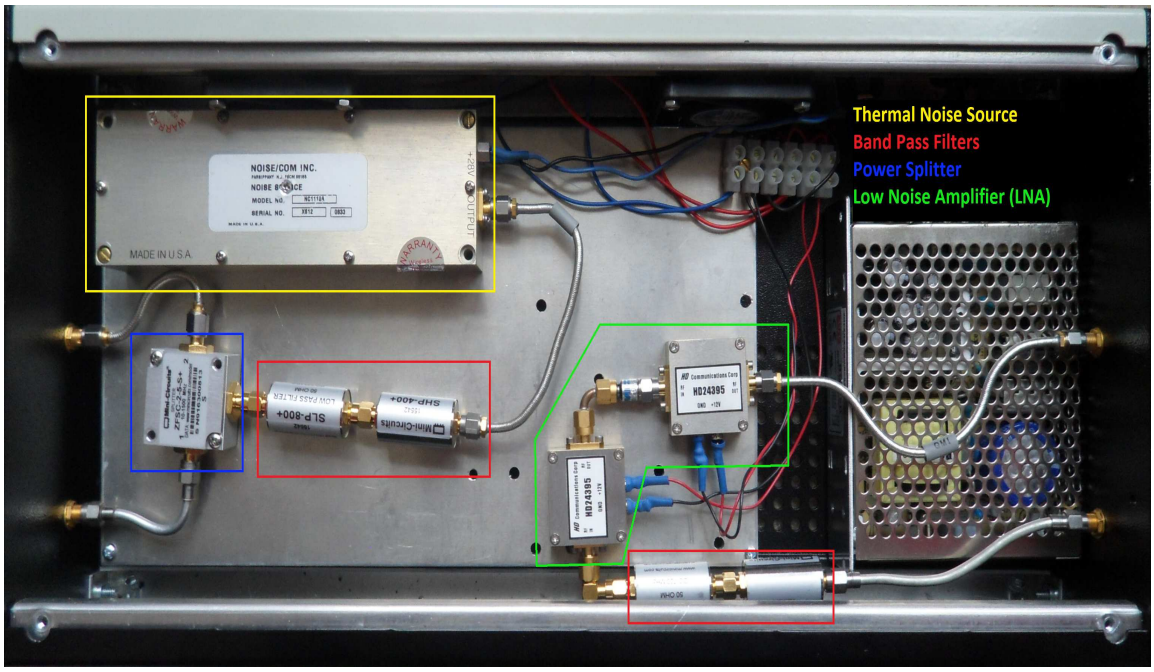

Figure 3.1: Key signal generation components for the AFIT RNR.

proved the received spectral characteristic assumption ($B_3 = 185$ MHz and $f_H = 520$ MHz) to be invalid. Figure 3.5 is an overlay of the antenna frequency response with the power spectral density (PSD) shown in Figure 3.2. It is now possible to grasp the extent to which the transmit and receive signals are colored due to the non-uniform gain of the antennas over the bandwidth. The ideal antenna frequency response would maintain a uniform gain over the bandwidth of the transmit signal. However, the expected receive signal from the receive antenna should have a PSD that resembles the combination of the signal PSD with the antenna frequency.

Figures 3.6 and 3.7 illustrate the theoretical difference in the range and velocity ambiguities between an ideal received signal and the assumed received signal with spectral characteristics shown in Figure 3.4. The ideal received signal would have the same signal parameters as s_{ref}, while the assumed received signal has s_r parameters. The reason the ambiguities grow are due to the difference in the parameters. Recall-

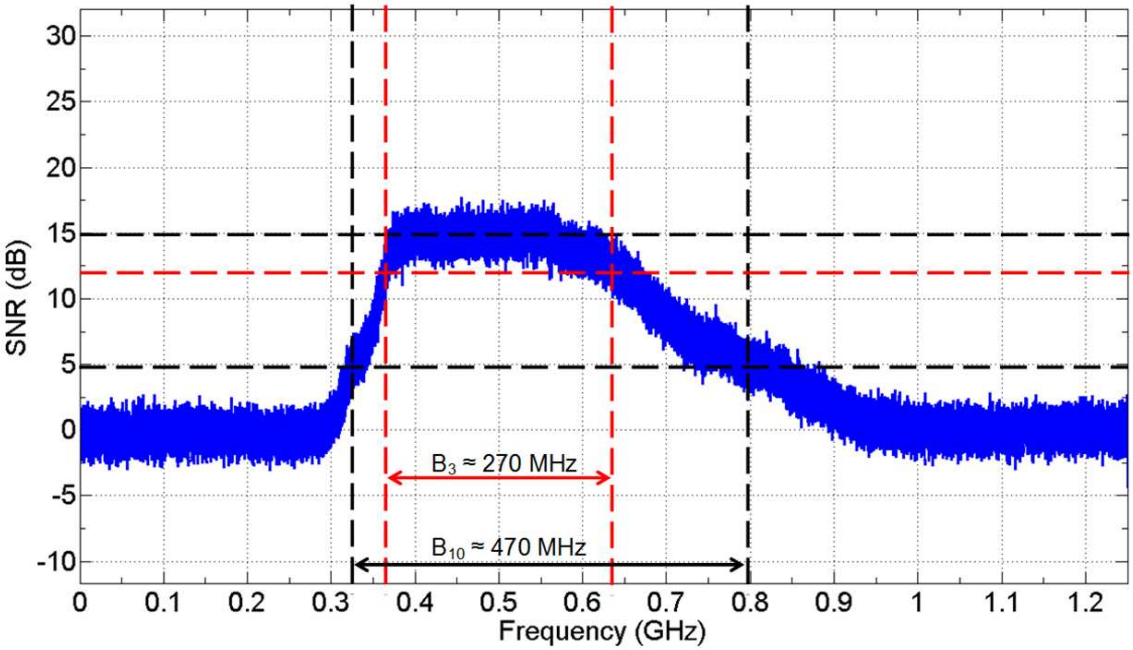

Figure 3.2: Power spectral density of input to transmit antenna.

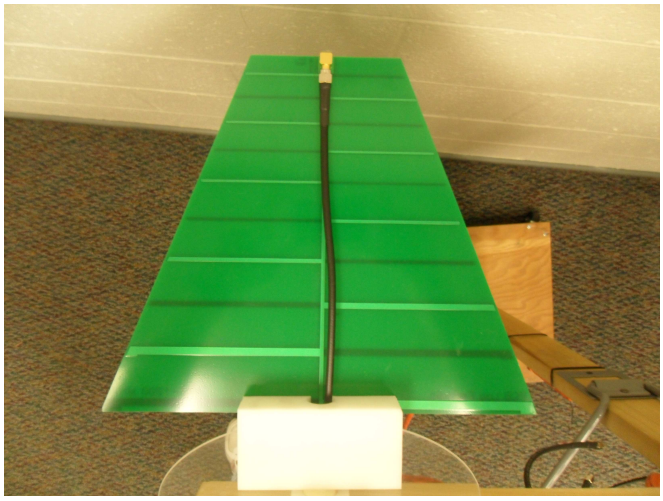

Figure 3.3: Two printed log periodic dipole array (LPDA) antenna made by Ramsey Electronics model LPY-41 are used as the transmit and receive antennas.

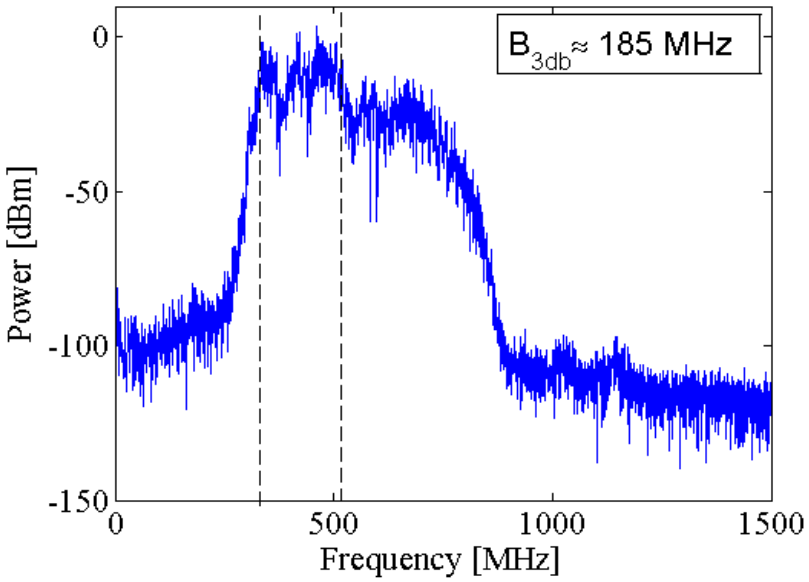

Figure 3.4: The half power (3 dB) bandwidth, B_3, of the AFIT RNR [29].

ing (2.22), range resolution improves as bandwidth increases. Therefore, s_{ref} range ambiguities are fewer when compared to s_r because 270 MHz $>$ 185 MHz.

Velocity resolution; though, is directly proportional to the measurement window, T, and the upper boundary bandwidth frequency, f_H. Therefore, when keeping the measurement windows equal, s_{ref} velocity ambiguities are fewer when compared to s_r since 630 MHz $>$ 520 MHz.

3.3 Simulation Procedure

The simulations require a high performance computer. In particular, the simulations require large amounts of random access memory (RAM) to handle the digitized signals of length L, where $L = \lceil f_s \cdot T \rceil$. Typical signal lengths tend to be 200 million samples. Therefore, a quad core Dell Precision 690 with a memory upgrade to 32 GB of RAM executes the simulations. The purpose of the simulations were to verify velocity estimation in the time domain through the use of digital correlation after (2.40) was applied to the reference signal. Therefore, it was assumed the radar

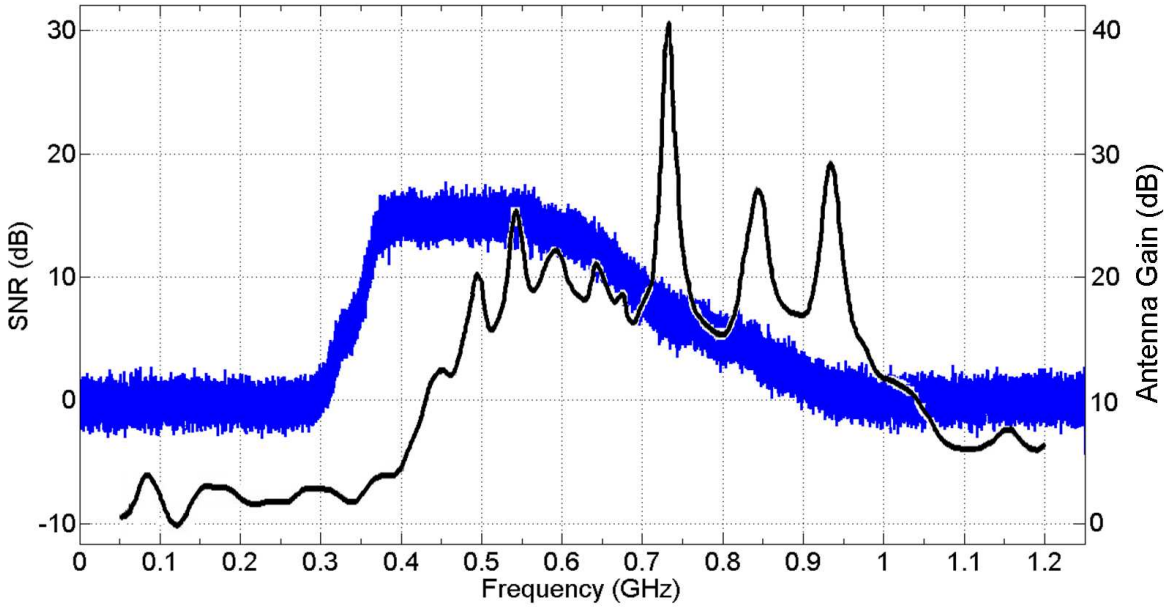

Figure 3.5: The frequency response for the Ramsey Electronics LPY-41 antenna, shown as the solid black line, is overlaid on the PSD plot for the the input to the LPY-41 antenna, shown in blue.

was perfectly matched in time delay and the antennas were ideal (uniform gain across signal bandwidth). With the assumption of the antennas being ideal, the received signal parameters were the same as the reference signal parameters. The ideal antenna assumption allowed simpler code and still tested whether velocity estimation was possible through interpolation of the reference signal in the time domain.

Following the block diagram in Figure 2.4 and recalling the antennas are assumed to be ideal, MATLAB® was used to conduct simulations. The process followed these steps:

1. Create real Gaussian distributed noise vector in double format of length $\lceil f_s \cdot T \rceil$
2. Bandlimit the noise vector to create the transmitted RNR signal vector
3. Create received signal vector from the transmitted RNR signal vector
   (a) Interpolate the simulated received signal to the target's velocity v.

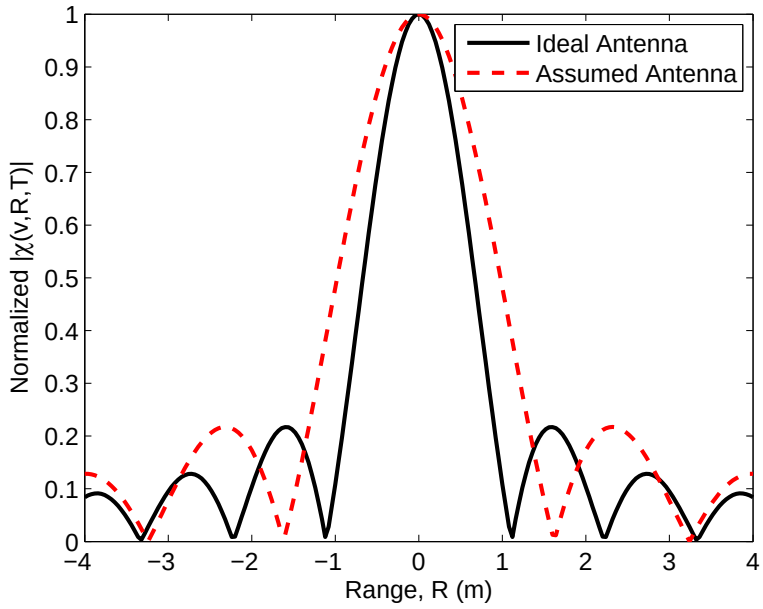

(a)

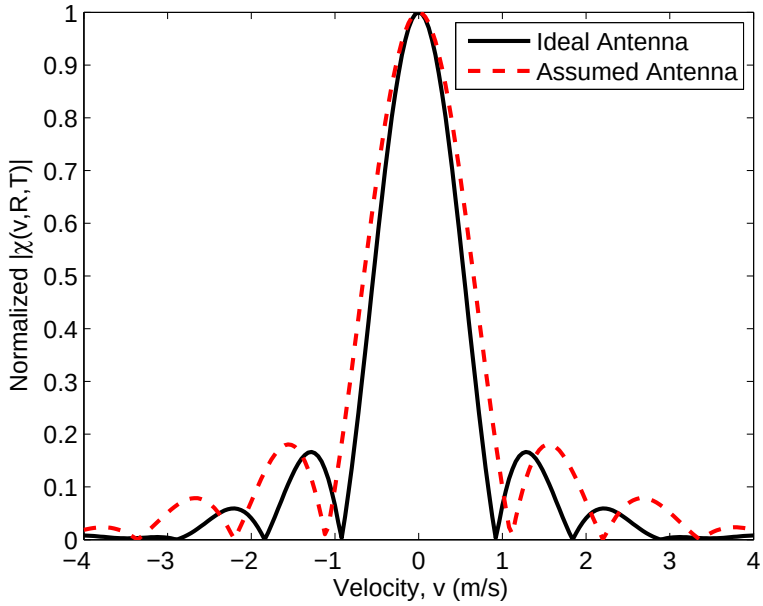

(b)

Figure 3.6: The solid represents an ideal antenna emitting the reference signal, $B_3 = 270$ MHz and $f_H = 630$ MHz. The red represents the assumed antenna emitting the reference signal, $B_3 = 185$ MHz and $f_H = 520$ MHz. These plots represent the principal axes of 2D ambiguity function and are for a measurement window of $T = 160$ ms. (a) The range ambiguities are compared. (b) The velocity ambiguities are compared.

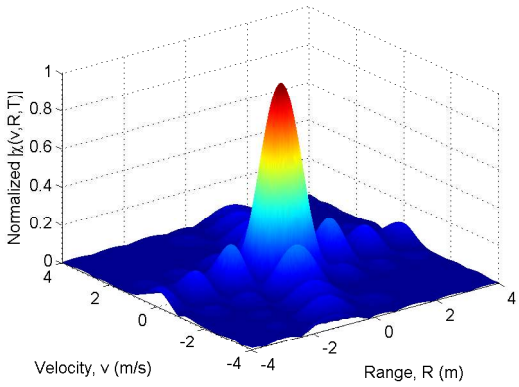

(a) Ideal Antenna

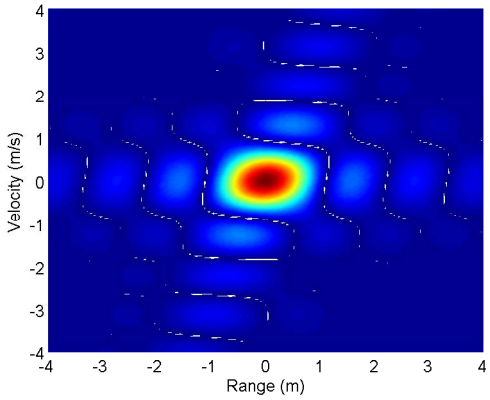

(b) Ideal Antenna

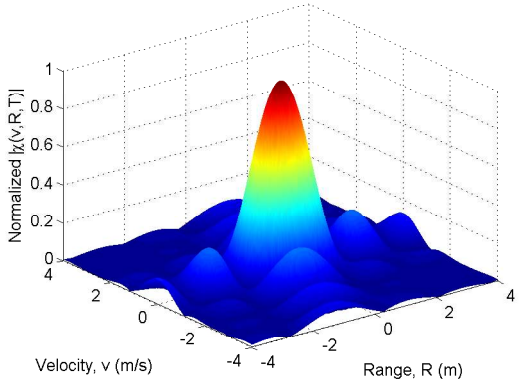

(c) Assumed Antenna

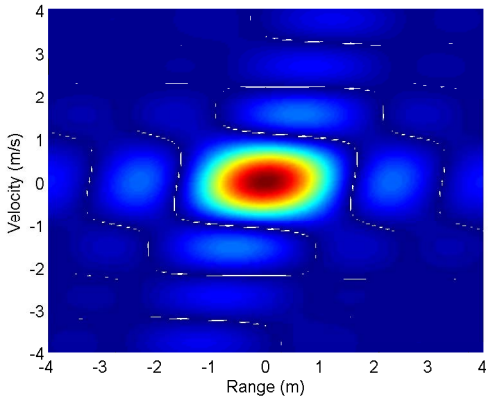

(d) Assumed Antenna

Figure 3.7: The 3D ambiguity plots for ideal and assumed signal parameters are depicted where $B_3 = 270$ MHz and $f_H = 630$ MHz are the ideal parameters and $B_3 = 185$ MHz and $f_H = 520$ MHz are the assumed parameters.

(b) Convert to 8-bit format to simulate the the quantization output of the AFIT RNR ADC

4. Create reference signals from the transmitted RNR signal vector

   (a) Convert the transmitted RNR signal vector to 8-bit

   (b) Interpolate one, 8-bit RNR reference signal vector for every reference velocity v_r

5. Compute the inner product between the simulated received signal and bank of reference velocity signals

6. Perform detection.

   Refer to Appendix B for the MATLAB code, "Simulation.m".

3.4 Calibrating Procedure and Results

The cross-correlation, $\mathbf{r}$, between a digitized transmit signal, $\mathbf{s}$, and digitized receive signal, $\mathbf{s_r}$, is found with a sliding dot product. The sliding dot product, commonly noted by $\star$, computes the inner dot product between two discrete signals with time lags applied to one signal. If the transmit signal is limited to L samples, while the receive signal is allowed M samples where $L < M$, then the sliding dot product is

$$r[m] = \mathbf{s} \star \mathbf{s_r} = \frac{1}{L} \sum_{k=1}^{L} s[k] s_r[k + m - 1], \tag{3.1}$$

where $m = 1, 2, \ldots, M - L$ and can be converted to an "absolute" time delay, t_d, where $t_d = (m - 1)/f_s$ s. Here, t_d is used to differentiate between τ so the reader understands that (2.23) does not apply to t_d. The absolute time delay cannot be converted to range because the required time needed for the signals to traverse through the radar hardware, η, does not represent a change in range. Once η is found, then $m_0 = \lfloor \eta f_s + 1 \rceil$ ($\lfloor \cdot \rceil$ means round to nearest integer) corresponds to $\tau = 0$ and in turn, $R = 0$. Therefore, the purpose of the calibration is to determine m_0 so the radar range estimates are accurate.

The calibration went as follows,

1. A stationary target was set at 5 m away in front of the radar.
2. Five collections lasting 8 μs (10,000 samples) were taken at $f_s = 1.25$ Gsamp/s.
3. The target was removed and five more collections with the same specifications were taken to represent the background.
4. The transmit signals were limited to 9,800 samples, while the receive signals were 10,000 samples.
5. Ten sliding dot products, one for each collection, were performed between the respective transmit and receive signals.
6. The five target cross-correlations were averaged, $\mathbf{r_t}$.
7. The five background cross-correlations were averaged, $\mathbf{r_{bg}}$.
8. The difference between the averaged cross-correlations was plotted (shown in Figure 3.8).
9. The highest cross-correlated sample, $m = 100$, was labeled $R = 5$ m.
10. The time delay corresponding to 5 m was calculated with (2.1) to be, $\tau_{5m} = 33.36$ ns.
11. The number of samples that occur during 33.36 ns is $\tau_{5m} \cdot f_s = 41.7 = 42$ samples.
12. Therefore, sample $m_0 = 100 - 42 = 58$ corresponds to a target range and time delay of zero for $f_s = 1.25$ Gsamp/s.

So the cross-correlation results from the hardware experiments in Chapter IV will utilize (3.1) where m ranges from m_0 to m_{end}.

The calibration testing was not reaccomplished for $f_s = 2.5$ Gsamp/s, but instead it was assumed that $m_0 = 117$. The assumption begins with the fact that $t_d = 46.4$ ns for $m = 58$ and $f_s = 1.25$ Gsamp/s. Then letting $\eta = 46.4$ ns and calculating m_0 for $f_s = 2.5$ Gsamp/s gives $m_0 = \lfloor \eta f_s \rceil + 1 = \lfloor (46.4\text{ns})(2.5\text{Gsamp/s}) \rceil + 1 = 116 + 1$.

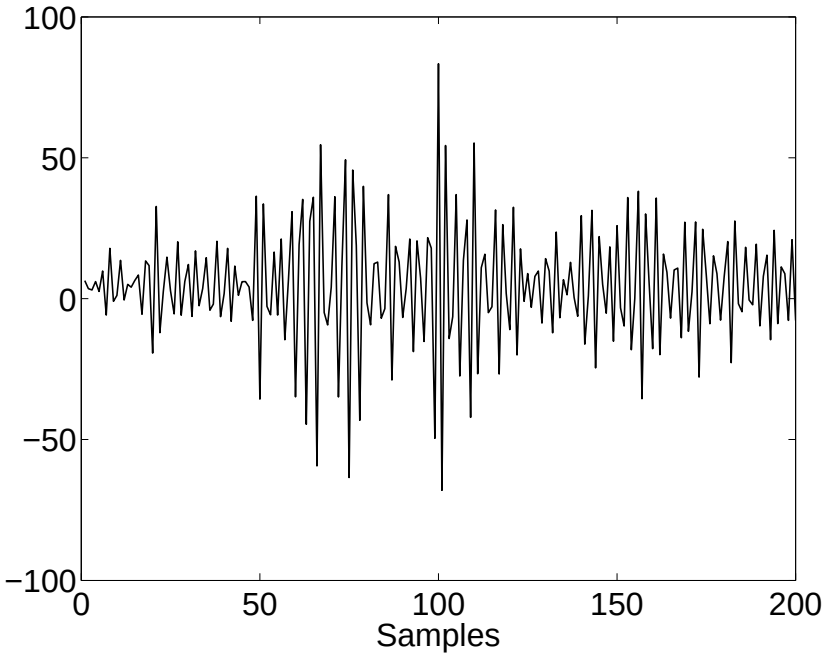

Figure 3.8: The correlation graph after the average background subtraction depicts a large return at sample 100 for a stationary target that exists at five meters. The 100th sample is then labeled as the $R = 5$ m sample.

3.5 Test Plan

The experiments involve three types of collections that are outlined in Table 3.1. The first collection type consists of gathering data from a ingressing target moving at a known velocity. This collection is referred to as a moving target collection, represented with prefix 'T' in Table 3.1. The second collection type captures the environment when no targets exist and is referred to as a background collection (labeled with 'B' prefixes). The final collection type involves replacing the receive antenna with a 50 Ω load and then collecting data from the receive channel in order to measure the internal noise of the system. This collection is referred to as a noise collection, represented with prefix 'N'. Once all collections have been accomplished, then the data is processed to test the theory covered in Chapter II. The required equipment includes: a moving target, the AFIT RNR, a digital oscilloscope for the data collection, and a high performance computer to analyze the data.

Table 3.1: Planned Collections

Collections	f_s (Gsamp/s)	v (m/s)	R (m)	T (ms)	Polarization
T01	1.25	-3	5	160	HH
T02	1.25	-3	5	160	VV
T03	1.25	-5	5	160	HH
T04	1.25	-5	5	160	VV
T05	1.25	-5	10	160	HH
T06	1.25	-5	10	160	VV
T07	2.5	-5	5	80	HH
T08	2.5	-5	5	80	VV
T09	2.5	-5	10	80	HH
T10	2.5	-5	10	80	VV
B01	1.25	N/A	N/A	160	HH
B02	1.25	N/A	N/A	160	VV
B03	2.5	N/A	N/A	80	HH
B04	2.5	N/A	N/A	80	VV
N01	1.25	N/A	N/A	160	N/A
N02	2.5	N/A	N/A	80	N/A

3.5.1 Equipment. For the moving target, the AFIT Advance Navigation Technology (ANT) Center Global Positioning System (GPS)-enabled golf cart was used and pictured in Figure 3.9. The golf cart uses the highly accurate, differential GPS (DGPS) enhancement for precision navigation and timing. The golf cart's DGPS relays to the driver the speed in meters per second via the laptop in the passenger seat. The cart reaches a maximum speed of roughly 5.7 m/s, which meets the desired velocities needed for the moving target collections in Table 3.1.

The original ADC for AFIT RNR is replaced with a Tektronix® Digital Phosphor Oscilloscope (DPO) 7254 with the memory upgrade option. The DPO 7254 is

Figure 3.9: The AFIT Advance Navigation Technology (ANT) Center golf cart equipped with differential GPS for enhanced precision navigation and timing.

capable of storing 250 million contiguous 8-bit voltage samples for each transmit and receive channel. The collections will have a measurement windows of 80 ms when $f_s = 2.5$ Gsamp/s and 160 ms when $f_s = 1.25$ Gsamp/s. These windows at their respective sample frequencies each equate to 200 million samples, which is well below the stated record length of the DPO 7254. The lower sampling frequency is assumed to meet Nyquist rate, because the assumed maximum frequency, f_H, is approximately 520 MHz according to Figure 3.4. The AFIT RNR and DPO 7254 are pictured in Figure 3.10.

Finally, three computers were utilized to process the collected data. The specifications of the computers are given in Table 3.2.

Table 3.2: Processing Hardware

	Computer 1	Computer 2	Computer 3
Make	Dell	Dell	Dell
Model	Precision 690	Precision T7500	Precision T7500
Operation System	Windows XP	Windows 7 Pro	Windows 7 Pro
Processor Make	Intel®	Intel®	Intel®
Processor Model	Xeon® 5160	Xeon® W5590	Xeon® X5677
Number of Processors	2	1	2
Processor Speed	3.000 GHz	3.333 GHz	3.466 GHz
L2 Cache	4 MB	1 MB	1 MB
L3 Cache	N/A	8 MB	12 MB
Multiple Core Capable	Yes (Dual)	Yes (Quad)	Yes (Quad)
Total Number of Cores	4	4	8
HT[a] Technology	No	Yes	Yes
64-bit Technology	Yes	Yes	Yes
Installed Memory	32 GB	48 GB	48 GB
Memory Speed	667 MHz	1333 MHz	1333 MHz
Number of Memory Slots	8	6	12
Size of Memory Per Slot	4 GB	8 GB	4 GB
Memory Technology	DDR2	DDR3	DDR3
NUMA[b] Capable	No	No	Yes

[a] Hyper-Threading
[b] Non-Uniform Memory Access

Figure 3.10: The antenna stand connected to the radar box (black box behind oscilloscope), which is connected to the Tektronix DPO 7254.

3.5.2 Collection Procedures. The Moving Target collection requires two people; one to drive the target and the other to operate the radar (initiates the collection of data). The test should abide by the following procedure:

1. Make three lines as in Figure 3.11 on the ingressing track that correspond to zero, five, and ten meters.
    - The zero meter line is the reference line and location of the transmit and receive antennas.
    - Data collection begins at either five or ten meters.
2. The driver must make practice runs before the radar is in place at the reference line to accomplish the following tasks:
    - Ensure the brakes work properly.
    - Establish an "end collection" marker.

Figure 3.11: Ingressing track setup where the lines correspond to zero, five, and ten meters.

  - The collection finishes in a distance of $v \cdot T$ meters, which equates to 0.8 meters for the longest distance for the collections shown in Table 3.1.

- Discover braking distance.

  (a) The driver must bring the golf cart to its maximum speed and then brake when the cart reaches the "end collection" marker.

  (b) Measure the distance from the front leading edge of the golf cart to the reference line.

- Establish a "must brake" marker

(a) With the knowledge of required distance needed to brake, create a "must brake" marker between the reference line and "collection over" marker.

(b) Once the golf cart reaches this marker during any test, the driver must brake in order to avoid damaging themselves or the equipment.

3. Once the practice run tasks are accomplished, set up the radar at the reference line with the correct antenna polarization for both antennas.
4. Make sure all coax cables and wires are correctly connected and appropriately tightened (use torque wrench).
5. Turn radar and DPO 7254 on.
6. Once the oscilloscope finishes initial calibration, the radar operator must set f_s on the Tektronix DPO 7254 to the desired sampling frequency, 1.25 or 2.5 Gsamp/s.
7. After confirmation is received from radar operator, driver may ingress with the golf cart at the desired speed.

    - Driver needs to make sure there is plenty of length on the ingressing track in order to reach and maintain the desired speed of the test. The golf cart must maintain constant velocity so the wideband condition in (2.19) is not violated.

8. When the driver reaches the predetermined collection line (five or ten meters) then the radar operator must start the collection.
9. When the driver reaches the "must brake" marker then driver must brake.
10. Save the data from both the transmit and receive channels of the Tektronix DPO 7254 onto portable media for post processing.
11. Return to step 3 and perform test again with new parameters taken from Table 3.1.

The second collection type, background collection, requires one person to operate the radar to initiate data collection. With the target removed from the environment, the radar operator must take four collections with the desired parameters from Table 3.1. After each collection, save the data from the transmit and receive channels onto portable media for later processing.

The third and final collection type, noise collection, requires one person to operate the radar. First, replace the receive antenna with a 50 Ω load, which closely resembles the output impedance of the LPY41 antenna. Then, with the transmitter on, take a collection with the desired parameters from Table 3.1. Finally, save the data from the receive channel as $\mathbf{n_{01}}$ or $\mathbf{n_{02}}$ onto portable media for later processing. The subscripts denote which collection, N01 or N02, the data comes from.

IV. Results

4.1 Overview

This chapter covers the simulated and measured results. The first section presents the simulation results and how those results sculpted the test plan described in Section 3.5. Then the measured results are discussed, where the measured results section covers how to incorporate the calibration data from Section 3.4 and then how the data were processed. Once the digital signal processing (DSP) is described, then the analysis of the results is presented.

4.2 Simulation Results

Eight simulations were accomplished to assess the feasibility of velocity estimation in the time domain through interpolation. Six simulations were conducted at sampling rates of $f_s = 1.25$ Gsamp/s with measurement windows of $T = 160$ ms, while the remaining two were simulated at $f_s = 2.5$ Gsamp/s with $T = 80$ ms. The number of samples, L, for all the simulations equaled 200 million. Of the six simulations at $f_s = 1.25$ Gsamp/s, three simulated a target moving at -3 m/s and the remaining three simulated the target's velocity to be -5 m/s. Within the respective sets of three, the simulated signal-to-noise ratio (SNR) was set to 0 dB, -20 dB, and -30 dB. The goal was to determine how robust the theory is and if the theory could be implemented in hardware.

Figure 4.1 depicts the simulation results for the six simulations at $f_s = 1.25$ Gsamp/s. The left column contains the simulations corresponding to a target moving at -3 m/s, while the right column represents the simulations with a target velocity of -5 m/s. The rows corresponds to a simulated SNR of either 0 dB, -20 dB, or -30 dB. From these results, it was decided that detecting a target at -5 m/s would be easier than detecting one at -3 m/s. By comparing the normalized matched filter outputs in Figure 1(e) and 1(f), the theory seems to be more robust with targets moving at higher speeds. This observation may be attributed to the fact that the amount of interpolation each k^{th} sample goes through is directly proportional to the

magnitude of the velocity. As each sample experiences a greater time shift for higher speeds, then the overall cross-correlation improves. Therefore, the planned collections focused more on targets moving at -5 m/s rather than -3 m/s.

The final two simulations were conducted with one goal in mind. If $f_s = 2.5$ Gsamp/s is required to meet Nyquist rate, would an 80 ms measurement window be long enough to accurately estimate velocity? Figure 4.2 answers the question by accurately estimating a targets speed at an SNR of 0 dB. As expected, the velocity resolution decreased, giving more validity to the simulation. Figure 2(a) depicts a simulated target at -3 m/s, while Figure 2(b) shows a target at -5 m/s. Only an SNR of 0 dB was considered, because experimental tests at $f_s = 2.5$ Gsamp/s were classified as backup tests. The classification was made based on the fact that velocity resolution increases with larger measurement windows. Therefore, the experimental tests at $f_s = 1.25$ Gsamp/s were of more interest since the measurement windows were twice as long, $T = 160$ ms.

4.3 Measured Results

4.3.1 Incorporating Calibration Results. Before processing the data, the calibration results from Section 3.4 need to be considered in order to shorten processing time. The goal was to reduce the range of m in (3.1). The start, m_0, was established in Section 3.4. The end, $m_{\text{end}} = M - L$, needed to be established where L was the length of the transmit signal, M was the length of the receive signal, and $L < M$.

To establish m_{end}, a desired maximum range, $R_{\max}$, must be set. The maximum range was set to be five meters beyond the target location; therefore, $R_{\max} = 10$ m when the target's location was five meters and $R_{\max} = 15$ m when the target was at ten meters.

Using $R_{\max} = 10$ m as an example, m_{end} is found by first converting $R_{\max}$ to the maximum time delay, $\tau_{\max}$, with (2.1). Thus, $\tau_{\max} = 2 \cdot 10/c = 66.7$ ns. Then find the number of samples needed, N, for a time delay of $\tau_{\max}$ by multiplying by the sample

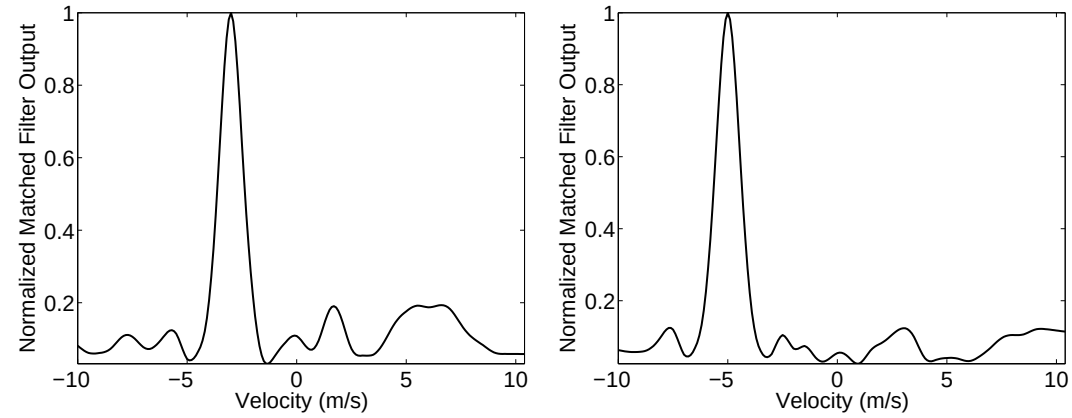

(a) SNR = 0 dB

(b) SNR = 0 dB

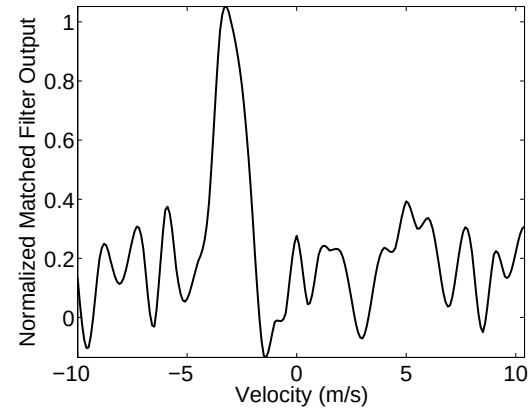

(c) SNR = -20 dB

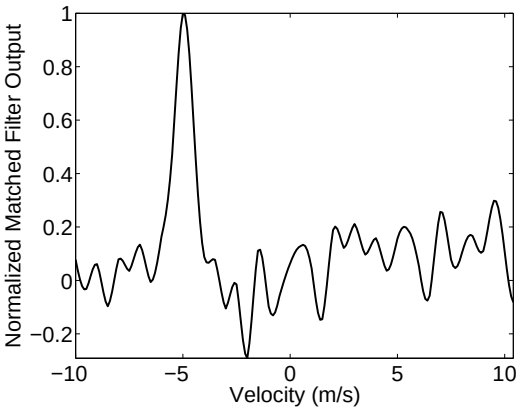

(d) SNR = -20 dB

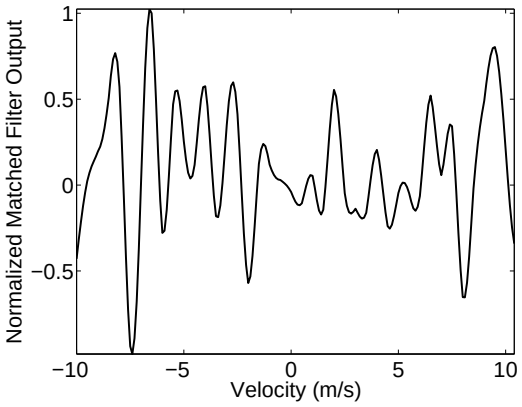

(e) SNR = -30 dB

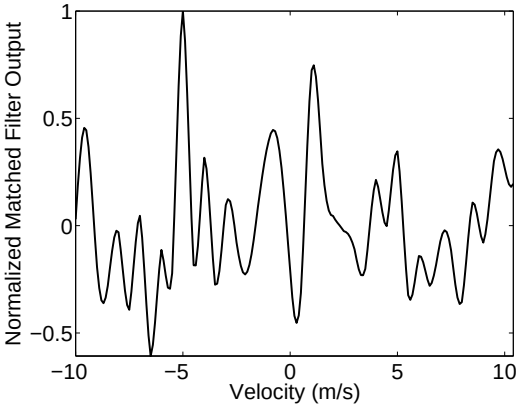

(f) SNR = -30 dB

Figure 4.1: The simulation results are for $T = 160$ ms. The left column represent the cross-correlated output (when perfectly matched in time delay) for a simulated velocity of -3 m/s while the right column graphs the simulated results for a target moving at -5 m/s. The rows correspond to varying SNRs of 0 dB, -20 dB, and -30 dB.

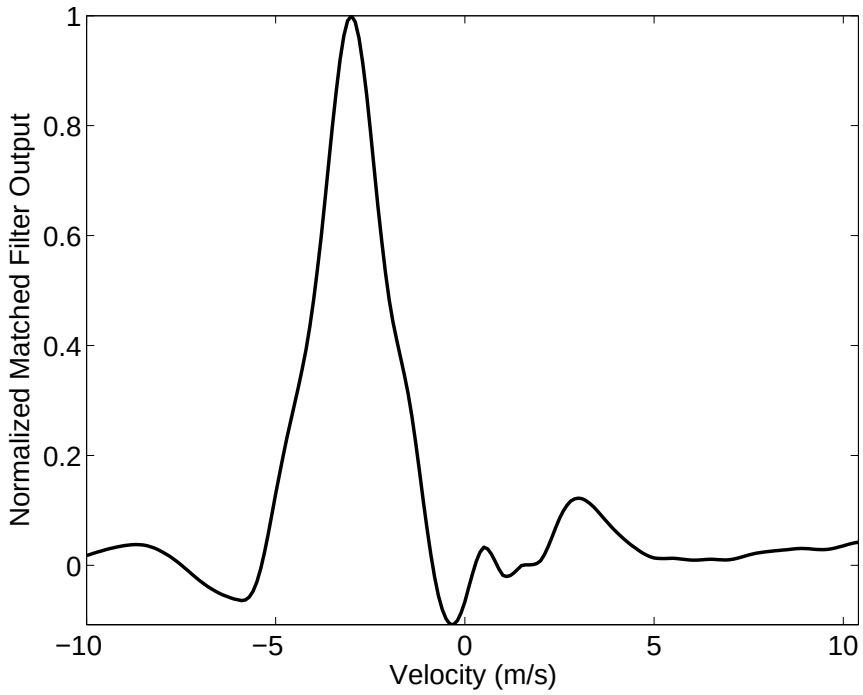

(a)

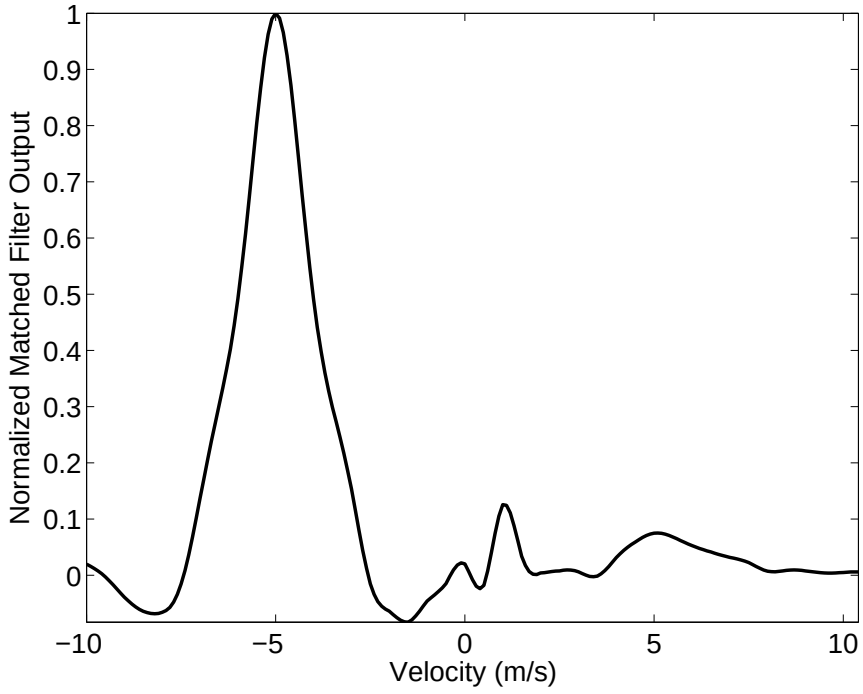

(b)

Figure 4.2: The simulation results are for $T = 80$ ms and an SNR of 0 dB where (a) represents a target with a velocity of -3 m/s while (b) corresponds to a target with a velocity of -5 m/s. Both assume the time delay, τ, is known.

Table 4.1: Data Processing Parameters

Process	f_s (Gsamp/s)	$R_{\max}$	m_0	Range Bins	m_{end}
P01	1.25	10	58	83	141
P02	1.25	15	58	125	183
P03	2.5	10	117	166	283
P04	2.5	15	117	250	367

frequency, f_s. Letting $f_s = 1.25$ Gsamp/s yields $N = \tau_{\max} \cdot f_s = 83$ samples needed to reach $\tau_{\max}$; thus, reaching $R_{\max}$. Solving for m_{end} gives $m_{\text{end}} = m_0 + N = 141$. So, when implementing (3.1), the cross-correlation output, $\mathbf{r}$, becomes length N and each cross-correlated value relates to a particular range, which causes there to be N range bins. Table 4.1 summarizes the data processing parameters.

4.3.2 Processing the Data. When processing the collected data, a cross-correlation matrix is the final output for the moving target and background collections, while a simple noise power estimate, σ^2, is the output for the noise collections. The following subsections will discuss the process for obtaining the cross-correlation matrix, the processing times required to obtain a matrix based on hardware and processing parameters, estimating the noise power, and finally how to combine different collection types into one final cross-correlation matrix.

4.3.2.1 Cross-Correlation Matrix. The data was processed for velocities ranging from -14 m/s to -2 m/s at 0.5 m/s increments, which equates to $V = 25$ different velocities. Processing the data followed these procedures:

1. Load the collection data from TXX or B0X, which consists of the transmit and receive signals that were simultaneously collected and contiguously digitized.
2. Limit the transmit data to length L, where $L = f_s \cdot T = 200$ million samples.

3. Limit the receive data to length M, where $M = L + m_{\text{end}}$ and m_{end} is specified by process type, P0X, in Table 4.1.
4. Preallocate a matrix $\mathbf{C}$ of size $V \times N + 1$ to later store cross-correlated data.
5. Use Equations (2.39) and (2.40) to create reference signal $s_{\text{ref}}[k]$ for each desired velocity.
6. Use Equation (3.1), where $\mathbf{s} = \mathbf{s}_{\text{ref}}$ to calculate the cross-correlation output, $\mathbf{r}$, for each reference velocity
7. Store row vector $\mathbf{r}$ in the row of $\mathbf{C}$ that corresponds to the respective reference velocity.
8. Save the final cross-correlation matrix output, $\mathbf{C}$, as either $\mathbf{C}_{\text{TXX}}$ or $\mathbf{C}_{\text{B0X}}$ depending on which collection was loaded in step 1.

In the final output, the matrix elements $c_{i,j}$ relate the cross-correlation between the reference and receive signals for the i^{th} reference velocity and j^{th} range bin.

4.3.2.2 Processing Times. Of the ten planned moving target collections, nine were accomplished and eight were processed. The T10 collection on Table 3.1 was not accomplished due to hardware complications that caused the test team to run out of time. The receive channel data from T02 was later found to be corrupted and unusable. The corrupt received data made the data for the transmit channel useless, since the transmit signal is completely random and never repeats. The remaining background and noise collections were accomplished and processed.

The total processing times to create a cross-correlation matrix were recorded and are given in Table 4.2. The times depend on the computers from Table 3.2 and the executed processing type, P0X, from Table 4.1. Table 4.2 relates the importance of advanced hardware combined with appropriate processing parameters.

Computers 2 and 3 execution times are over twice as fast as computer 1. The memory speed is believed to be a major reason for the difference. The main differences between computers 2 and 3 are computer 2 has six 8 GB of RAM while computer 3

Table 4.2: Processing Times

Collection	Computer Used	Process	Completion Time
T01	2	P01	1 hr 19 min
T03	1	P01	3 hr 28 min
T04	2	P01	1 hr 16 min
T05	2	P02	1 hr 44 min
T06	2[c]	P02	2 hr 39 min
T07	3	P03	3 hr 21 min
T08	3[b]	P03	3 hr 4 min
T09	2[a]	P04	3 hr 9 min
B01	3	P02	1 hr 50 min
B02	3	P02	1 hr 54 min
B03	3[b]	P04	3 hr 7 min
B04	3[b]	P04	3 hr 13 min

[a] Hyper-threading technology enabled
[b] Hyper-threading and non-uniform memory access technology enabled
[c] Computer entered sleep mode causing the time to lengthen

has twelve 4 GB of RAM, and unlike computer 2, computer 3 is non-uniform memory access (NUMA) capable. Initially, computers 2 and 3 did not have the hyper-threading (HT) and NUMA (for computer 3 only) technology enabled. During this initial setup, computer 2 averaged faster processing times than computer 3, which may be contributed to the difference in memory size allocations. Once the technologies were enabled, computer 3 processing times decreased while the times for computer 2 roughly remained the same. This makes sense, because HT technology speeds up parallel processing while NUMA helps to improve memory speed through the use of separating the memory out between processors. Since the DSP required 31.9 GB of memory and does not utilize parallel processing due to the memory constraints, the decrease in processing time can be contributed to the NUMA technology.

4.3.2.3 Faster Cross-Correlation with the FFT. After processing the data and recording the times, a faster implementation of the sliding dot product in (3.1) was found with the help of the fast Fourier transform (FFT) [19]. Ifeachor and Jervis give the proof of the fast correlation theorem [19, pg. 267-269] and once applied, (3.1) becomes

$$r[m] = \mathbf{s} \star \mathbf{s_r} = \frac{1}{L}\mathcal{F}^{-1}\{S^*[j]S_r[j]\}, \tag{4.1}$$

where $\mathcal{F}^{-1}$ is the inverse FFT, $S[j]$ and $S_r[j]$ are the reference and receive signals in the frequency domain, and $*$ represents a conjugate.

4.3.2.4 Cross-Correlation Matrix Revised. The data processing procedure previously described in Section 4.3.2.1 was altered in order to incorporate (4.1). The revised procedure followed these steps:

1. Load the collection data from TXX or B0X, which consists of the transmit and receive signals that were simultaneously collected and contiguously digitized.
2. Limit the transmit data to length L, where $L = f_s \cdot T = 200$ million samples.
3. Limit the receive data to length M, where $M = L + m_{\text{end}}$ where $m_{\text{end}} = 183$ for $f_s = 1.25$ Gsamp/s or $m_{\text{end}} = 367$ for $f_s = 2.5$ Gsamp/s. This ensures a maximum range of 15 meters regardless of where the target is located (see Table 4.1).
4. Preallocate a matrix $\mathbf{C}$ of size $V \times N + 1$ to later store cross-correlated data, where V are the number of reference velocities and N are the number of range bins (125 or 250).
5. Use Equations (2.39) and (2.40) to create reference signal $s_{\text{ref}}[k]$ for each desired velocity.
6. Zero pad $s_{\text{ref}}[k]$ to length M.
7. Perform the FFT on $s_{\text{ref}}[k]$ and $s_r[k]$ to get $S_{\text{ref}}[j]$ and $S_r[j]$ respectively.

8. Conjugate the reference signal to get $S^*_{\text{ref}}[j]$
9. Use Equation (4.1), where $S^*[j] = S^*_{\text{ref}}[j]$ to calculate the cross-correlation output, $\mathbf{r}$, for each reference velocity
10. Store the elements ranging from $m_0, m_0 + 1, \ldots, m_0 + N$ of the row vector $\mathbf{r}$ in the row of $\mathbf{C}$ that corresponds to the respective reference velocity. These elements correspond to ranges zero through 15 meters for the respective reference velocities.
11. Save the final cross-correlation matrix output, $\mathbf{C}$, as either $\mathbf{C}_{\text{TXX}}$ or $\mathbf{C}_{\text{B0X}}$ depending on which collection was loaded in step 1.

4.3.2.5 Reduced Processing Times. The revised data processing procedure that incorporated (4.1) was used for collections T01 and T09. Table 4.3 gives the original and reduced processing times for T01 and T09. From the comparison in Table 4.3, the revised procedure not only decreased the completion times, but is also independent of which processing parameters are chosen from Table 4.1. The problem with the original procedure required careful consideration of the maximum range for the cross-correlator because the goal was to minimize the number of inner dot products within (3.1). By using the revised procedure with (4.1), all desired ranges can be cross-correlated without an impact to the completion time. Now the completion time is primarily controlled by the number of reference velocities, V, along with the length of the signals, L and M.

4.3.2.6 Noise Power. The noise power, P_n, was easily calculated with the collected data, $\mathbf{n}_{01}$ and $\mathbf{n}_{02}$, taken from the receive channel during the noise collections N01 and N02. Since P_n was used for power ratio estimations such as SNR, the resistance was not needed and was assumed to be one ohm. Therefore, the noise power was estimated by the statistical second moment of $\mathbf{n}_{0X}$,

$$P_n = \frac{1}{L}\mathbf{n}_{0X}^{\text{T}}\mathbf{n}_{0X}, \tag{4.2}$$

Table 4.3: Revised Processing Times

Collection	Computer Used	Process Parameters	Procedure	Completion Time
T01	2	P01	Original	1 hr 19 min
T09	2[a]	P04	Original	3 hr 9 min
T01	3[b]	P02	Revised	42 min
T09	3[b]	P04	Revised	42 min

[a] Hyper-threading technology enabled
[b] Hyper-threading and non-uniform memory access technology enabled

where L is the number of samples in the collected noise column vector and $^{\mathrm{T}}$ represents the transpose.

For additive white Gaussian noise (AWGN), the noise power equals the variance, σ^2 because AWGN has zero mean, making the second moment and variance equal. However, the numerical results showed $\mathbf{n}_{01}$ and $\mathbf{n}_{02}$ had approximately equal variances, but non-zero and non-equal means as given in Table 4.4. Since the noise means of N01 and N02 are not equal, it leads to different noise powers based on the sample frequency used during a collection. The different noise powers is most likely due to the fact that the noise collections were sampled after the bandpass filter, and in turn, caused the PSD of the noise to no longer be uniform across all frequencies. Figure 4.3 illustrates how the noise was bandlimited by the filters.

Table 4.4: Noise Power

Collection	P_{N0X} (dBW)	σ^2 (dBW)	μ (dBW)
N01	-23.53	-25.62	-13.86
N02	-23.00	-25.69	-13.18

4.3.2.7 Combining All Processed Collection Types. Once the cross-correlation matrices and noise powers have been calculated for the collection types, it is possible to execute the background subtraction and convert the data to units of dB to illustrate the SNR. Since the Tektronix DPO 7254 digitized the signal into 8-bit voltage readouts, the SNR cross-correlation matrix, $\mathbf{C}_{\text{SNR}}$ was easily calculated as $\mathbf{C}_{\text{SNR}} = 10\log_{10}(\mathbf{C}_{\text{TXX}}) - P_{N0X}$. It must be noted that the no background subtraction occurred on $\mathbf{C}_{\text{SNR}}$, which means the signal contains the target plus clutter information.

Incorporating both cross-correlation matrices yielded the background subtraction SNR cross-correlation matrix, $\mathbf{C}_{\text{Tot}} = 10\log_{10}(\mathbf{C}_{\text{TXX}} - \mathbf{C}_{\text{B0X}}) - P_{N0X})$. The $\mathbf{C}_{\text{Tot}}$ matrix represents the SNR for a signal with the target information only.

The problem that occurs with the background subtraction is it assumes that the background is stationary during all collections. Also, rather than averaging multiple background collections at the same processing parameters, it was assumed that one collection at a measurement window of at least 80 ms would be sufficient to statistically represent the clutter.

4.3.3 Analysis of Results. Figure 4.4 depicts the power spectral density (PSD) of transmit and receive signal along with the frequency response of the antenna. The figure was used to decide whether the receive signal bandwidth assumption, $B_3 = 185$ MHz with $f_H = 520$ MHz, made in Section 3.2 was valid. This assumption led to using a sample frequency of 1.25 Gsamp/s to meet the Nyquist rate. However, Figure 4.4 shows a narrowband of frequencies within the 3 dB bandwidth at 640 MHz. Even though these frequencies are aliased, it was assumed the cross-correlation results did not degrade. This assumption was made based on the fact that the narrowband of frequencies were aliased to 15 MHz where the transmit signal is very low; leading to a low cross-correlation at the aliased frequencies.

The collections occurred over two days and the order the collections were taken is given in Table 4.5. At the end of day one, the radar was packed up and stored away for the night. The ingressing track was left alone so the radar could be placed

Table 4.5: Order of Collections Taken

Day	Order	Collection	v (m/s)	R (m)	T (ms)	LPDA
	1	T02	-3	5	160	VV
	2	T04	-5	5	160	VV
1	3	T06	-5	10	160	VV
	4	T08	-5	5	80	VV
	5	T03	-5	5	160	HH
	6	T05	-5	10	160	HH
	7	T01	-3	5	160	HH
	8	T07	-5	5	80	HH
	9	T09	-5	10	80	HH
	10	B03	N/A	N/A	80	HH
2	11	B01	N/A	N/A	160	HH
	12	N01	N/A	N/A	160	N/A
	13	N02	N/A	N/A	80	N/A
	14	B04	N/A	N/A	80	VV
	15	B02	N/A	N/A	160	VV

in the same location on day two. Unfortunately, though, background collections were not taken on day one, which leads to degraded background subtraction results for the day one collections.

Figures 4.5–4.11 compare the results of $\mathbf{C}_{\text{SNR}}$ and $\mathbf{C}_{\text{Tot}}$ for different collections. Figures 4.5 and 4.6 show the processed data for the collections T01, B01, and N01. Here the background collection, B01, accurately represents the background in T01, which allowed the target response to be clearly visible at a velocity of -3 m/s and range near 5 m. This outcome was contributed to the fact that all three collections were taken on the same day (refer to Table 4.5).

Figures 4.7 and 4.8 illustrate the processed results for collections T07, B03, and N02. Since T07 and B03 were collected on day two, the background was accurately represented and resulted in good background subtraction. The results also show how a measurement window of 80 ms reduces the target velocity resolution as expected.

The results for the final moving target collection taken, T09, are shown in Figures 4.9 and 4.10. These results emphasize the importance of accurate background subtraction. Since the target is at 10 m during this collection, the power received from the target is much weaker than the collections with targets at 5 m due to spreading loss. Without accurate background subtraction, the target in Figure 4.9 might go unnoticed. Also note, that like the previous results, the measurement window is again 80 ms. Figure 4.9 once again illustrates the dependence of velocity resolution has on correlation time window, T.

The results shown in Figures 9(c) and 10(c) also illustrate the importance of accurately knowing the background by noting that the z-axis is not SNR after the background subtraction. This is because the average received power for B03 was -11.45 dBW (calculated using (4.2) where $\mathbf{n}$ was the B03 received channel data), while the average received power for T09 was -11.48 dbW. Since the received power was greater in the background data, the numerator of $\mathbf{C}_{\text{Tot}}$, $\mathbf{C_{T09}} - \mathbf{C}_{B03}$, cannot be converted to dBW. The cross-correlation technique still extracts the target's range and velocity, but the background subtraction would have given $\mathbf{C}_{\text{Tot}}$ as an SNR if the background had been more accurately estimated. Therefore, multiple background collections should be averaged together in any future experiments.

Figure 4.11 illustrates the poor results the background subtraction caused when the day two background data was applied to day one moving target data. The processed collections in Figure 4.11 are T03, B01, and N01. The collection T03 was taken day one because it met several test goals. First, the velocity was -5 m/s, which as discussed previously, should be easier to detect based on simulation results. Second, the measurement window was 160 m/s, allowing for the better theoretical velocity res-

olution based on the ambiguity plots presented in Chapter III. Lastly, the antennas were horizontally polarized, which created less cross-talk interference than vertically polarized log-periodic dipole array (LPDA) antennas. Therefore, collection T03 was collected on day one, while the background collection occurred on day two. The results are not as impressive as the previous three figures, showing the importance of accurate background data. However, on the plus side, the strong response from the target before background subtraction emphasizes how well 2D cross-correlation in the time domain works.

All the results are given in larger scales in Appendix A, where the minimum correlated range is two meters.

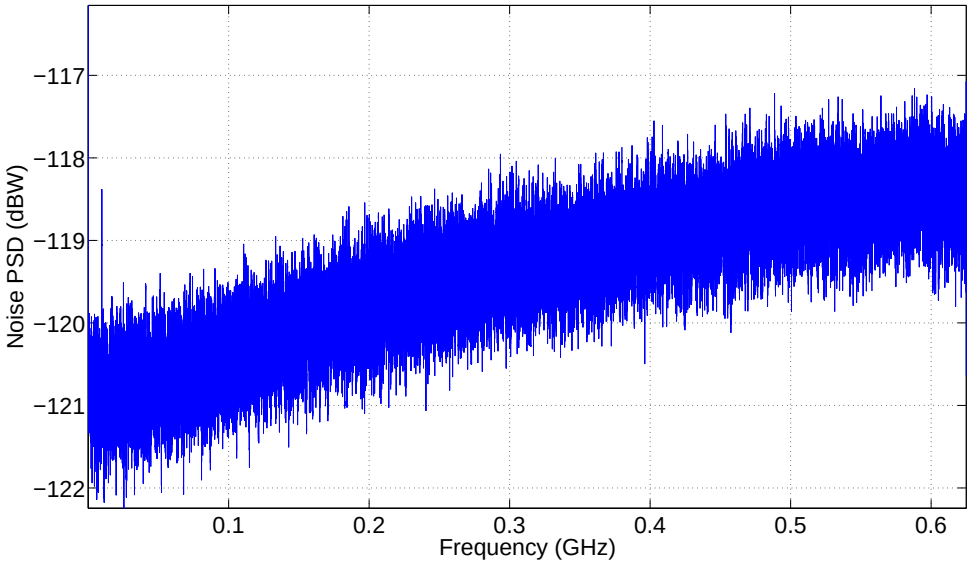

(a) N01

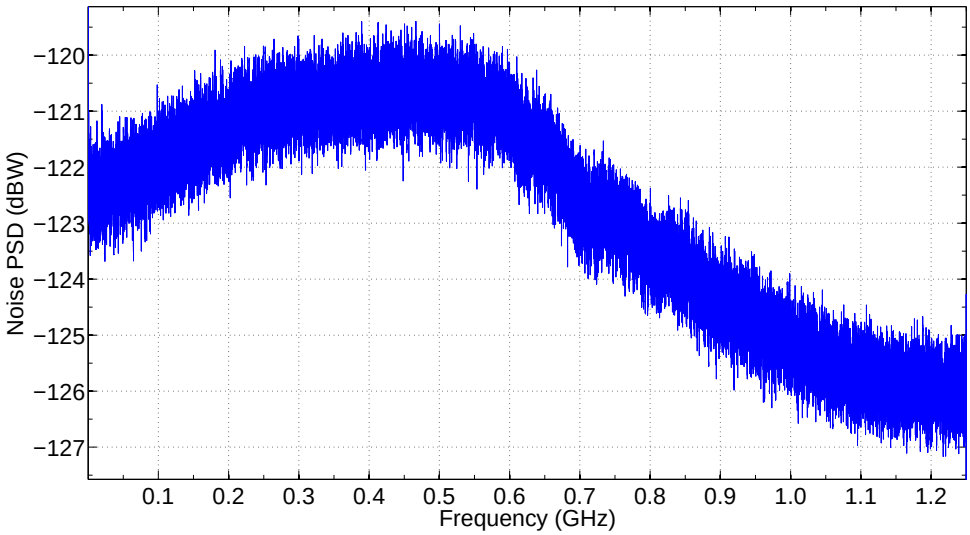

(b) N02

Figure 4.3: The noise PSD where (a) shows the PSD for the N01 collection, which was sampled at 1.25 Gsamp/s, and (b) depicts the PSD for the N02 collection where $f_s = 2.5$ Gsamp/s

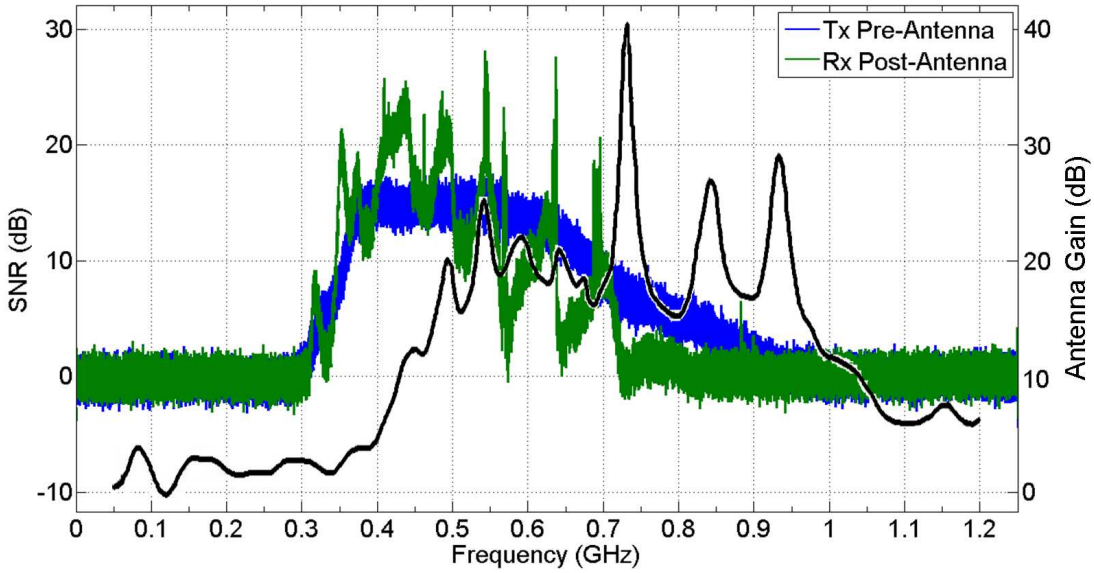

Figure 4.4: The frequency response of the antenna represented as a solid black line is overlaid on the SNR of the transmit and receive signals.

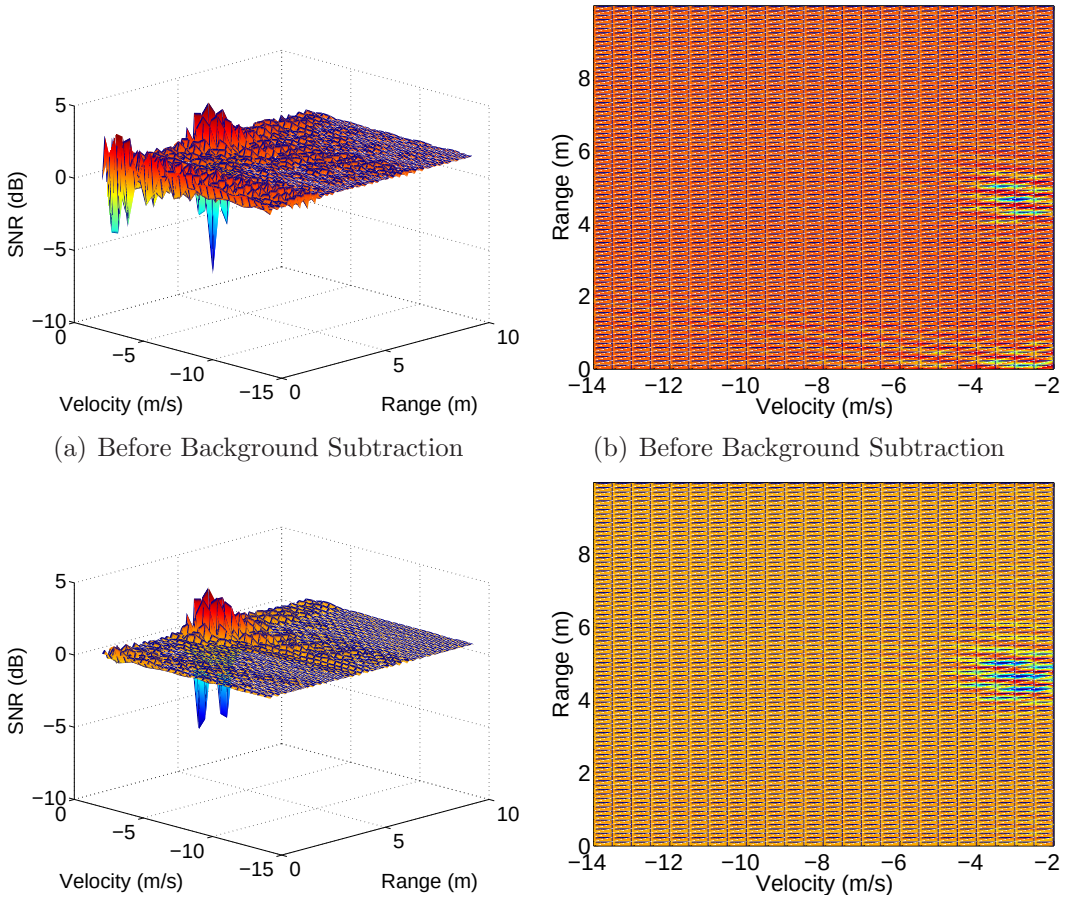

(a) Before Background Subtraction

(b) Before Background Subtraction

(c) After Background Subtraction

(d) After Background Subtraction

Figure 4.5: Results for target parameters of $v = -3$ m/s and $R = 5$ m and collection parameters of $T = 160$ ms, and horizontal antenna polarization.

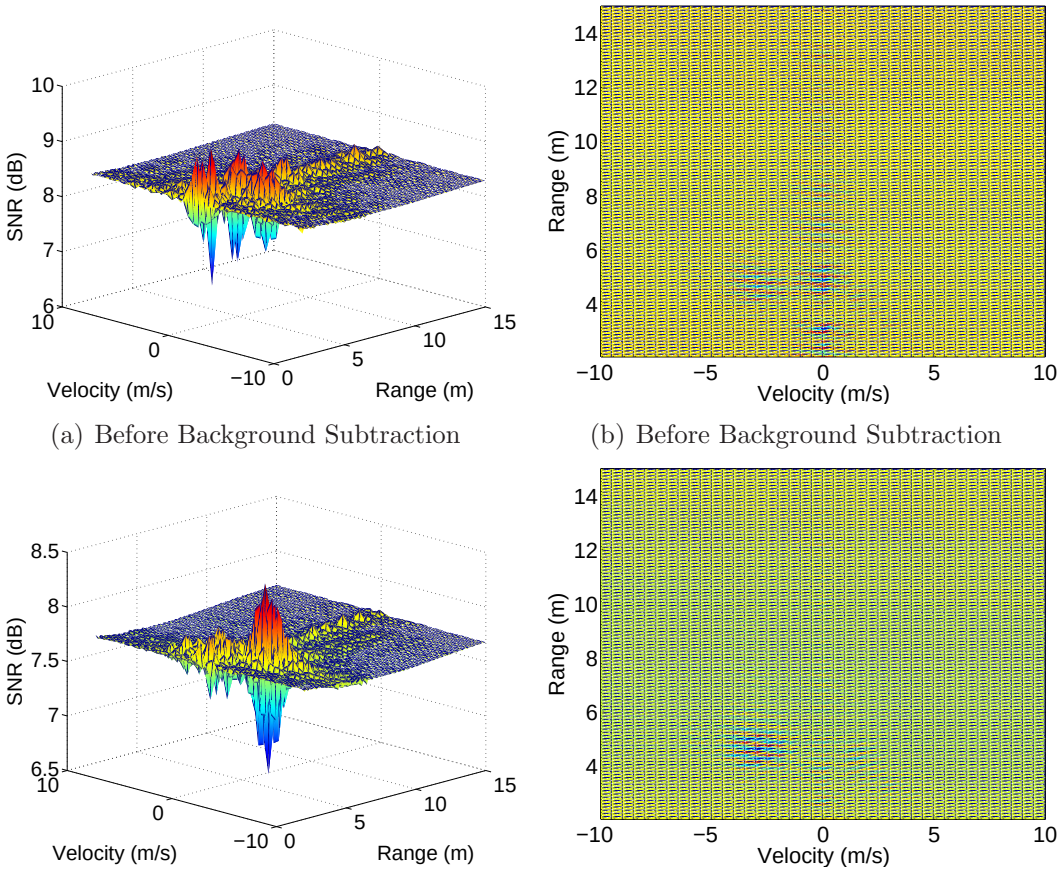

(a) Before Background Subtraction

(b) Before Background Subtraction

(c) After Background Subtraction

(d) After Background Subtraction

Figure 4.6: Results for reference velocities ranging from -10 m/s to 10 m/s at 0.5 m/s increments for the target parameters described in Figure 4.5

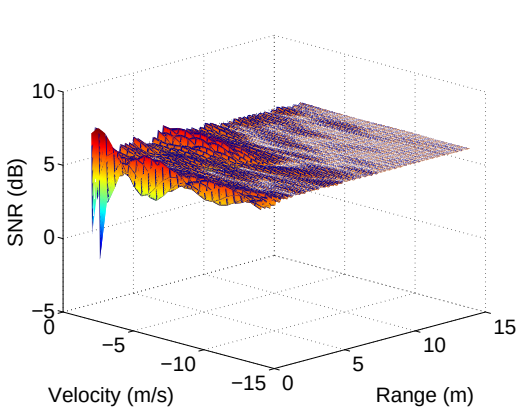

(a) Before Background Subtraction

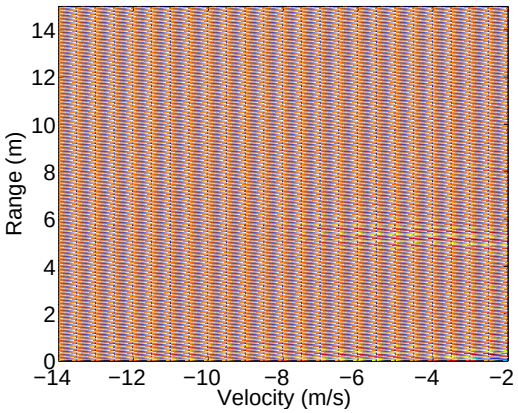

(b) Before Background Subtraction

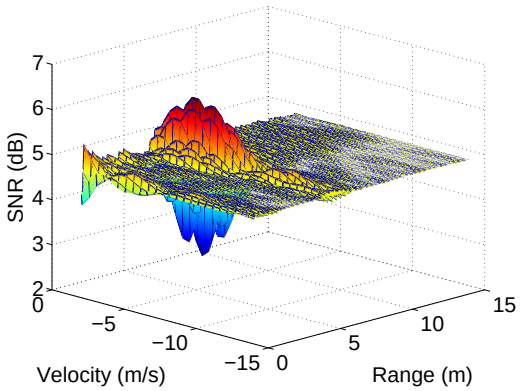

(c) After Background Subtraction

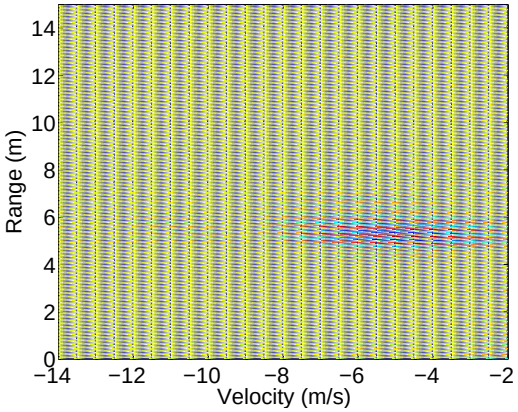

(d) After Background Subtraction

Figure 4.7: Results for target parameters of $v = -5$ m/s and $R = 5$ m and collection parameters of $T = 80$ ms, and horizontal antenna polarization.

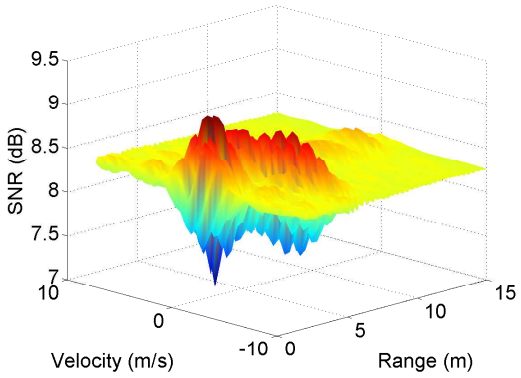

(a) Before Background Subtraction

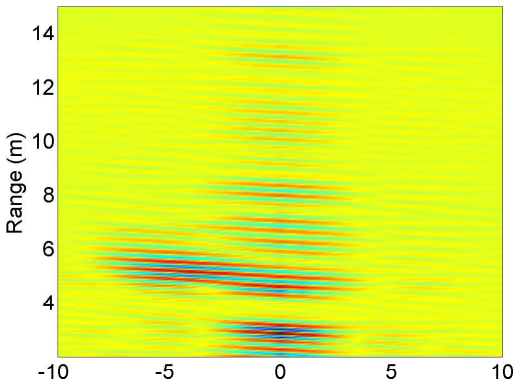

(b) Before Background Subtraction

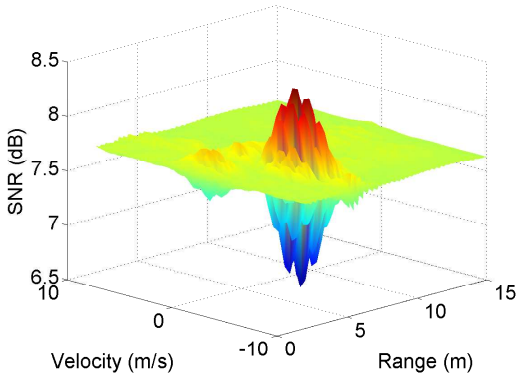

(c) After Background Subtraction

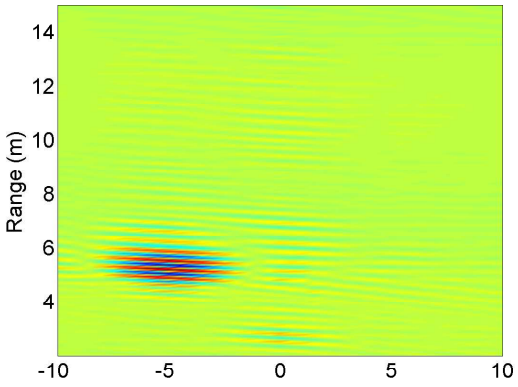

(d) After Background Subtraction

Figure 4.8: Results for reference velocities ranging from -10 m/s to 10 m/s at 0.5 m/s increments for the target parameters described in Figure 4.7

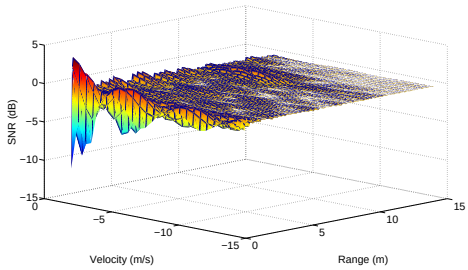

(a) Before Background Subtraction

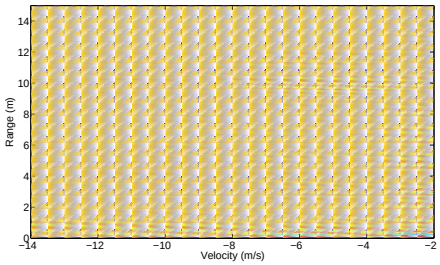

(b) Before Background Subtraction

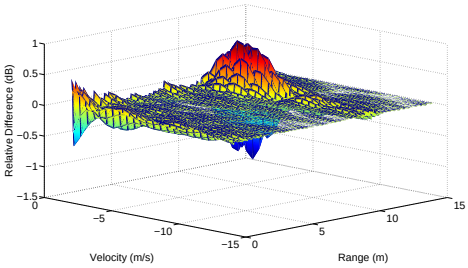

(c) After Background Subtraction

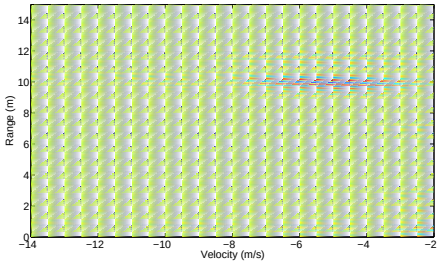

(d) After Background Subtraction

Figure 4.9: Results for target parameters of $v = -5$ m/s and $R = 10$ m and collection parameters of $T = 80$ ms, and horizontal antenna polarization.

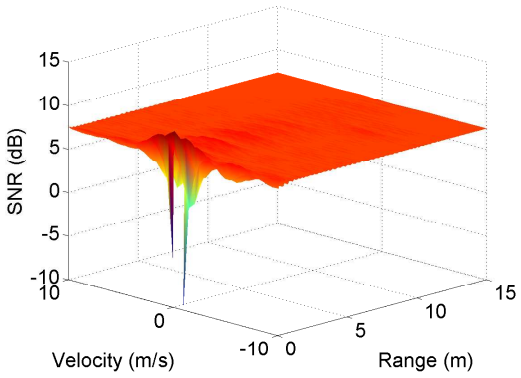

(a) Before Background Subtraction

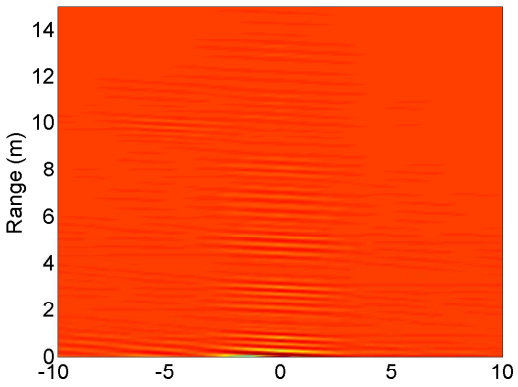

(b) After Background Subtraction

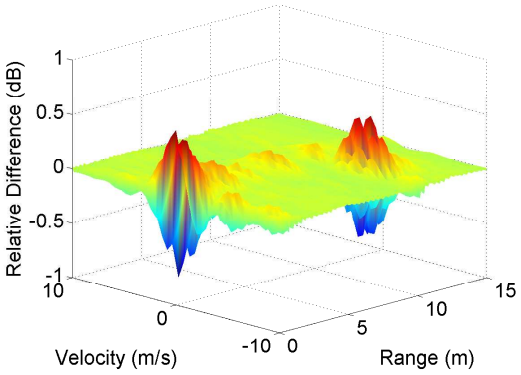

(c) Before Background Subtraction

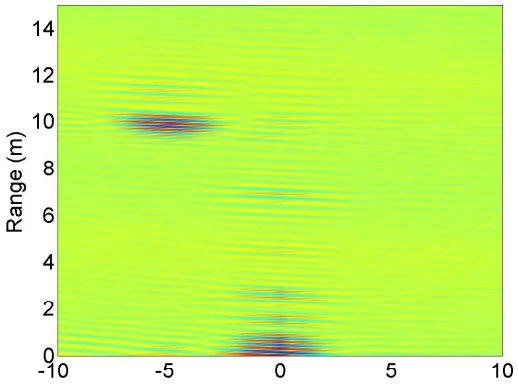

(d) After Background Subtraction

Figure 4.10: Results for reference velocities ranging from -10 m/s to 10 m/s at 0.5 m/s increments for the target parameters described in Figure 4.9.

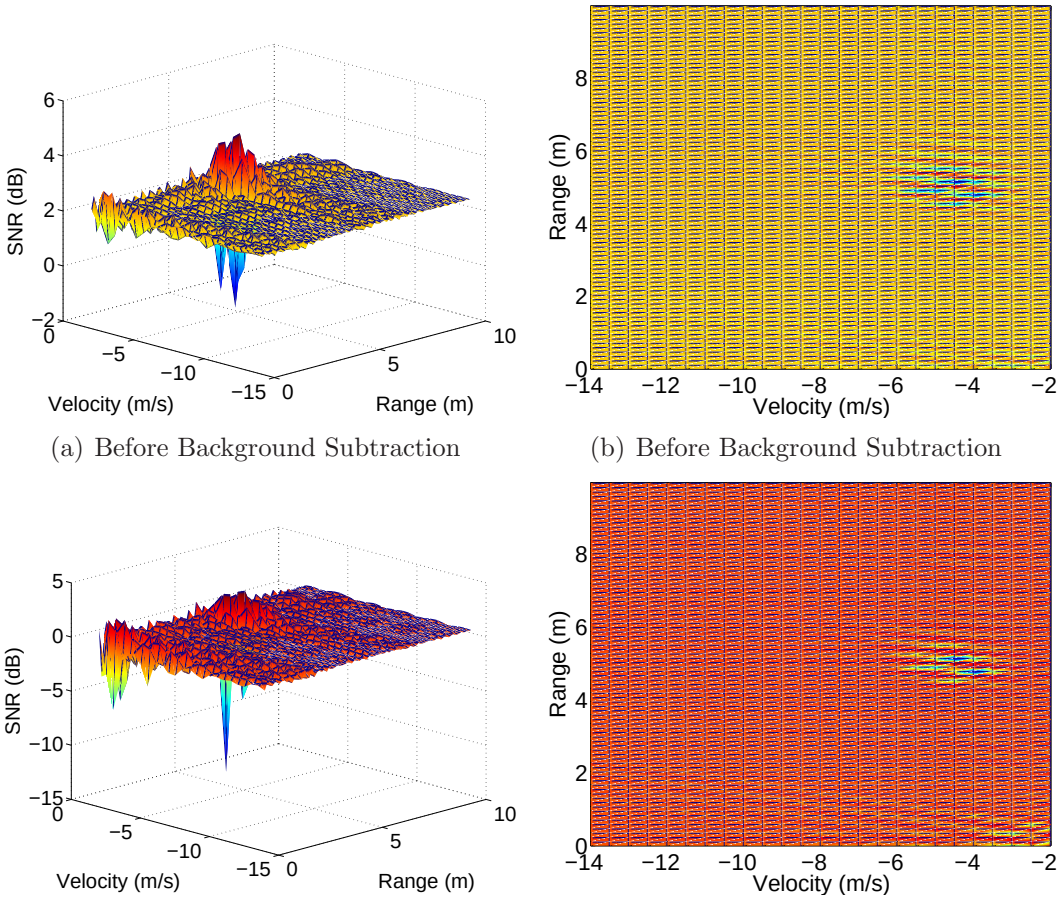

(a) Before Background Subtraction

(b) Before Background Subtraction

(c) After Background Subtraction

(d) After Background Subtraction

Figure 4.11: Results for target parameters of $v = -5$ m/s and $R = 5$ m and collection parameters of $T = 160$ ms, and horizontal antenna polarization.

V. Conclusions

5.1 Overview

This chapter will restate the original research goals and then provide a summary of the results and what contributions were made. Lastly, suggested changes for future work are given.

5.2 Research Goals

The primary goal was to demonstrate the AFIT UWB RNR's capability to extract the velocity from a moving target through non-coherent, digital correlation in the time domain. The secondary goal expands the previous to include extracting a target's velocity and range simultaneously with the AFIT UWB RNR through non-coherent, 2D, digital cross-correlation in the time domain. These goals can greatly improve the AFIT UWB RNR system.

5.3 Results and Contribution

The results shown in Chapter IV and Appendix A illustrate the level of accuracy the AFIT UWB RNR contained when performing a 2D, digital cross-correlation in the time domain. The correct velocity and range were depicted with the respective resolutions of approximately $\Delta v = 3$ m/s and $\Delta R = 1$ m when the measurement time was $T = 160$ ms. The velocity and range resolutions when $T = 80$ ms were approximately $\Delta v = 6$ m/s and $\Delta R = 1$ m. The benefit of 2D correlation requires multiple targets to be within both resolutions in order for the radar to detect only one target. For a 2D correlation over $T = 160$ ms, if two point scatterers are moving at the same speed but separated by more than one meter, the AFIT UWB RNR would still see two targets.

The results matched the expected range resolution given in Figure 3.6, $\Delta R = 1$ m. However, the expected velocity resolution for $f_H = 520$ MHz and $T = 160$ ms was roughly 0.5 m/s, while the results showed a $\Delta v = 3$ m/s. It is believed the difference between the theoretical and measured velocity resolutions can be attributed

to the timing accuracy and quantization error of the Tektronix® digital phosphor oscilloscope (DPO) 7254.

The time accuracy for the DPO 7254 is given as ±2.5 parts per million (ppm). For a desired measurement window of $T = 160$ ms, the timing accuracy causes the measurement window to be $T = 160 \pm 0.004$ ms. Since the measured signal is of length 200 million, each sample can have a timing error of ± 4 μs$/200e6 = \pm 20$ fs. A timing error of ±20 fs is relatively large when compared to the time shifts that the initial samples experience, $(k-1)\Delta t$. For example, the smallest time shift in the received signal sampled at 1.25 Gsamp/s for a target moving at -5 m/s is $\Delta t = 2v/((c-v)f_s) = 2(-5)/((c+5)1.25e9) = -27$ as $= -0.027$fs, while the largest time shift is $(200e6-1)\Delta t = -5.337$ ns $= -5,337,000$ fs.

The major drawback is the same as it was in the 1960s, the number of computations. The velocity resolution is controlled by the maximum sampled frequency, which in the AFIT UWB RNR equals the maximum transmitted frequency f_H, and the measurement window, T. According to Figure 2.9, the velocity resolution is equally dependent on f_H and T. Therefore, the length of the cross-correlated signals, L, cannot be lessoned since $L = \lceil f_s \cdot T \rceil = \lceil 2f_H \cdot T \rceil$, assuming the transmit and receive signals are not modulated down to intermediate or baseband frequencies. Therefore, if the maximum transmitted frequency is doubled, then the measurement window would decrease by half to achieve the same original velocity resolution. However, the length of the signals would remain unchanged and thus offering no benefit to the number of computations.

As technology continues advancing, this method of 2D digital cross-correlation in the time domain will become very useful in extracting a target's range and velocity simultaneously.

5.4 Future Work

The future work has been divided up into system hardware improvements and transmit waveform alterations. Each plays an important role in the size of the system and the processing speed for 2D cross-correlation in the time domain.

5.4.1 System Hardware Improvements. System improvements can offer some of the greatest potential benefits to the AFIT UWB RNR. With more capable equipment, it is believed that 2D cross-correlation in the time domain can become faster and more accurate for range/velocity estimates. Some system improvements include:

- Upgraded wideband antennas that maintain a uniform gain across the bandwidth of the signal. This improvement should not only help estimation, but also improve the low probability of intercept (LPI) characteristics the RNR possesses.
- Upgraded analog-to-digital converter (ADC) that not only collects long contiguous data from for two channels, but also needs to be smaller for easy transportation.
- Program a field programmable gate array (FPGA) to run the data processing procedure outlined in Section 4.3.2.4. This will greatly decrease the processing time and may allow near real-time range/velocity estimation. However, the amount of RAM needed will be a limiting factor.

5.4.2 Transmit Waveform Alterations. Other system improvements pertain to the altering the transmitted waveform to achieve faster range/velocity estimation and also help in creating a smaller overall system. The suggested waveform alterations include:

- Use a pseudo random number generator (PRNG) to create the transmit signal.
  - This would allow for a priori knowledge of the signal and greatly improve processing times.

  - Ideally the period of the waveform would be very long so the LPI characteristics are maintained as much as possible.
  - A long waveform period also eliminates any ambiguous range estimations that are caused from the periodicity nature of the waveform.
- Increase the transmit frequency and bandwidth of the signal
  - Increasing both frequency and bandwidth allows the fractional bandwidth to remain relatively unchanged and in turn, causes minor impact to the LPI characteristics of the radar.
  - Increasing the transmit frequency also allows for smaller antennas to be utilized.
  - An increased bandwidth will also improve range resolution.
  - Processing time for 2D cross-correlation in the time domain should not be affected because increasing the frequencies does not change the needed number of samples for accurate velocity estimation. It would require higher sampling rates; therefore, it might be best to modulate down to an intermediate frequency before digital signal processing.

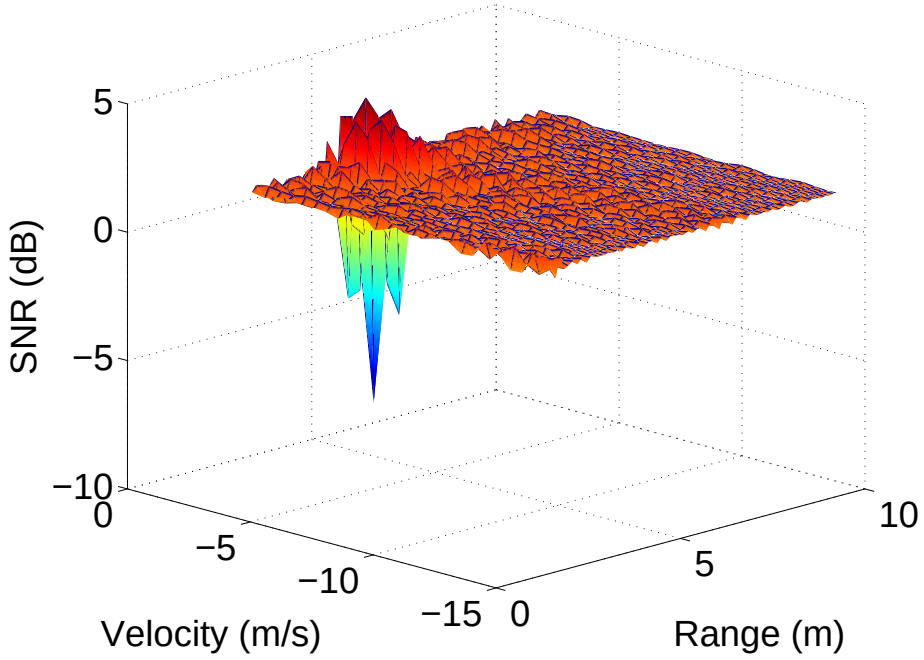

(a) Before Background Subtraction

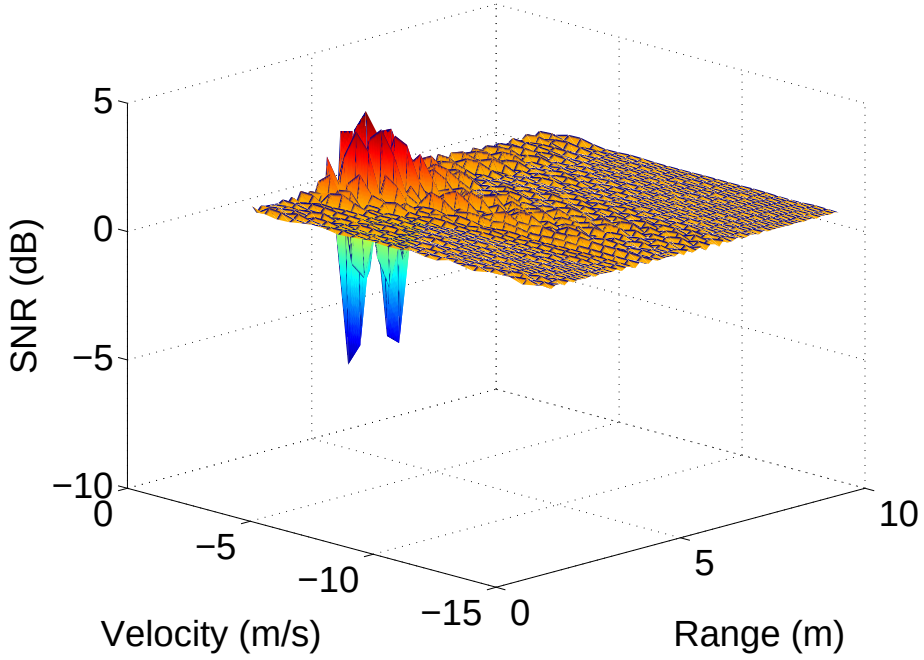

(b) After Background Subtraction

Figure A.1: Results for target parameters of $v = -3$ m/s and $R = 5$ m and collection parameters of $T = 160$ ms, $f_s = 1.25$ Gsamp/s, and horizontal antenna polarization.

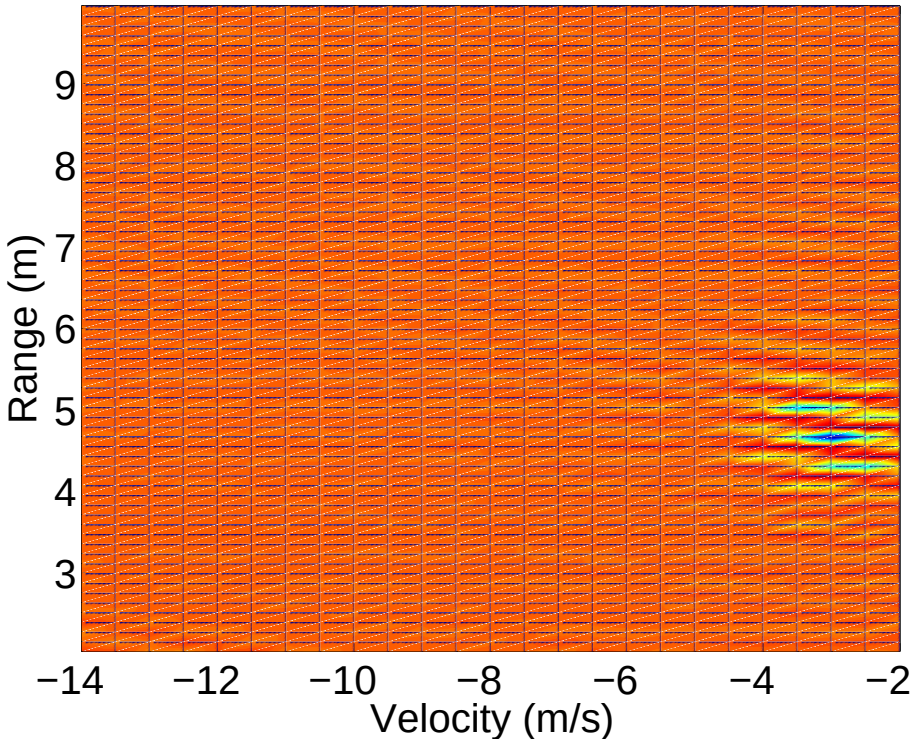

(a) Before Background Subtraction

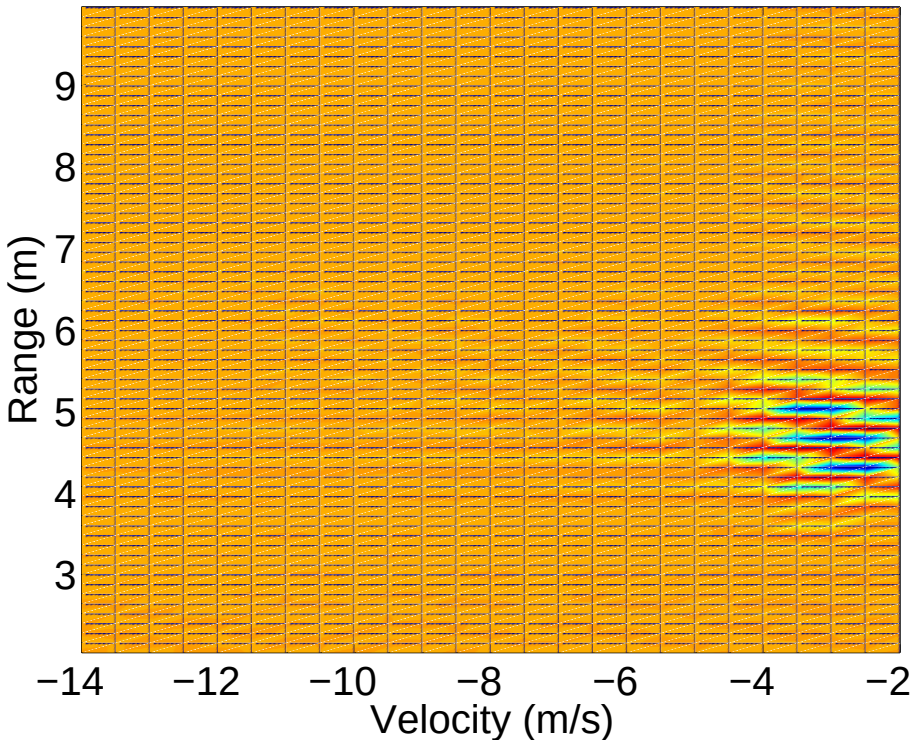

(b) After Background Subtraction

Figure A.2: Top view of Figure A.1

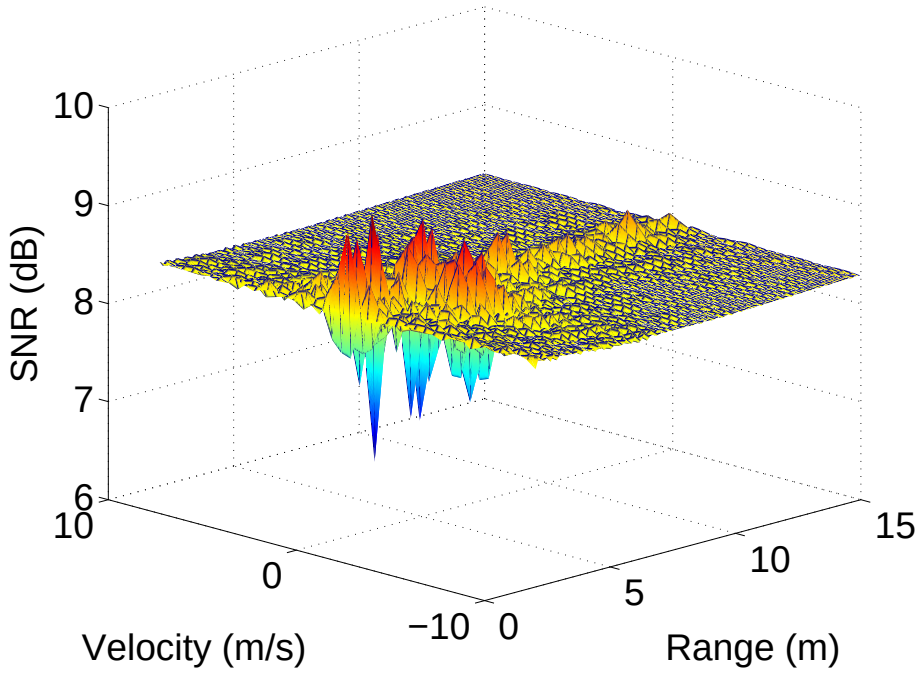

(a) Before Background Subtraction

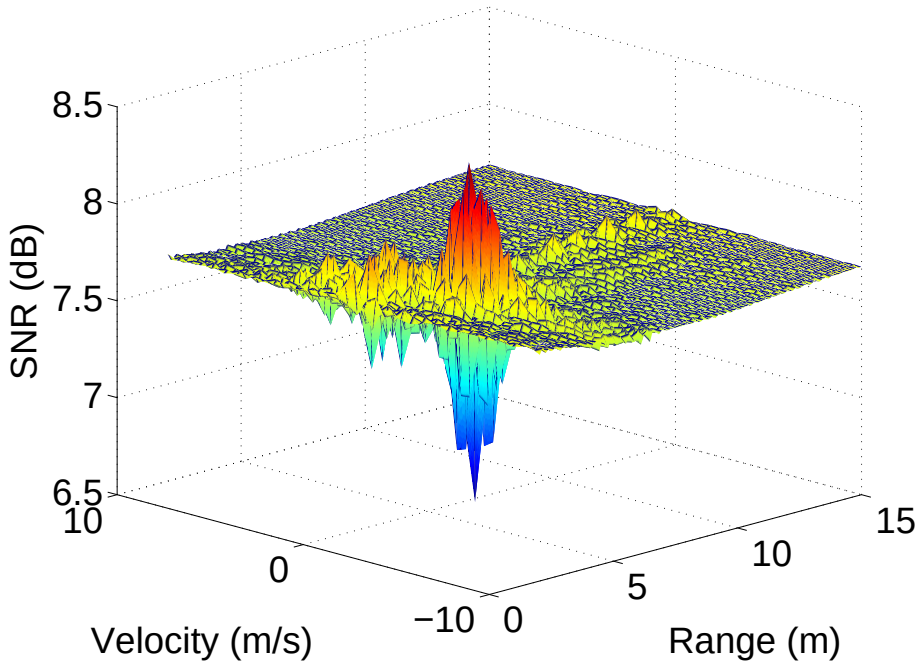

(b) After Background Subtraction

Figure A.3: Results for target parameters of $v = -3$ m/s and $R = 5$ m and collection parameters of $T = 160$ ms, $f_s = 1.25$ Gsamp/s, and horizontal antenna polarization.

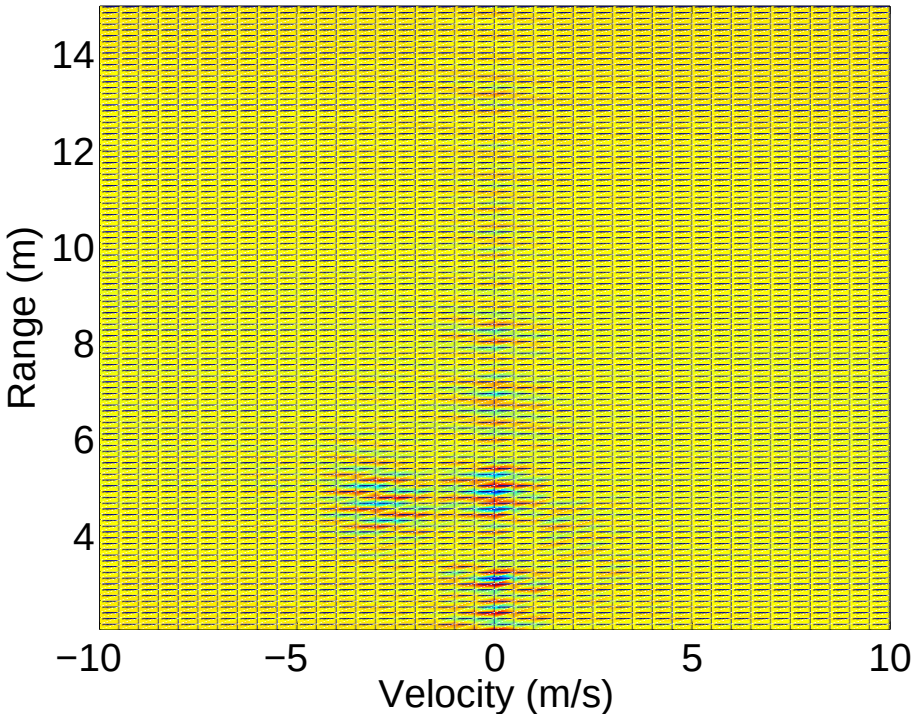

(a) Before Background Subtraction

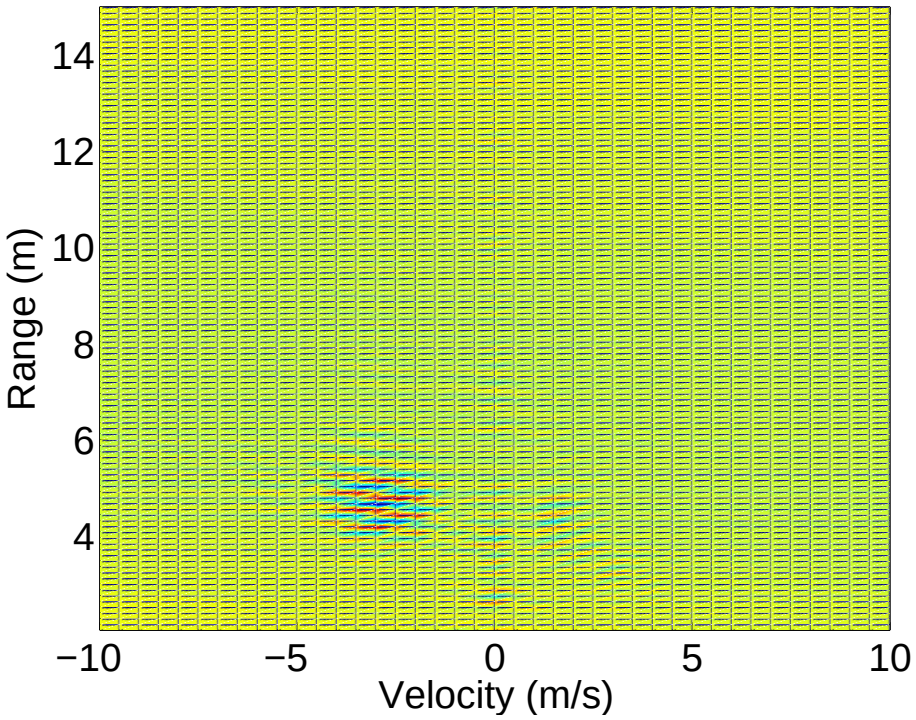

(b) After Background Subtraction

Figure A.4: Top view of Figure A.3

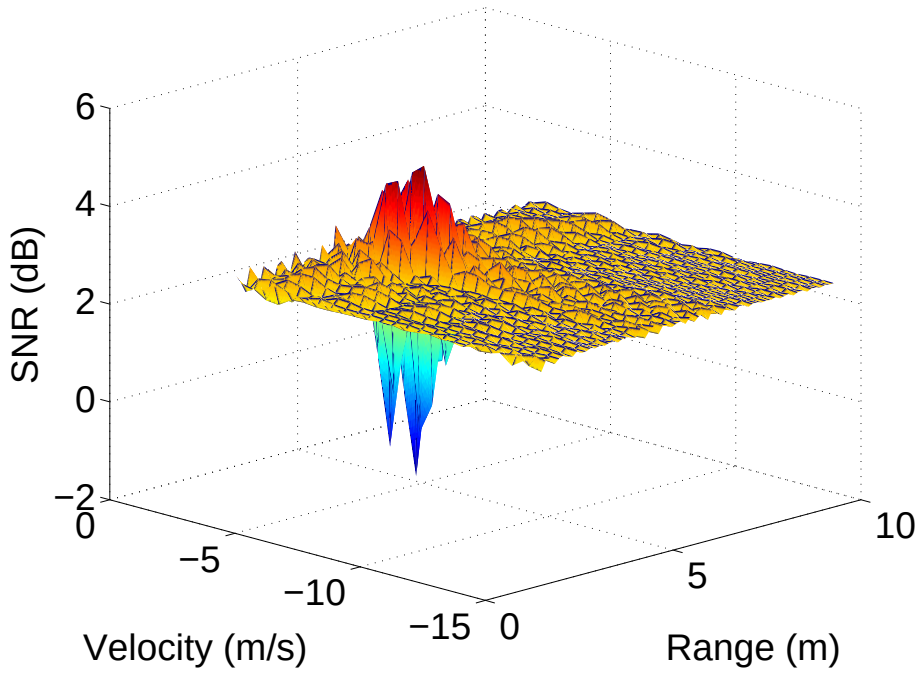

(a) Before Background Subtraction

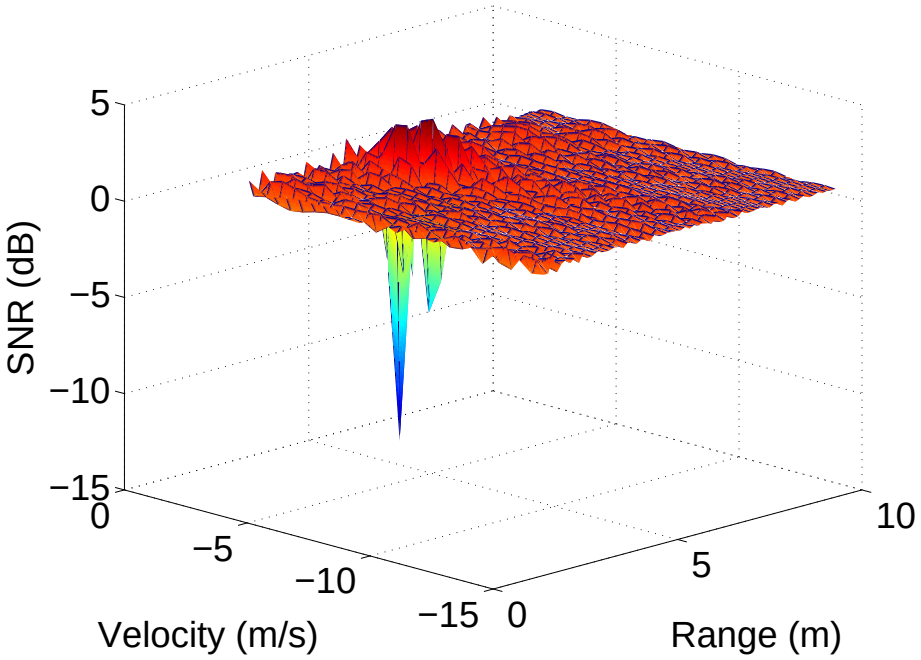

(b) After Background Subtraction

Figure A.5: Results for target parameters of $v = -5$ m/s and $R = 5$ m and collection parameters of $T = 160$ ms, $f_s = 1.25$ Gsamp/s, and horizontal antenna polarization.

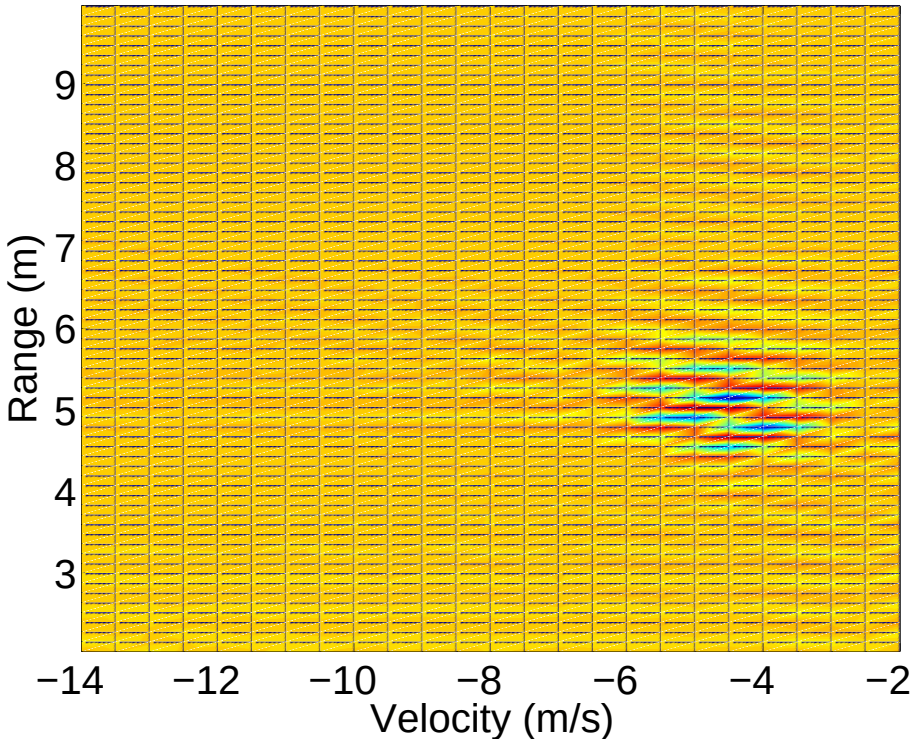

(a) Before Background Subtraction

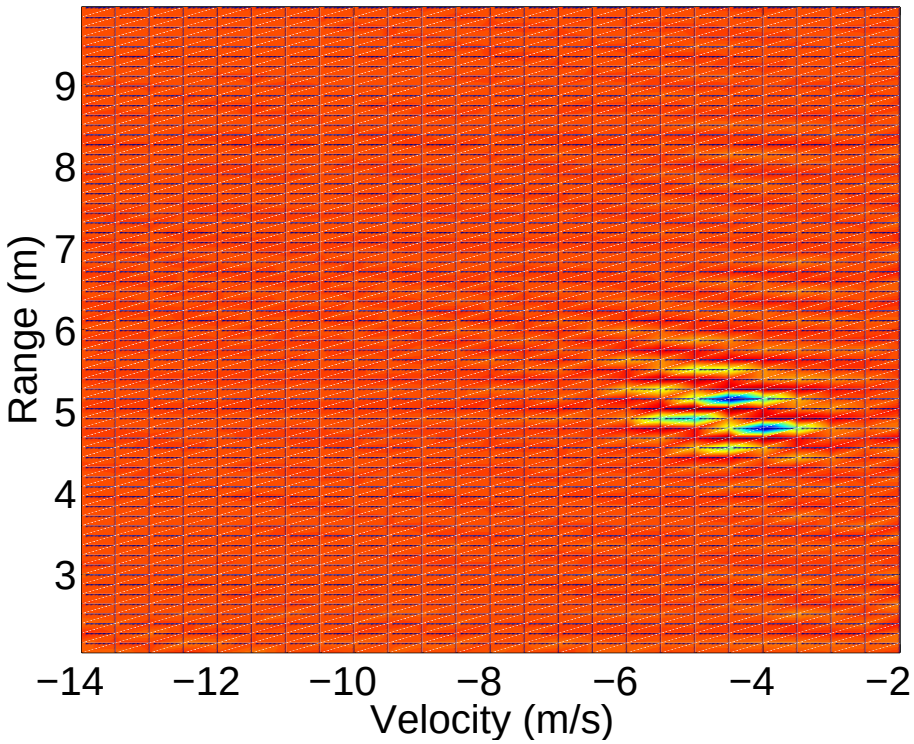

(b) After Background Subtraction

Figure A.6: Top view of Figure A.5

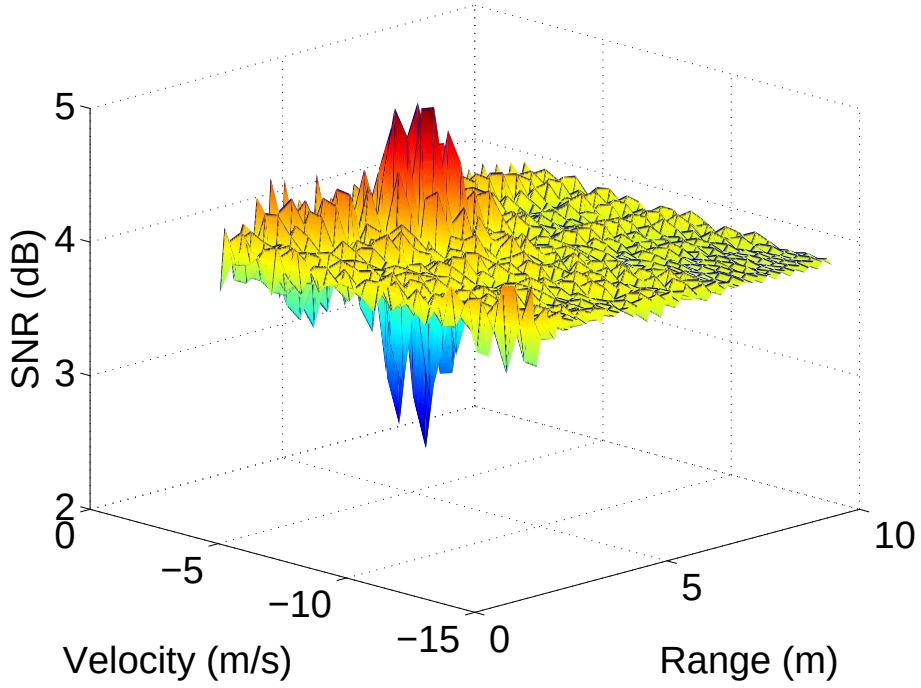

(a) Before Background Subtraction

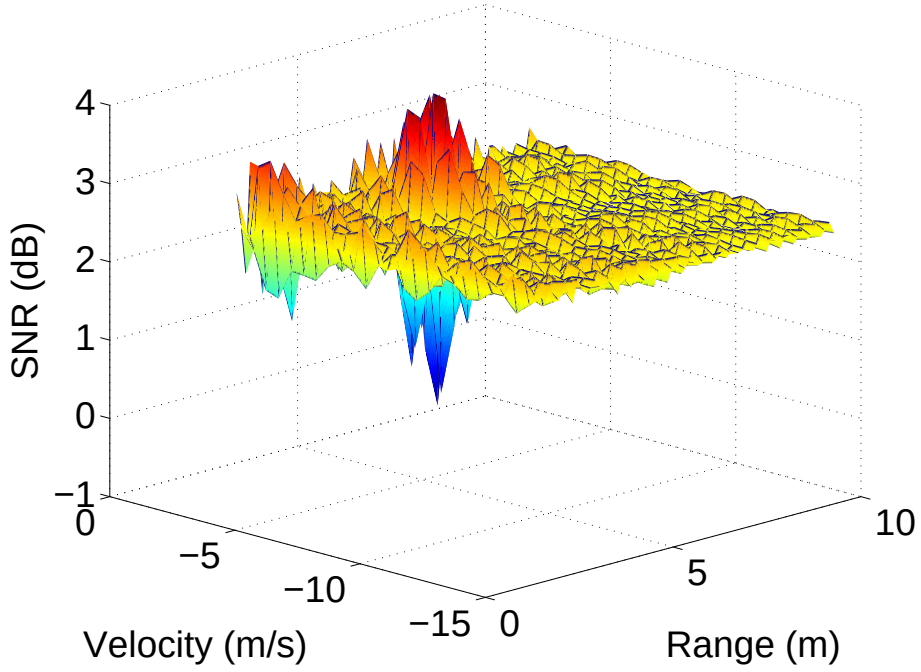

(b) After Background Subtraction

Figure A.7: Results for target parameters of $v = -5$ m/s and $R = 5$ m and collection parameters of $T = 160$ ms, $f_s = 1.25$ Gsamp/s, and vertical antenna polarization.

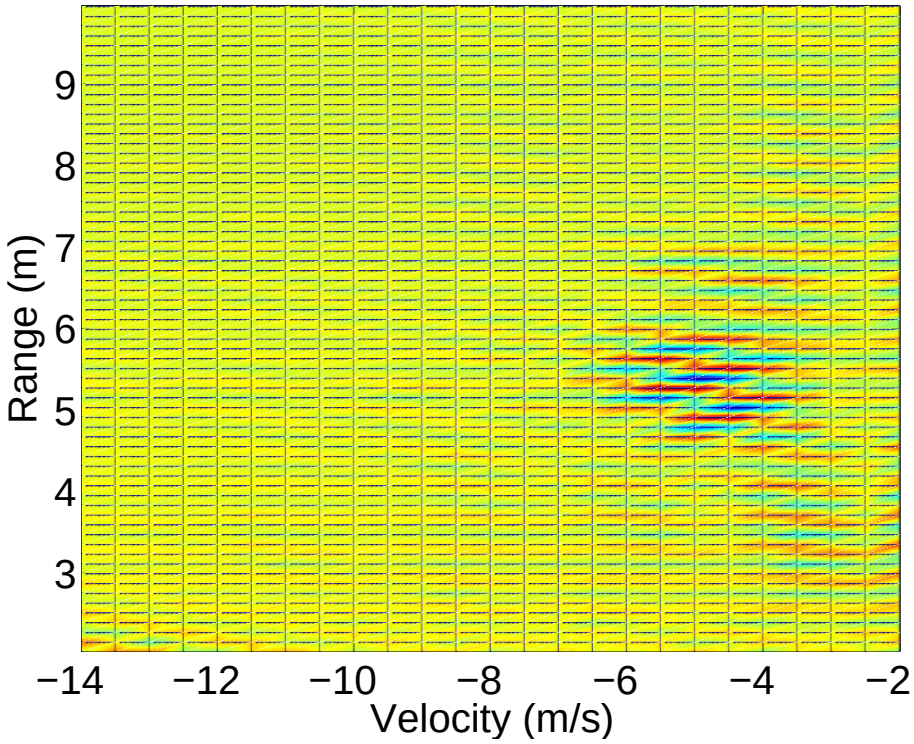

(a) Before Background Subtraction

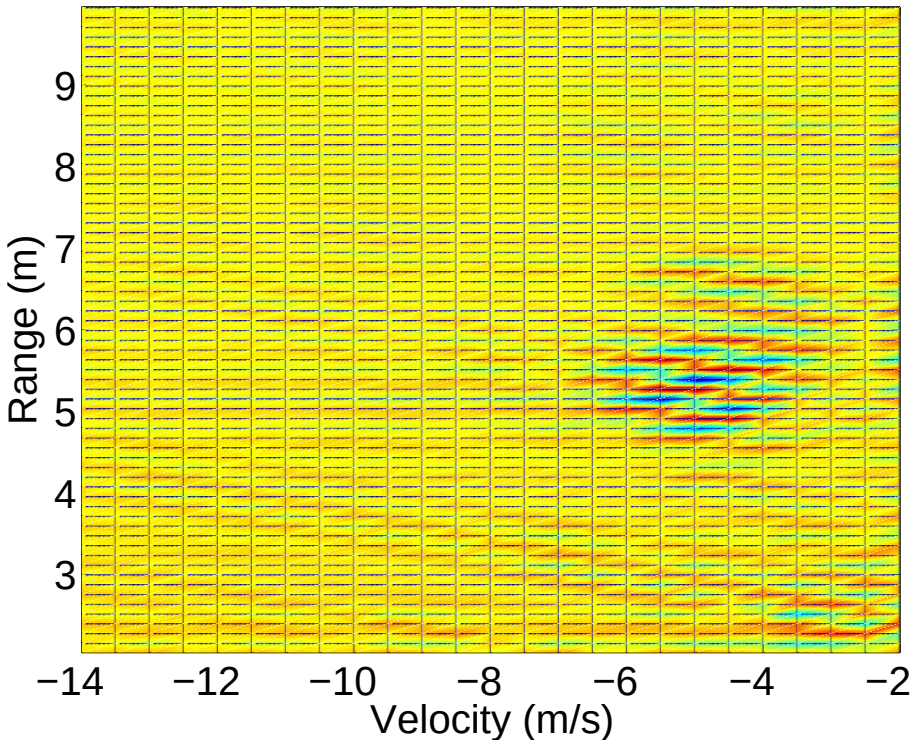

(b) After Background Subtraction

Figure A.8: Top view of Figure A.7

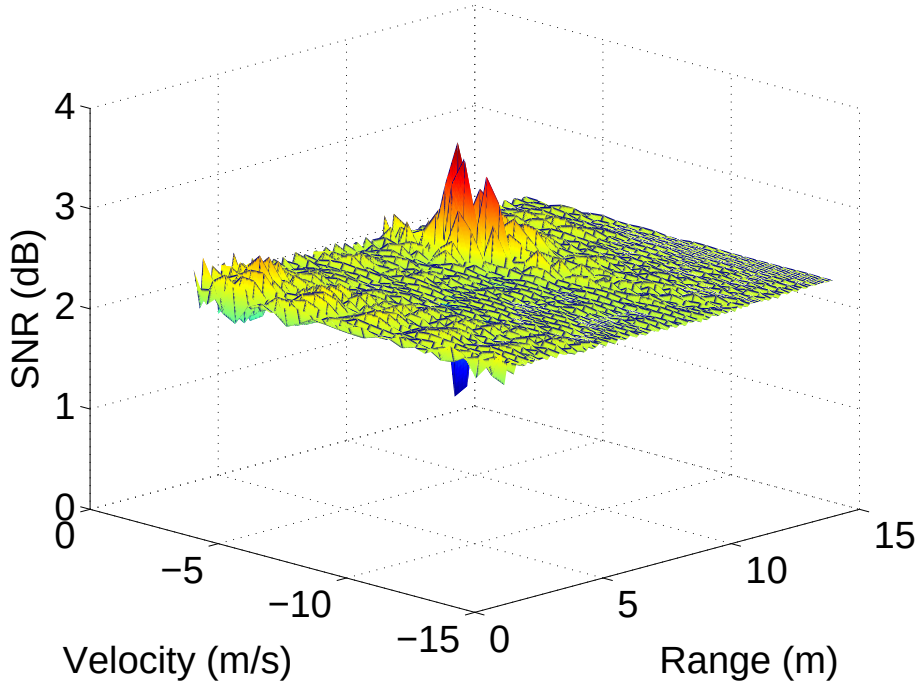

(a) Before Background Subtraction

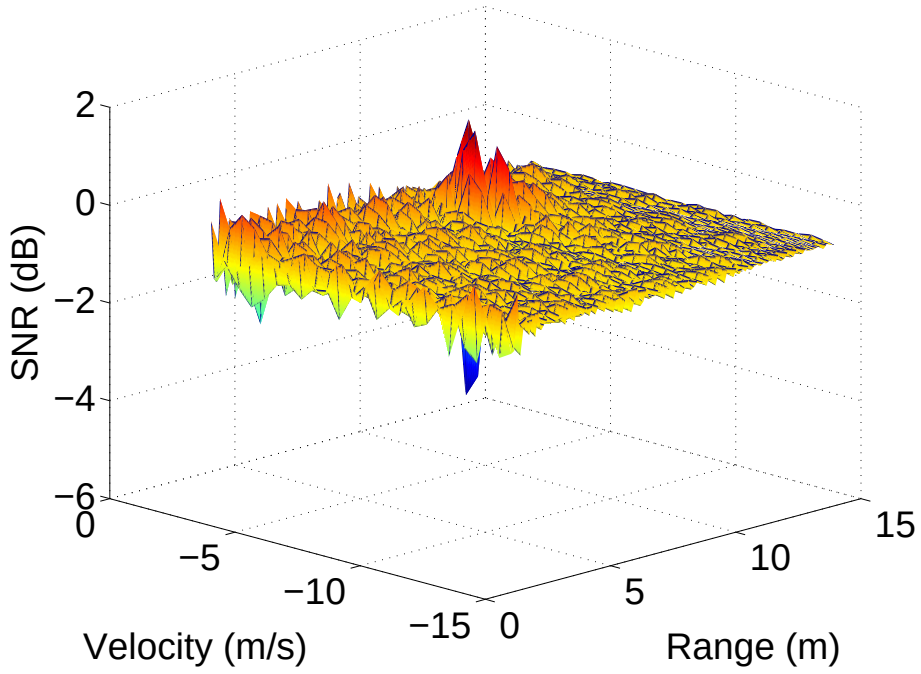

(b) After Background Subtraction

Figure A.9: Results for target parameters of $v = -5$ m/s and $R = 10$ m and collection parameters of $T = 160$ ms, $f_s = 1.25$ Gsamp/s, and horizontal antenna polarization.

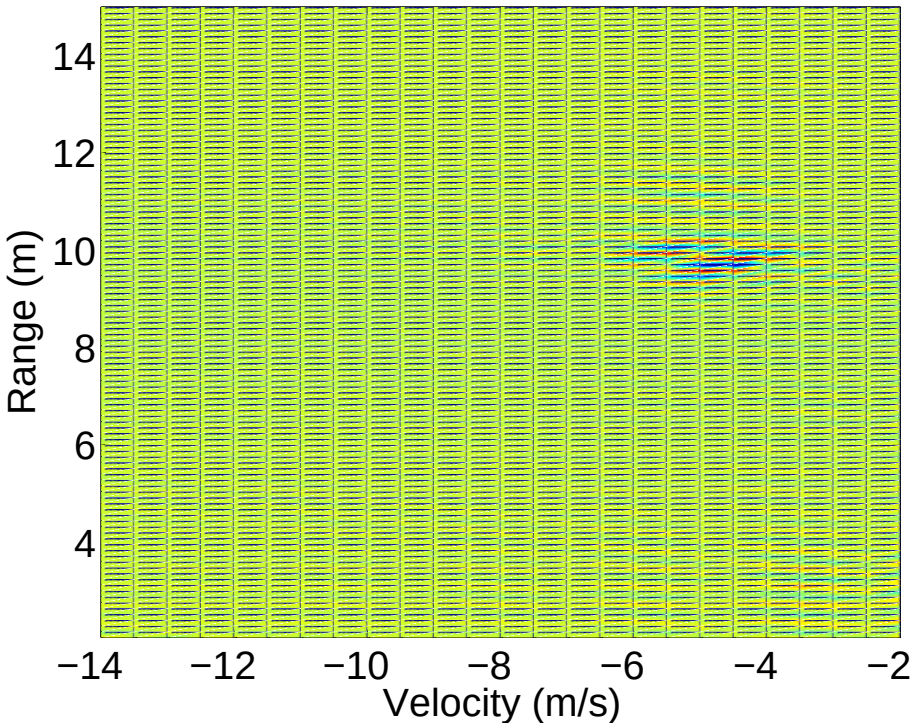

(a) Before Background Subtraction

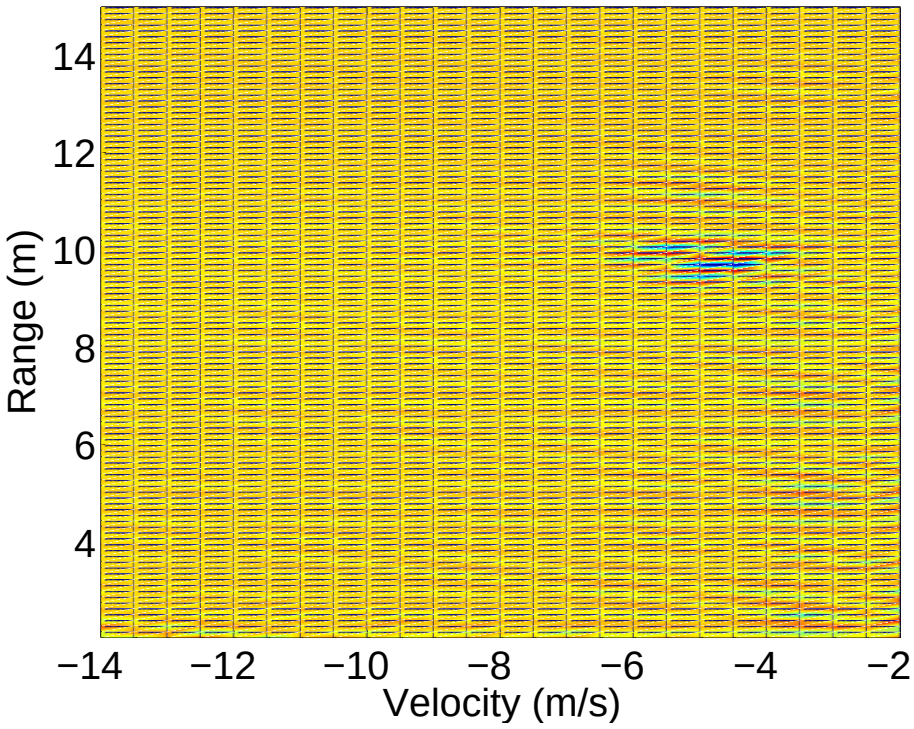

(b) After Background Subtraction

Figure A.10: Top view of Figure A.9

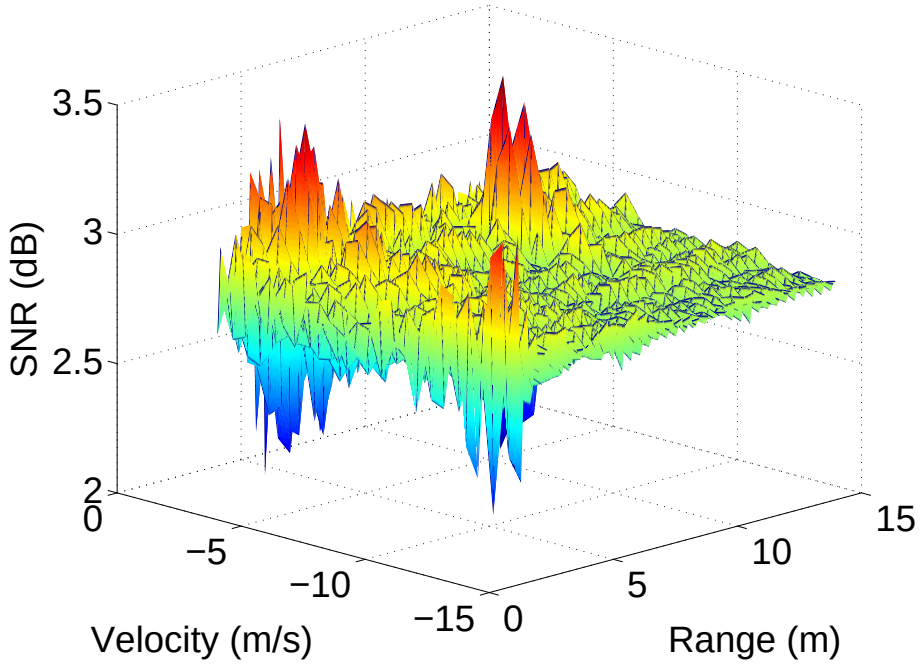

(a) Before Background Subtraction

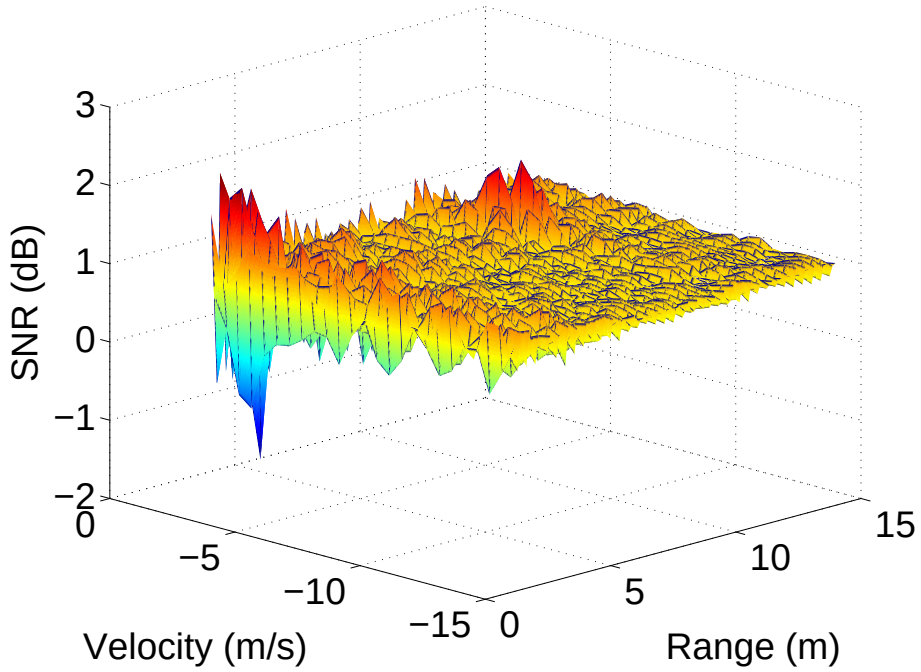

(b) After Background Subtraction

Figure A.11: Results for target parameters of $v = -5$ m/s and $R = 10$ m and collection parameters of $T = 160$ ms, $f_s = 1.25$ Gsamp/s, and vertical antenna polarization.

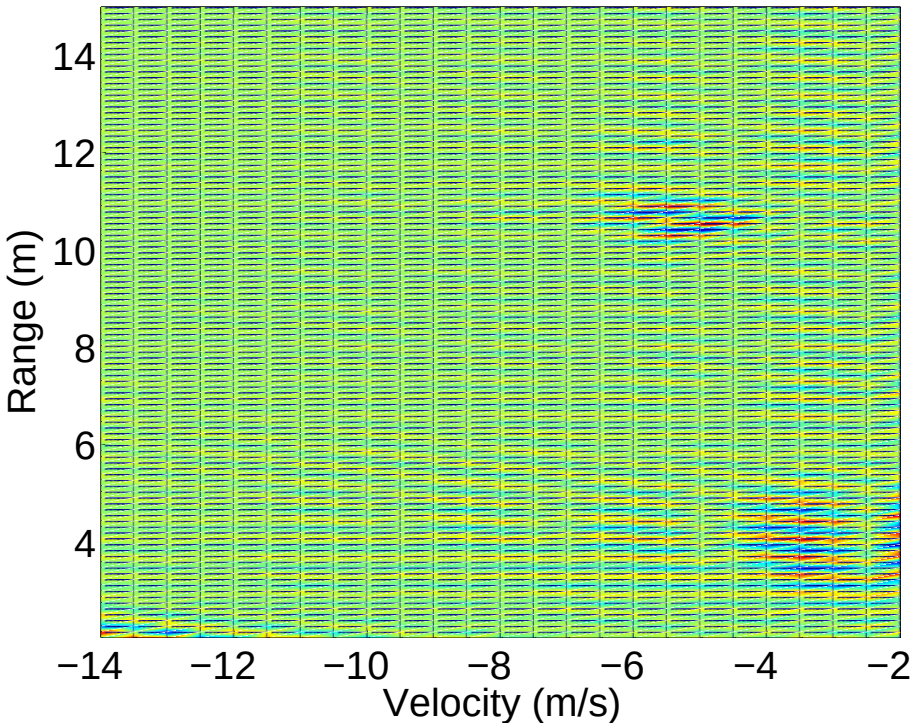

(a) Before Background Subtraction

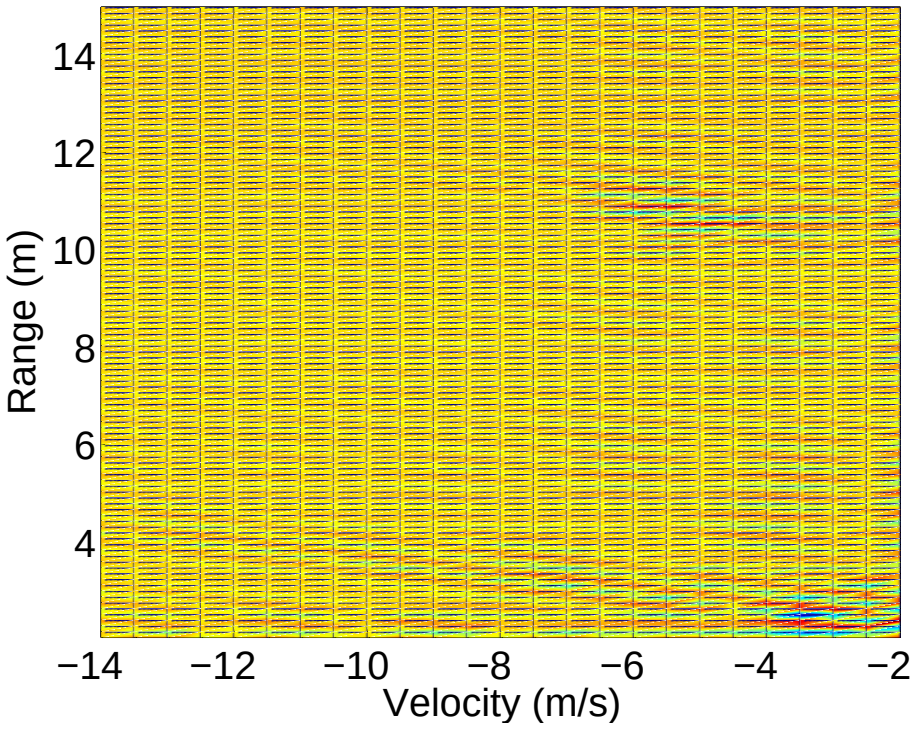

(b) After Background Subtraction

Figure A.12: Top view of Figure A.11

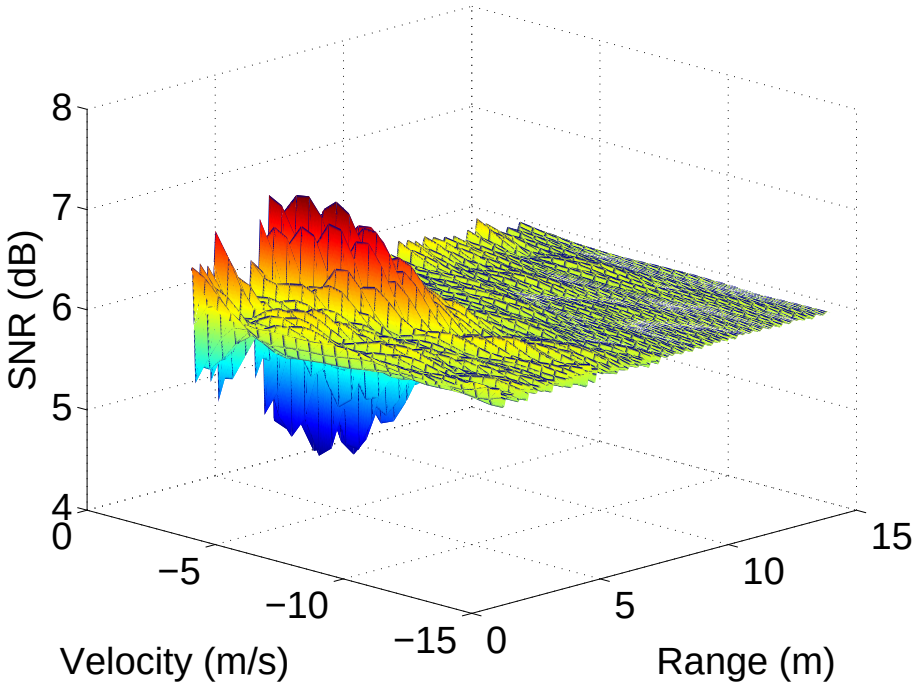

(a) Before Background Subtraction

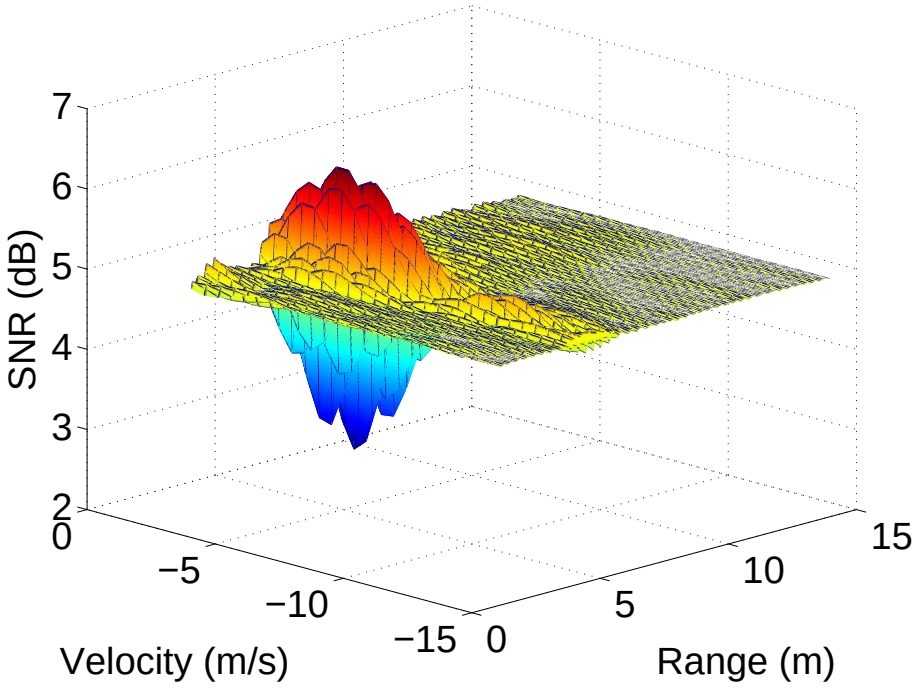

(b) After Background Subtraction

Figure A.13: Results for target parameters of $v = -5$ m/s and $R = 5$ m and collection parameters of $T = 80$ ms, $f_s = 2.5$ Gsamp/s, and horizontal antenna polarization.

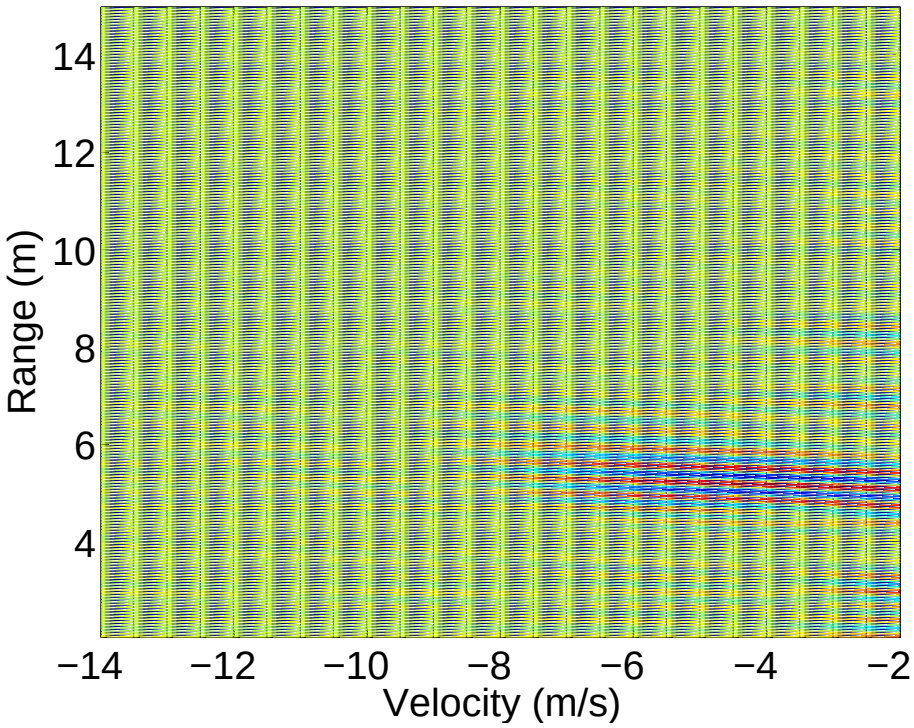

(a) Before Background Subtraction

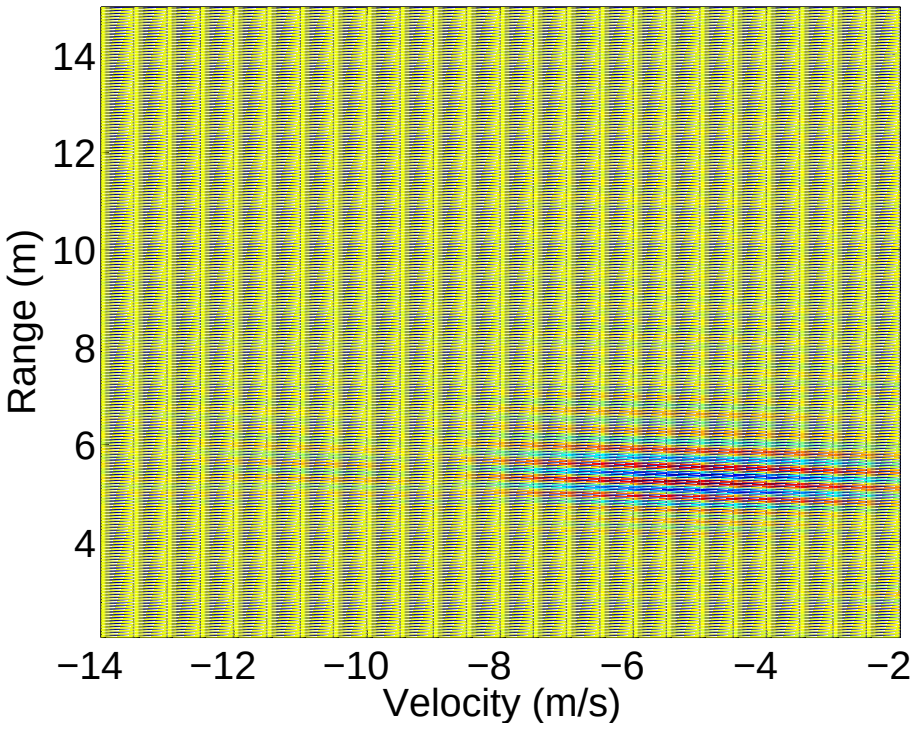

(b) After Background Subtraction

Figure A.14: Top view of Figure A.13

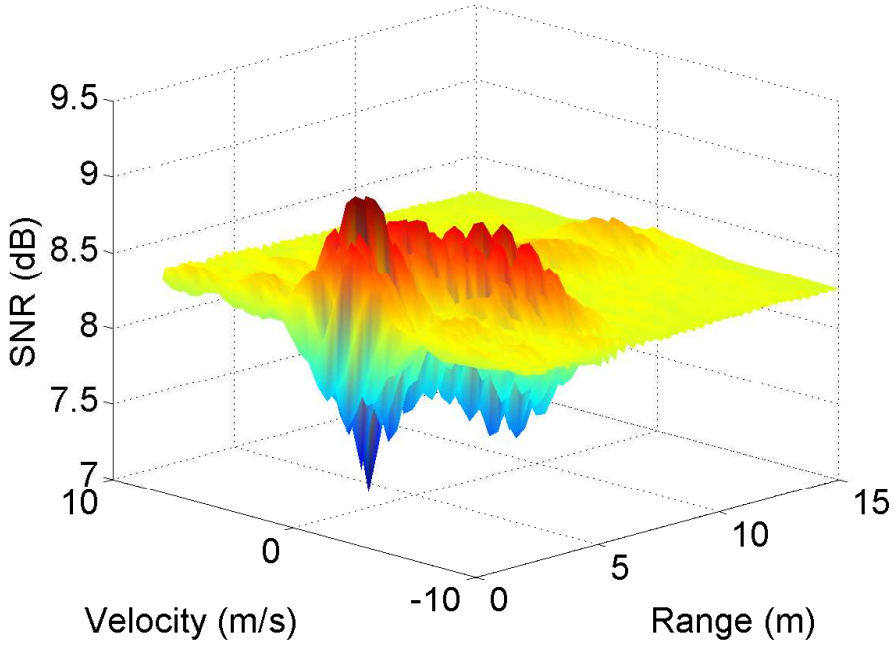

(a) Before Background Subtraction

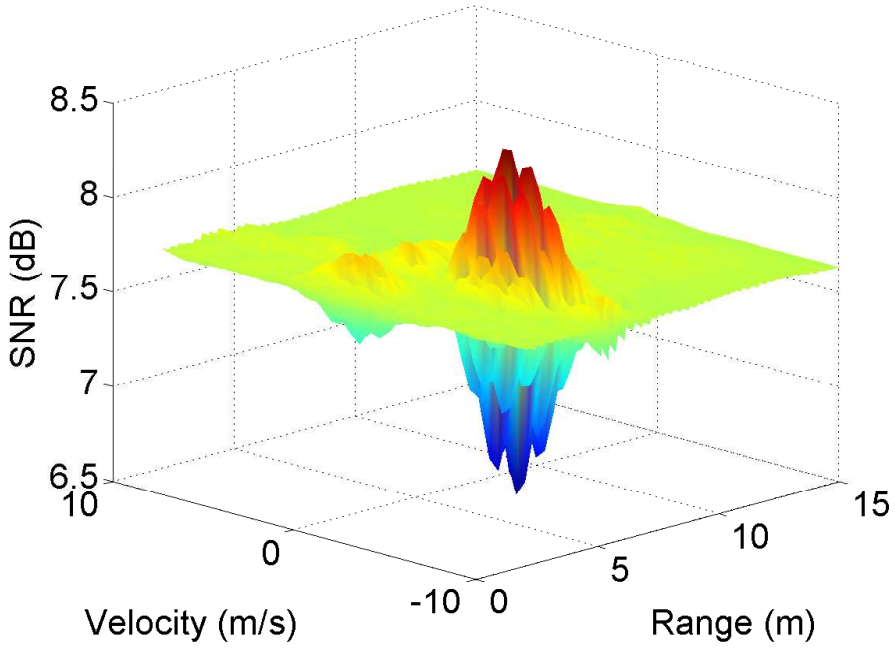

(b) After Background Subtraction

Figure A.15: Results for target parameters of $v = -5$ m/s and $R = 5$ m and collection parameters of $T = 80$ ms, $f_s = 2.5$ Gsamp/s, and horizontal antenna polarization.

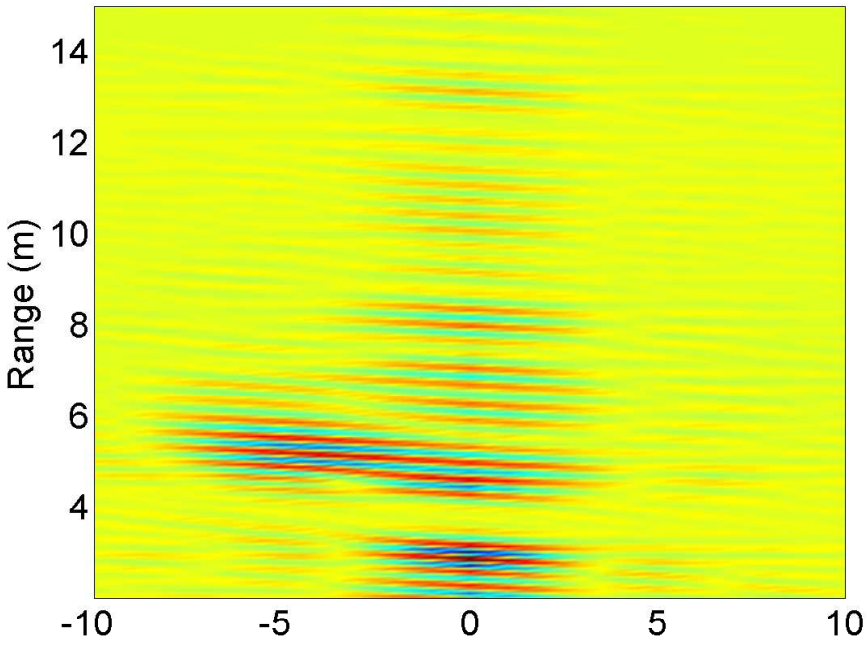

(a) Before Background Subtraction

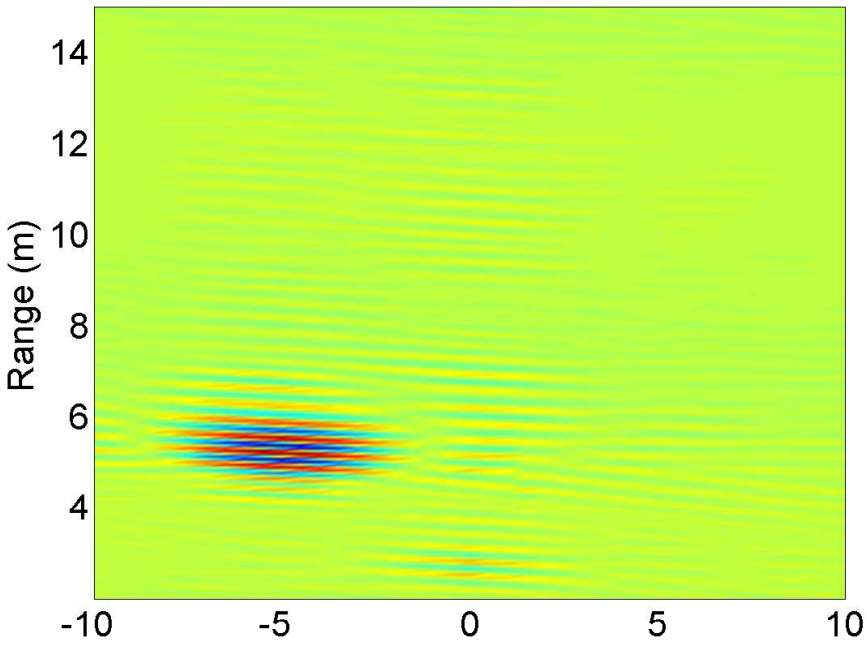

(b) After Background Subtraction

Figure A.16: Top view of Figure A.15

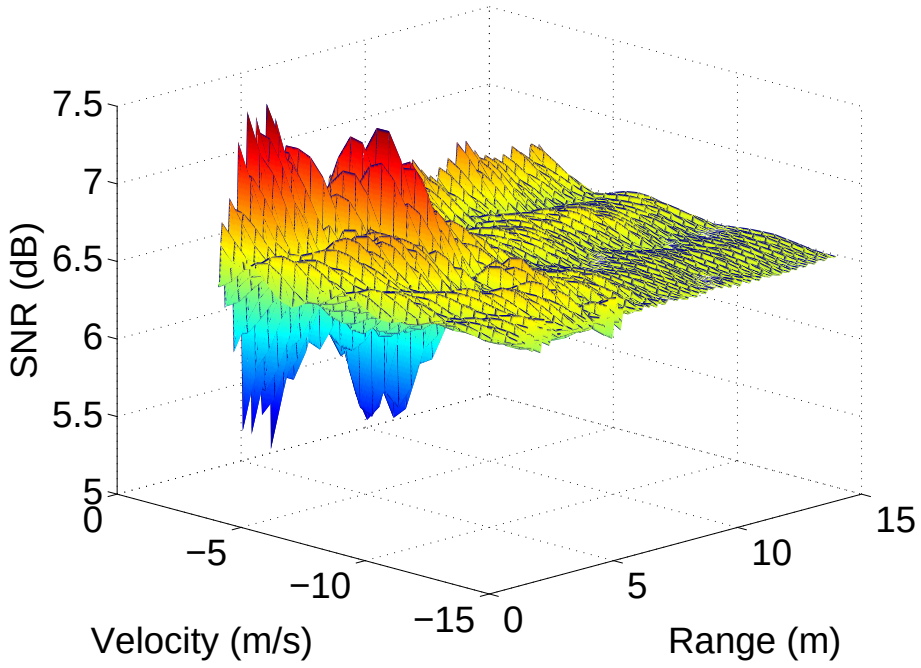

(a) Before Background Subtraction

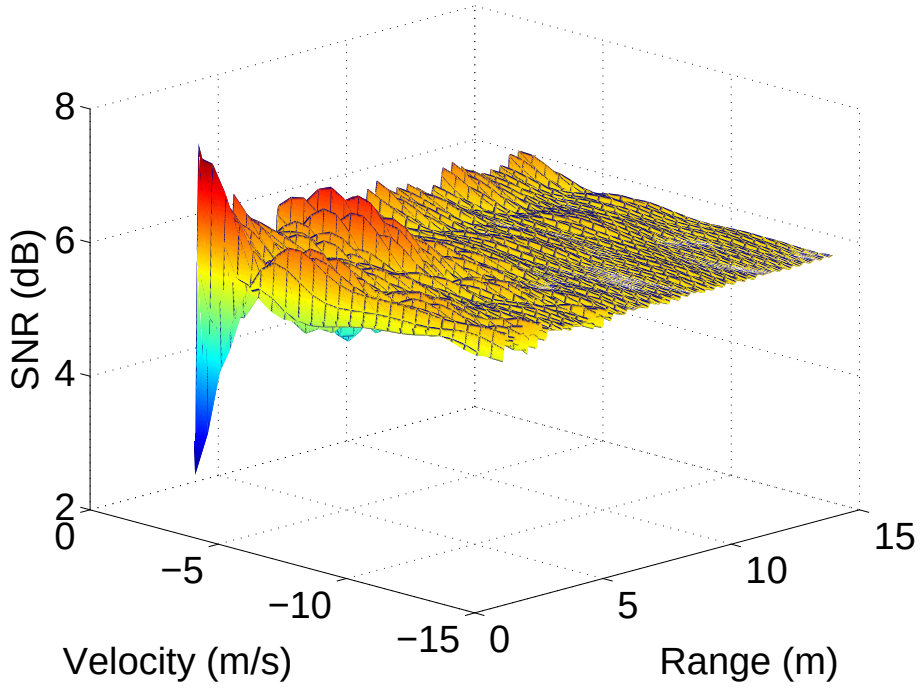

(b) After Background Subtraction

Figure A.17: Results for target parameters of $v = -5$ m/s and $R = 5$ m and collection parameters of $T = 80$ ms, $f_s = 2.5$ Gsamp/s, and vertical antenna polarization.

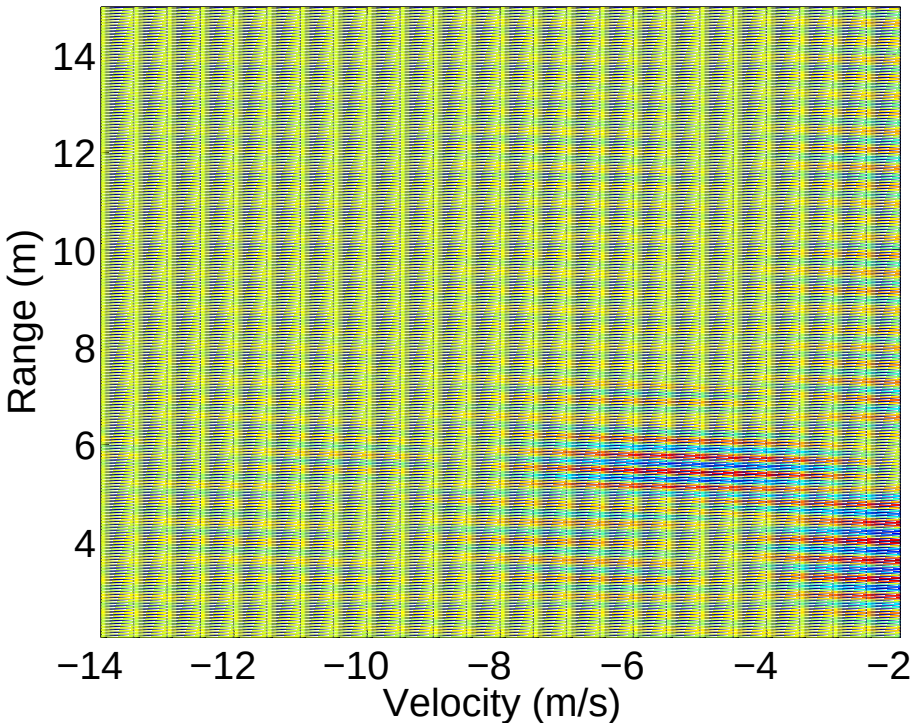

(a) Before Background Subtraction

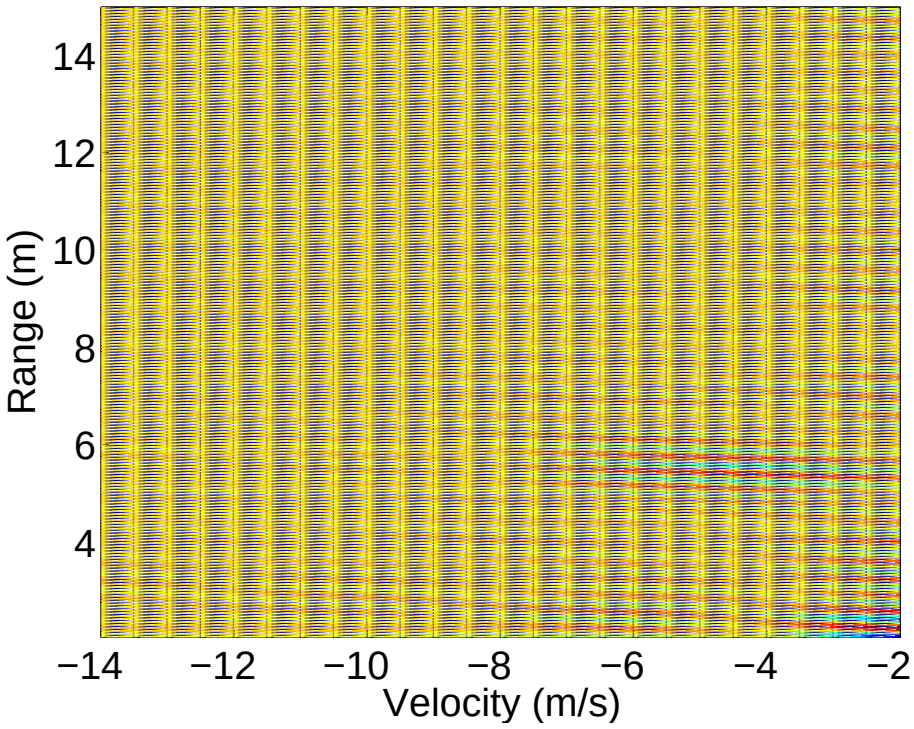

(b) After Background Subtraction

Figure A.18: Top view of Figure A.17

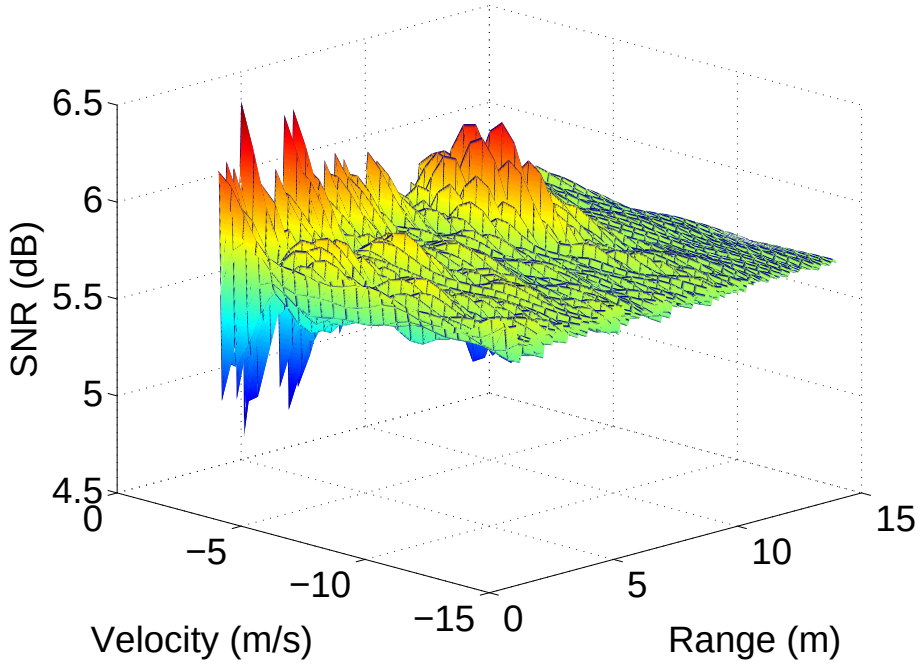

(a) Before Background Subtraction

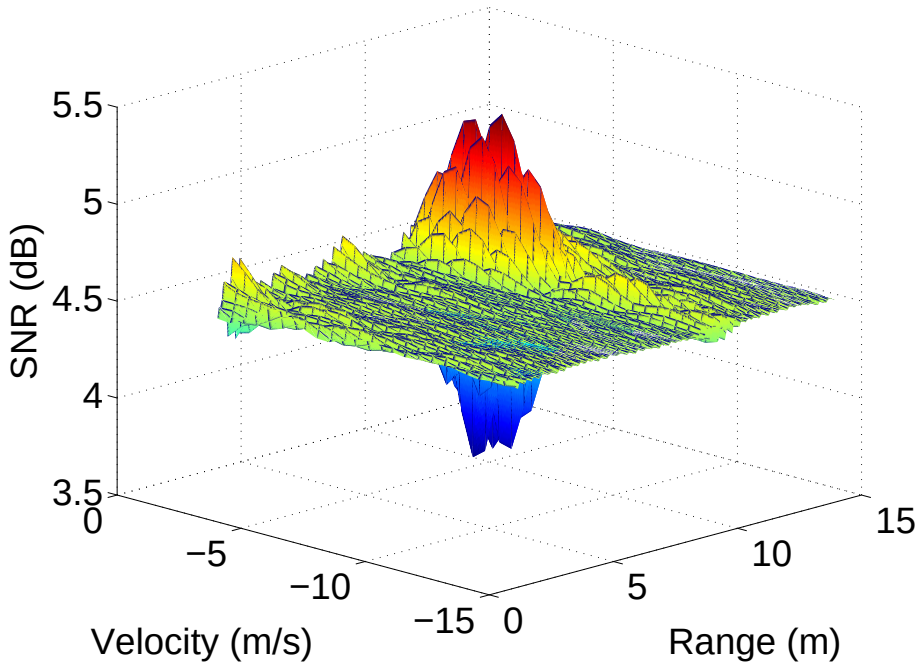

(b) After Background Subtraction

Figure A.19: Results for target parameters of $v = -5$ m/s and $R = 10$ m and collection parameters of $T = 80$ ms, $f_s = 2.5$ Gsamp/s, and horizontal antenna polarization.

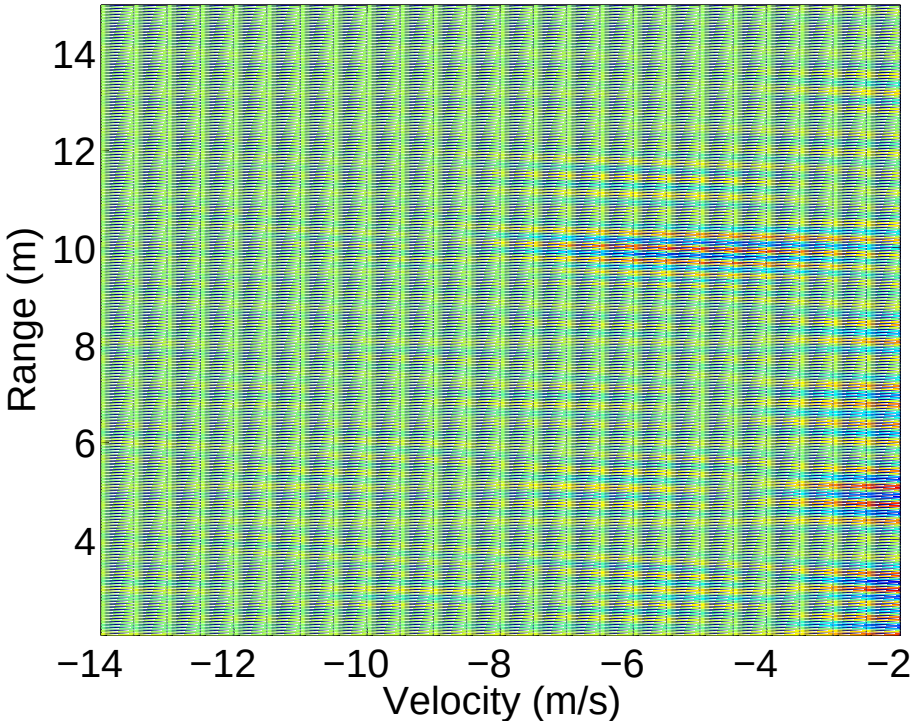

(a) Before Background Subtraction

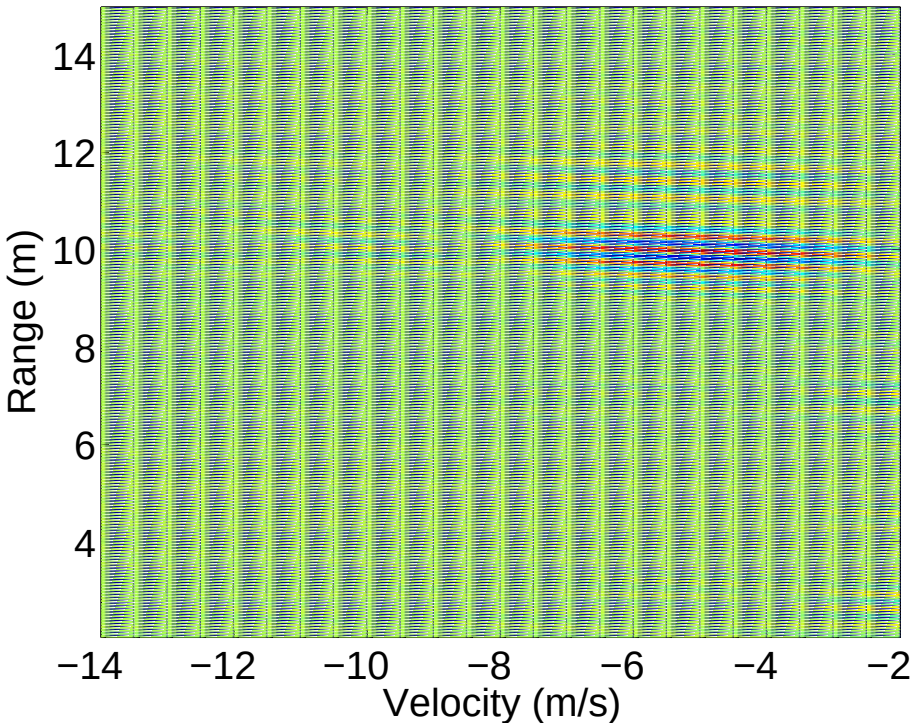

(b) After Background Subtraction

Figure A.20: Top view of Figure A.19

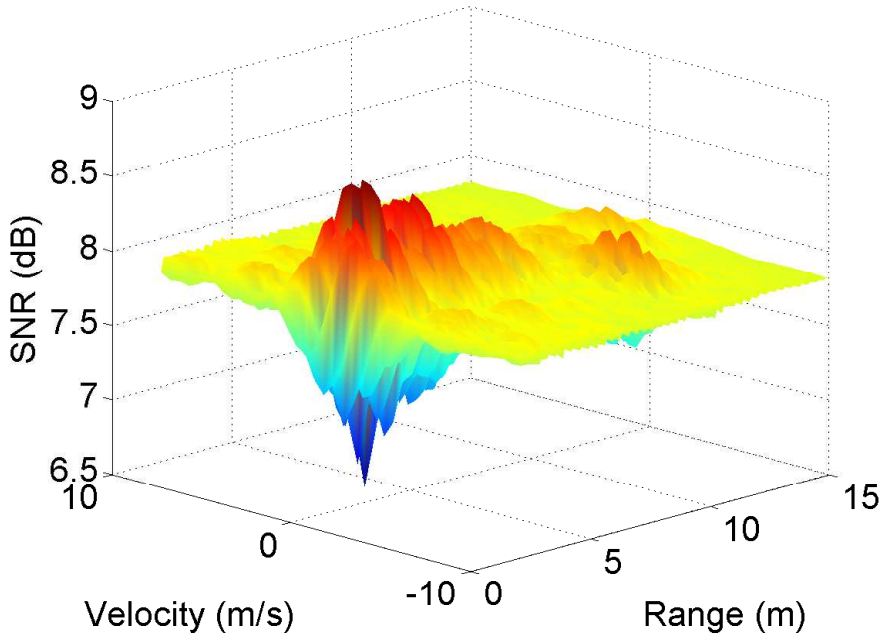

(a) Before Background Subtraction

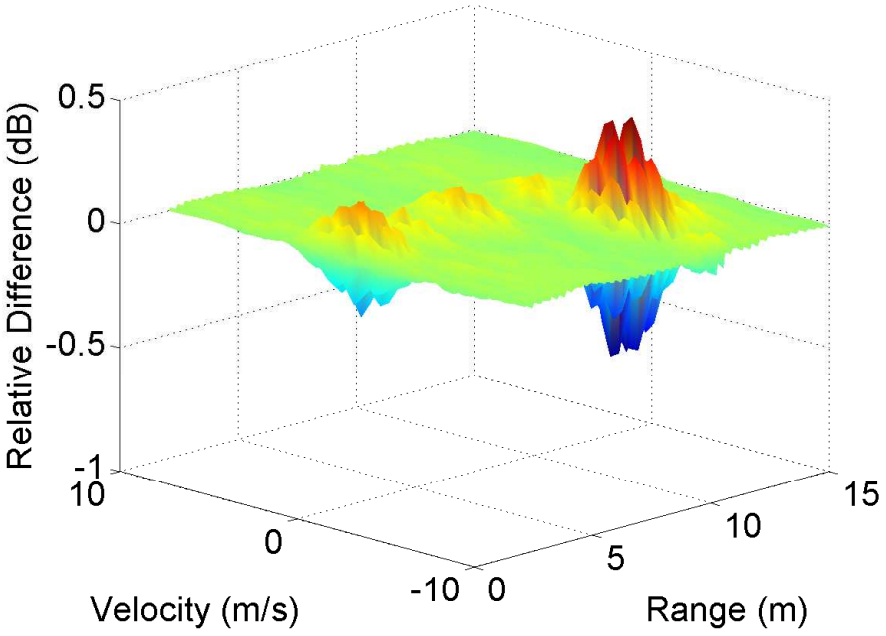

(b) After Background Subtraction

Figure A.21: Results for target parameters of $v = -5$ m/s and $R = 10$ m and collection parameters of $T = 80$ ms, $f_s = 2.5$ Gsamp/s, and horizontal antenna polarization.

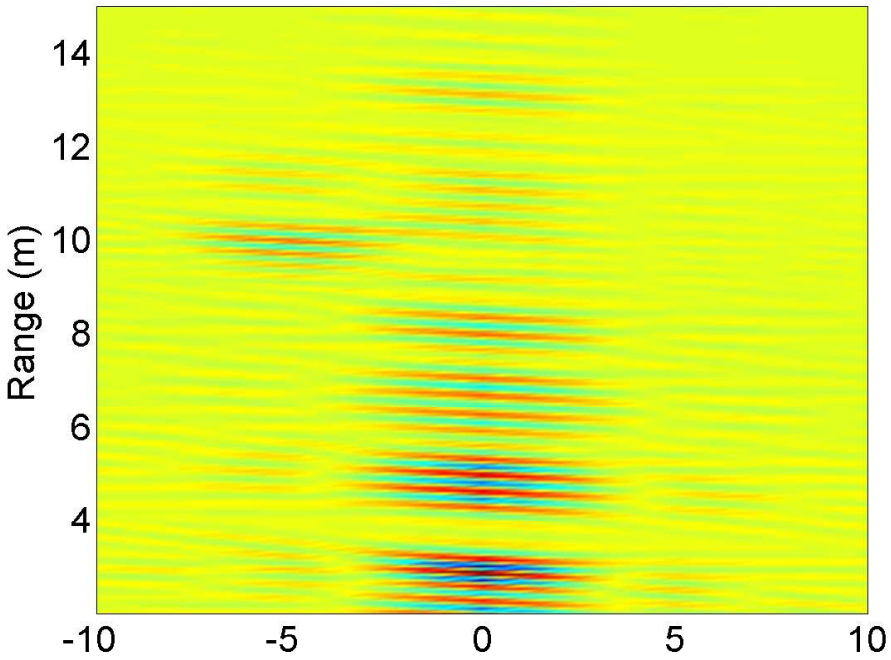

(a) Before Background Subtraction

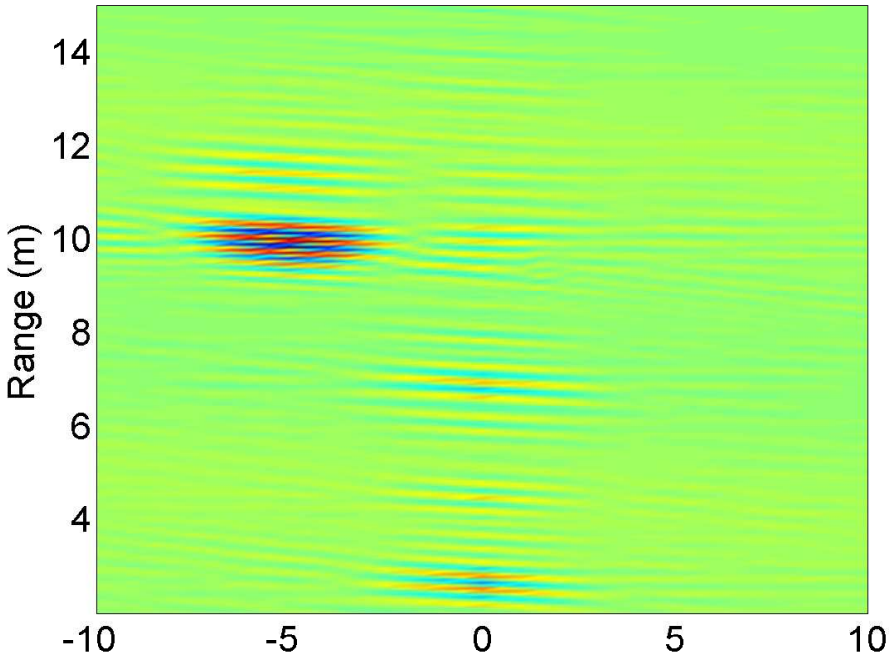

(b) After Background Subtraction

Figure A.22: Top view of Figure A.21

Listing B.1: Transmit_Sig.m

```
function[sig,t]=Transmit_Sig(Bandwidth,Measurement_Window,...
    Sample_Frequency,Center_Frequency)

%%%%%%%%%%%%%%%%%%%%%%%%%%%%%%%%%%%%%%%%%%%%%%%%%%%%%%%%%%%%%%%%%%%%%%%
%  This function simulates the transmitted signal for a random
%  noise radar (RNR) based on user inputs
%
%  Inputs:
%   Bandwidth - Bandwidth of transmit signal
%   Measurement_Window - Time duration of transmit signal
%   Sample_Frequency - Ensure sample freq is at least two times
%       maximum frequency so no aliasing occurs
%   Center_Frequency - Carrier frequency of signal.  Ensure
%       center freq is larger than half the bandwidth
%
%  Outputs:
%   sig - Real band-limited noise signal
%   t - time vector for noise signal
%   Figure(1) - plot of noise signal before and after Butterworth
%       filter is applied.  The "return" at bottom of code must
%       be commented out for the figure to plot
%
%%%%%%%%%%%%%%%%%%%%%%%%%%%%%%%%%%%%%%%%%%%%%%%%%%%%%%%%%%%%%%%%%%%%%%%

%%%%%%%%%%%%%%%% Initial Vectors and Variables %%%%%%%%%%%%%%%%

L = round(Measurement_Window*Sample_Frequency); % Length of ...
    transmit signal
t=(0:1/Sample_Frequency:Measurement_Window-1/Sample_Frequency)'; %...
     Time vector
f=(-Sample_Frequency/2:1/Measurement_Window:Sample_Frequency/2-1/...
    Measurement_Window)'; % Frequency vector used for plotting
```

```
NFFT=length(L); % Length of FFT

%%%%%%%%%%%% Noise Signal that is Not Band-Limited %%%%%%%%%%%%

s=randn(round(L),1)+1i*randn(round(L),1); % Initial noise vector ...
    that is not band limited

%%%%%%%%%%%%%%%%%%%%%% Butterworth Filter %%%%%%%%%%%%%%%%%%%%%%

fcut=Bandwidth/2; % Cutoff freq for Butterworth Filter
fb=(f-Center_Frequency)/fcut; % Lowpass Butterworth relation
n=20; %Butterworth filter order
T=1./sqrt(1+(fb).^(2*n)); % Butterworth transfer function

%%%%%%%%%%%%%%%%%% Band-Limited Noise Signal %%%%%%%%%%%%%%%%%%

S=fftshift(fft(s,NFFT))/sqrt(L); % Initial noise vector in the ...
    frequency domain
Sb=S.*T; % Complex band-limited noise signal in the frequency ...
    domain
sig=ifft(fftshift(Sb),NFFT); % Complex noise signal in the time ...
    domain
sig=real(sig); % Real noise signal, which is what the AFIT UWB RNR...
     transmits

return % Comment out if the transmit signal wants to be viewed in ...
    the frequency domain
figure(1)
plot(f,abs(S),f,abs(Sb),'r')
```

Listing B.2: Simulation.m

```
function [] = Simulation(Target_Velocity, Reference_Velocity_Low, ...
    Reference_Velocity_High, Number_of_Reference_Velocities, ...
    Bandwidth, Measurement_Window, Maximum_Frequency, ...
    Sample_Frequency, SNRdB)

%%%%%%%%%%%%%%%%%%%%%%%%%%%%%%%%%%%%%%%%%%%%%%%%%%%%%%%%%%%%%%%%%%%%%%%
%
% The function simulates the normalized matched filter ouput for
%   a Random Noise Radar (RNR) when the radar is perfectly matched
%   in range.
%
%  Inputs:
%   Target_Velocity - Truth data for simulated target
%   Reference_Velocity_Low - Minimum reference velocity
%   Reference_Velocity_High - Maximum reference velocity
%   Number_of_Reference_Velocities - Number of velocities to
%       correlate
%   Bandwidth - Bandwidth of signal
%   Measurement_Window - Time duration of transmit signal, T
%   Maximum_Frequency - Upper limit of bandwidth
%   Sample_Frequency - Ensure sample freq is at least two times
%       Maximum_Frequency, fs
%   SNRdB - Signal to noise ratio in dB for the simulated receive
%       signal
%
%  Outputs:
%   Figure(1) - Velocity correlation stem plot
%   Figure(2) - Velocity correlation line plot
%
%%%%%%%%%%%%%%%%%%%%%%%%%%%%%%%%%%%%%%%%%%%%%%%%%%%%%%%%%%%%%%%%%%%%%%%

fc = Maximum_Frequency-Bandwidth/2; %convert max freq to center ...
    freq
```

```
[sig,t] = Transmit_Sig(Bandwidth, Measurement_Window, ...
    Sample_Frequency,fc); %input BW, T, fs, and fc to create ...
    simulated transmit signal

SNR = 10^(SNRdB/10); % Change from log to linear ratio
sigint = int8(sig*100000); % Simulated 8-bit sampled transmit ...
    signal
L = length(sig); % Number of samples = fs*T

%%%%%%%%%%%%%%%%%% Simulated Receive Signal %%%%%%%%%%%%%%%%%%%%

c = 299792458; % Speed of light
fs = Sample_Frequency;
deltr = 2*Target_Velocity/((c-Target_Velocity)*fs); % Time shift ...
    every sample experiences for constant moving target
mult = (0:L-1)';
tr = t-mult*deltr; % Vector of where the receive samples are at in...
     time
if Target_Velocity < 0
    tr = reshape([t,tr]',[],1); % Sorts the vector used for ...
        interp1 function
    tr(1)=[]; % First two values are zero and one needs to be ...
        deleted
    recsig=interp1(t,sig,tr); % Interpolated signal with original ...
        signal
    recsig=recsig(1:2:end); % Simulated received signal for ...
        negative target velocity
    clear sig tr
    recsig=int8(recsig*100000); % Convert to 8-bit to simulate ...
        sampled receive signal
    recsig(find(isnan(recsig)))=0; % Interp1 function does not ...
        extrapolate data and this sets any NaN to 0 so the inner ...
        dot product does change with those samples
elseif Target_Velocity==0
```

```
        recsig=int8(sig*100000); % If target velocity is zero than no ...
            interpolation takes place
    else
        tr=reshape([tr,t]',[],1); % Changed order because of positive ...
            target velocity
        tr(1)=[];
        recsig=interp1(t,sig,tr);
        recsig=[recsig(1);recsig(2:2:end)]; % Simulated received ...
            signal for positive target velocity
        clear sig tr
        recsig=int8(recsig*100000); % Convert to 8-bit to simulate ...
            sampled receive signal for positive target velocity
    end

    %%%%%%%%%%%%%%%%%% Simulated Reference Signal %%%%%%%%%%%%%%%%%%

    vref = linspace(Reference_Velocity_Low,Reference_Velocity_High,...
        Number_of_Reference_Velocities); % Creates the range of ...
        reference velocities base on user input
    corr = zeros(length(vref),1); % Preallocated vector
    for ii = 1:length(vref) % Same process as above, only there can be...
        many reference velocities and only one target velocity
        delt = 2*vref(ii)/((c-vref(ii))*fs); % Time shift every sample...
            experiences the specific reference velocity
        ti = t-mult*delt; % Vector of where the reference samples are ...
            at in time
        if vref(ii) < 0
            ti = reshape([t,ti]',[],1);
            ti(1) = [];
            sigref = interp1(t,double(sigint),ti);
            sigref = sigref(1:2:end);
            sigref(find(isnan(sigref))) = 0;
        elseif vref(ii) == 0
            sigref = sigint;
        else
```

```
            ti = reshape([ti,t]',[],1);
            ti(1) = [];
            sigref = interp1(t,double(sigint),ti);
            sigref = [sigref(1);sigref(2:2:end)];
        end
        corr(ii) = (double(recsig)+1/SNR*randn(L,1)).'*double(sigref);...
            % Correlates the signals by converting the simulated ...
            receive and reference signals to double format and then ...
            taking the inner dot product between the noisy receive ...
            signal and reference signal
        fprintf('%d of %d Completed\n',ii,length(vref)); % Displays ...
            how many reference velocities have been completed
    end
    corr=corr/max(corr); % Normalized matched filter output vector
    [dummy, I]=max(abs(corr));
    Velocity=vref(I) % Displays velocity estimation

    %%%%%%%%%%%%%%%%%% Plot Simulated Results %%%%%%%%%%%%%%%%%%%%%

    figure(1)
    clf;
    set(0,'DefaultAxesFontSize',14);
    stem(vref,corr)
    xlabel('Velocity (m/s)')
    ylabel('Normalized Matched Filter Output')

    figure(2)
    clf;
    set(0,'DefaultAxesFontSize',14);
    plot(vref,corr,'linewidth',2)
    xlabel('Velocity (m/s)')
    ylabel('Normalized Matched Filter Output')
```

Listing B.3: Analyze_Data.m

```
function [] = Analyze_Data(tx, rx, Reference_Velocity_Low, ...
    Reference_Velocity_High, Number_of_Reference_Velocities, ...
    Sample_Frequency, Rmax, filename)

%%%%%%%%%%%%%%%%%%%%%%%%%%%%%%%%%%%%%%%%%%%%%%%%%%%%%%%%%%%%%%%%%%%%%%%%
%
% The function simulates the normalized matched filter ouput for
%   a Random Noise Radar (RNR) when the radar is perfectly matched
%   in range.
%
%  Inputs:
%   tx - Raw data from transmit channel
%   rx - Raw data from receive channel
%   Reference_Velocity_Low - Minimum reference velocity
%   Reference_Velocity_High - Maximum reference velocity
%   Number_of_Reference_Velocities - Number of velocities to ...
    correlate
%   Sample_Frequency - Should be either 1.25e9 or 2.5 e9 GS/s
%   Rmax - Maximum range in meters the user want to correlate out ...
    to
%   filename - The filename for the saved data to be saved in.  An
%       example is 'MyData', notice the single quotes are ...
    necessary
%
%  Output:
%   .mat file that contains the correlation matrix, the sample
%       frequency, the range vector, and reference velocity vector
%
%%%%%%%%%%%%%%%%%%%%%%%%%%%%%%%%%%%%%%%%%%%%%%%%%%%%%%%%%%%%%%%%%%%%%%%%

c=299792458; % Speed of light
fs=Sample_Frequency;

if fs == 1.25e9
```

```
        R0 = 58; % Sample 58 corresponds to 0 meters for fs = 1.25e9 ...
            based on calibration testing
        T = .16;
    elseif fs == 2.5e9
        R0 = 117; % Sample 58 corresponds to 0 meters for fs = 2.5e9 ...
            based on calibration testing
        T = .08;
    else
        disp('Sample frequency must be either 1.25e9 or 2.5e9.')
        return
    end

    L = round(fs*T); % Length of signal
    d = c/fs; % Distance = Rate * Time
    Rmax = round(2*Rmax/d); % Finds the number of samples that equals ...
        Rmax
    range=(0:Rmax)*d/2; % Range vector that gets saved and used for ...
        plotting purposes

    tx=tx(1:L); % Limit tx to length L
    rx=rx(1:L+R0+Rmax); % Limit rx to length L+R0+Rmax

    vref = linspace(Reference_Velocity_Low,Reference_Velocity_High,...
        Number_of_Reference_Velocities); % Creates the range of ...
        reference velocities base on user input

    t=(0:1/fs:(L-1)/fs)'; % Time stamps for each sample

    corr=zeros(Number_of_Reference_Velocities,Rmax+1); % Preallocated ...
        correlation matrix
    mult=(0:L-1)'; % Each sample gets shift in time based on target ...
        velocity, sample frequency, and sample number which is where ...
        mult comes in
    for ii=1:Number_of_Reference_Velocities
```

```
    if vref(ii)<0 % For Negative Reference Velocities
        delt=2*vref(ii)/((c-vref(ii))*fs); % Time shift every ...
            sample experiences for constant moving target
        ti=t-mult*delt; % Vector of where the reference samples ...
            are at in time
        ti=reshape([t,ti]',[],1); % Sorts the vector used for ...
            interp1 function
        ti(1)=[]; % First two values are zero and one needs to be ...
            deleted
        sigref=interp1(t,tx,ti); % Interpolated signal with ...
            original signal
        sigref=sigref(1:2:end); % Reference signal for negative ...
            velocity for negative target velocity
        sigref(find(isnan(sigref)))=0; % Interp1 function does not...
             extrapolate data and this sets any NaN to 0 so the ...
            inner dot product does change with those samples
    elseif vref(ii)==0
        sigref=tx; % At this velocity is where the majority of the...
             clutter will appear
    else % For Positive Reference Velocities
        delt=2*vref(ii)/((c-vref(ii))*fs);
        ti=t-mult*delt;
        ti=reshape([ti,t]',[],1);
        ti(1)=[];
        sigref=interp1(t,tx,ti);
        sigref=[sigref(1);sigref(2:2:end)];
    end

    temp = ifft(fft([sigref;zeros(R0+Rmax)]).*fft(rx)); % ...
        Effectively performs a sliding dot product in order to ...
        calculate the range correlations all at once without a for ...
        loop
    corr(ii,:) = temp(R0:Rmax); % Stores the correlated data that ...
        starts with R0 and goes to Rmax
```

```
    fprintf('%d of %d Completed\n',ii,...
        Number_of_Reference_Velocities); % Displays how many ...
        reference velocities have been completed
end

save(filename,'corr','fs','range','vref') % Saves the processed ...
    data for later plotting
```

Bibliography

1. Axelsson, S. R. J. "On the theory of noise Doppler radar." *Geoscience and Remote Sensing Symposium, 2000. Proceedings. IGARSS 2000. IEEE 2000 International2*. 856–860 vol.2. 2000.

2. Axelsson, S. R. J. "Noise radar for range/Doppler processing and digital beamforming using binary ADC." *Geoscience and Remote Sensing Symposium, 2001. IGARSS '01. IEEE 2001 International5*. 2001 –2005 vol.5. 2001.

3. Axelsson, S. R. J. "Noise Radar for range/Doppler processing and digital beamforming using low-bit ADC," *Geoscience and Remote Sensing, IEEE Transactions on*, *41*(12):2703 – 2720 (Dec 2003).

4. Axelsson, S. R. J. "Noise Radar for range/Doppler processing and digital beamforming using low-bit ADC," *Geoscience and Remote Sensing, IEEE Transactions on*, *41*(12):2703–2720 (2003).

5. Axelsson, S. R. J. "Noise radar using random phase and frequency modulation." *Geoscience and Remote Sensing Symposium, 2003. IGARSS '03. Proceedings. 2003 IEEE International7*. 4226 – 4231 vol.7. July 2003.

6. Axelsson, S. R. J. "Noise radar using random phase and frequency modulation," *Geoscience and Remote Sensing, IEEE Transactions on*, *42*(11):2370–2384 (2004).

7. Axelsson, S. R. J. "Generalized Ambiguity Functions for Ultra Wide Band Random Waveforms." *Radar Symposium, 2006. IRS 2006. International*. 1 –4. May 2006.

8. Breed, G., editor. *A Summary of FCC Rules for Ultra Wideband Communications*, 2005.

9. Byrnes, J. S. *Advances in sensing with security applications*, *2*. Dordrecht ; Great Britain: Springer, 2006.

10. Cook, C. E. and M. Bernfeld. *Radar signals; an introduction to theory and application*. New York: Academic Press, 1967.

11. Cooper, G. R. and C. D. McGillem. *Random Signal Radar*. NASA Grant NSG 543, Lafayette, Indiana: Purdue University, June 1967.

12. Craig, S. E., et al. "Continuous-wave radar with high range resolution and unambiguous velocity determination," *IRE Transactions MIL-6*, 153 (April 1962).

13. Dawood, M. and R. M. Narayanan. "Doppler measurements using a coherent ultrawideband random noise radar." *Antennas and Propagation Society International Symposium, 1999. IEEE4*. 2226 –2229 vol.4. August 1999.

14. Dawood, M. and R. M. Narayanan. "Receiver operating characteristics for the coherent UWB random noise radar," *Aerospace and Electronic Systems, IEEE Transactions on*, *37*(2):586–594 (2001).

15. Dawood, M. and R. M. Narayanan. "Generalised wideband ambiguity function of a coherent ultrawideband random noise radar," *Radar, Sonar and Navigation, IEE Proceedings* -, *150*(5):379–386 (Oct 2003).

16. Grant, S. E., et al. "A class of noise radar systems," *Proceedings of the IEEE*, *51*(7):1060–1061 (July 1963).

17. Guosui, L., et al. "The present and the future of random noise signals," *Aerospace and Electronic Systems Magazine, IEEE*, *12*(10):35–40 (Oct 1997).

18. Horton, B. M. "Noise-modulated distance measuring system," *Proceedings of the IRE*, *49*(5):821–828 (May 1959).

19. Ifeachor, E. C. and B. W. Jervis. *Digital Signal Processing: A Practical Approach* (Second Edition). Pearson Education Limited, 2002.

20. "www.dictionary.com."

21. Kaiser, G. *A Friendly Guide to Wavelets*. Birkhäuser, 1994.

22. Levanon, N. and E. Mozeson. *Radar signals*. Wiley, 2004.

23. Li, Z. and R. M. Narayanan. "Doppler visibility of coherent ultrawideband random noise radar systems," *Aerospace and Electronic Systems, IEEE Transactions on*, *42; 42*(3):904–916 (2006).

24. Mahafza, B. R. and A. Z. Elsherbeni. *MATLAB simulations for radar systems design*. Chapman & Hall/CRC, 2004.

25. McGillem, C. D., et al. "An experimental random signal radar." *Proceedings of the National Electronics Conference*. 409–411. October 1967.

26. Narayanan, R. M. and M. Dawood. "Doppler estimation using a coherent ultrawide-band random noise radar," *Antennas and Propagation, IEEE Transactions on*, *48*(6):868–878 (2000).

27. Narayanan, R. M., et al. "Design and performance of a polarimetric random noise radar for detection of shallow buried targets." *Proceedings SPIE Meet. Detection Technol. Mines Minelike Targets*. 20–30. Apr 1995.

28. Narayanan, R. M., et al. "Design, performance, and applications of a coherent ultra-wideband random noise radar," *Optical Engineering*, *37*(6):1855–1869 (June 1998).

29. Nelms, M. *Development and Evaluation of a Multistatic Ultrawideband Random Noise Radar*. MS thesis, Air Force Institute of Technology, March 2010.

30. Pace, P. E. *Detecting and Classifying Low Probability of Intercept Radar*. Norwood, MA: Artech House, 2009.

31. Schmitt, A. L. *Radar Imaging with a Network of Digital Noise Radar Systems*. MS thesis, Air Force Institute of Technology, Mar 2009.

32. Stremler, F. G. *Introduction to Communication Systems* (3rd Edition). Addison-Wesley Series in Electrical Engineering, Addison-Wesley Publishing Company, Inc., 1990.

33. Theron, I.P., et al. "Ultrawide-band noise radar in the VHF/UHF band," *Antennas and Propagation, IEEE Transactions on*, *47*(6):1080 –1084 (June 1999).

34. Walton, E. K., et al. "Moving vehicle range profiles measured using a noise radar." *Antennas and Propagation Society International Symposium, 1997. IEEE., 1997 Digest4*. 2597 –2600 vol.4. July 1997.

35. Weiss, L. G. "Wavelets and wideband correlation processing," *Signal Processing Magazine, IEEE*, *11*(1):13 –32 (January 1994).

36. Young, R. K. *Wavelet Theory and its Applications*. Kluwer Academic Publishers, 1993.

REPORT DOCUMENTATION PAGE

Form Approved
OMB No. 0704–0188

1. REPORT DATE *(DD–MM–YYYY)*	2. REPORT TYPE	3. DATES COVERED *(From — To)*
24–03–2011	Master's Thesis	Aug 2009 — Mar 2011

4. TITLE AND SUBTITLE

Simultaneous Range/Velocity Detection with an Ultra-Wideband Random Noise Radar Through Fully Digital Cross-Correlation in the Time Domain

5a. CONTRACT NUMBER

5b. GRANT NUMBER

5c. PROGRAM ELEMENT NUMBER

6. AUTHOR(S)

James R. Lievsay, Capt, USAF

5d. PROJECT NUMBER

5e. TASK NUMBER

5f. WORK UNIT NUMBER

7. PERFORMING ORGANIZATION NAME(S) AND ADDRESS(ES)

Air Force Institute of Technology
Graduate School of Engineering and Management (AFIT/EN)
2950 Hobson Way
Wright-Patterson AFB, OH 45433-7765

8. PERFORMING ORGANIZATION REPORT NUMBER

AFIT/GE/ENG/11-24

9. SPONSORING / MONITORING AGENCY NAME(S) AND ADDRESS(ES)

INTENTIALLY LEFT BLANK

10. SPONSOR/MONITOR'S ACRONYM(S)

11. SPONSOR/MONITOR'S REPORT NUMBER(S)

12. DISTRIBUTION / AVAILABILITY STATEMENT

13. SUPPLEMENTARY NOTES

14. ABSTRACT

This research effort examines the theory, application, and results of applying two-dimensional cross-correlation in the time domain to ultra-wideband (UWB) random noise waveforms for simultaneous range and velocity estimation. When applying common Doppler processing techniques to random noise waveforms for the purpose of velocity estimation, the velocity resolution degrades as the signal bandwidth or the target speed increase. To mitigate the degradation, the Doppler approximation is not utilized, and instead, wideband signal processing theory is applied in the time domain. The results show that by accurately interpolating each sample in the digitized reference signal, a target's velocity and range can be extracted simultaneously. However, the drawback consists of the amount of time involved in processing the data. As technology continues to advance, it is believed that the Air Force Institute of Technology UWB Random Noise Radar (RNR) will be capable of simultaneously estimating a target's range and velocity near real-time through 2D non-coherent cross-correlation in the time domain.

15. SUBJECT TERMS

Random Noise Radar, Ultra-Wideband, Low Probability of Intercept Radar, Simultaneous Detection

16. SECURITY CLASSIFICATION OF:			17. LIMITATION OF ABSTRACT	18. NUMBER OF PAGES	19a. NAME OF RESPONSIBLE PERSON
a. REPORT	b. ABSTRACT	c. THIS PAGE			Maj Geoffrey Akers, PhD
U	U	U	UU	118	19b. TELEPHONE NUMBER *(include area code)* (937) 785-3636 x 4659; geoffrey.akers@afit.edu